INFORMATION TO USERS

This manuscript has been reproduced from the microfilm master. UMI films the text directly from the original or copy submitted. Thus, some thesis and dissertation copies are in typewriter face, while others may be from any type of computer printer.

The quality of this reproduction is dependent upon the quality of the copy submitted. Broken or indistinct print, colored or poor quality illustrations and photographs, print bleedthrough, substandard margins, and improper alignment can adversely affect reproduction.

In the unlikely event that the author did not send UMI a complete manuscript and there are missing pages, these will be noted. Also, if unauthorized copyright material had to be removed, a note will indicate the deletion.

Oversize materials (e.g., maps, drawings, charts) are reproduced by sectioning the original, beginning at the upper left-hand corner and continuing from left to right in equal sections with small overlaps.

ProQuest Information and Learning
300 North Zeeb Road, Ann Arbor, MI 48106-1346 USA
800-521-0600

NOTE TO USERS

Page(s) not included in the original manuscript are unavailable from the author or university. The manuscript was microfilmed as received.

120

This reproduction is the best copy available.

UMI

Impact of Gel Morphology on Pore-Filled Membranes

By

Christopher T.C. McCrory, M.Sc.

A Thesis

Submitted to the School of Graduate Studies

in Partial Fulfilment of the Requirements

for the Degree

Doctor of Philosophy in Chemistry

McMaster University

© Copyright by Christopher T.C. McCrory, July 2001

IMPACT OF GEL MORPHOLOGY ON PORE-FILLED MEMBRANES

DOCTOR OF PHILOSOPHY (2001)
(Chemistry)

McMaster University
Hamilton, Ontario

TITLE: Impact of Gel Morphology on Pore-Filled Membranes

AUTHOR: Christopher T.C. McCrory, M.Sc. (McMaster University)

SUPERVISOR: Professor R. F. Childs

NUMBER OF PAGES: xxiii. 162

Abstract

Pore-filled cation exchange membranes were prepared by the co-polymerization of acrylic acid and N,N'-methylenebisacrylamide within the pores of a microporous polypropylene substrate. The poly(acrylic acid) gels in the membranes exhibited heterogeneity when synthesized with 1,4-dioxane, a poor solvent for poly(acrylic acid), or with increase in degree of cross-linking. Corresponding bulk gels were prepared and revealed heterogeneity as the volume percent of 1,4-dioxane was increased in the DMF mixture, or as the cross-linking ratio was increased. Confocal laser scanning microscopy revealed a globular morphology of both the bulk gel and the pore-filling gel in the membrane when formed in a poor solvent, however, no difference in morphology was detected with the change in degree of cross-linking. The degree of swelling of the membranes was consistent with a change in gel morphology associated with change in reaction solvent or degree of cross-linking.

The hydrodynamic (Darcy) permeabilities of the membranes were determined by measuring the fluxes at various pressures. The pure water-fluxes were found to be dependent on the mass-loading and morphology of the gel within the membranes. It was found that the permeability of the membranes decreased with increasing polymer volume fraction. The reaction solvent and degree of cross-linking used in the polymerization step were both found to have a direct impact on permeability. For example, a 9 fold increase in hydrodynamic permeability was observed when a poorer solvent was used in the

formation step and a 4 fold increase in permeability was observed with increase in cross linking. A recently developed model based on fundamental scaling principles allows further insight in understanding the impact of gel morphology on permeability.

The membranes were evaluated in terms of their nanofiltration capabilities with 5 mM solutions of NaCl. The extended Nernst-Planck equation, which takes account of the effective charge densities, was used to model rejection of single electrolyte solutions. The separation properties of the PAA membranes are good and the salt rejection was found to be practically constant, at constant pressure, over a wide range of gel concentrations. However, the performance was affected by the morphology of the gel.

Asymmetric membranes were synthesized by photopolymerization of acrylic acid within a porous substrate. The monomer solution contained 2,2'-dihydroxy-4,4'-dimethoxybenzophenone (DDB), a UV absorber, which controlled the penetration depth of UV radiation. The asymmetric distribution of gel within the membrane was varied by changing the concentration of DDB in the polymerization mixture.

Singular value decomposition analysis of X-ray microscopy images recorded at carefully selected photon energies is shown to be a useful method to obtain quantitative maps of chemical components. The method is illustrated by a quantitative study by Scanning Transmission X-ray Microscopy (STXM) of the distribution of poly(acrylic acid) in a series of microporous polypropylene support membranes. The polymeric system was studied fully hydrated in order to perform the quantitative mapping when the membrane is the same as in its state of application. The effect of concentration of DDB on

morphology of the gel fill was analyzed by STXM and related to the hydrodynamic permeability and nanofiltration performance.

It was found that the polymerization conditions led to a denser, thinner poly(acrylic acid) gel morphology within the membrane with increasing amount of photoblocker. The hydrodynamic permeability of the asymmetric membranes decreased with increase in gradient morphology. Also, the flux during nanofiltration of 5 mM NaCl decreased, while the rejection remained constant for all membranes.

The quantitative description of the gel structure obtained in this work allows the prediction of the properties of poly(acrylic acid) gel separation devices, and provides a basis for the further design and optimization of poly-electrolyte filled membranes for nanofiltration applications.

Acknowledgements

I wish to express my thanks to my research supervisor, Professor Ron Childs, for his knowledge and guidance, and especially for his encouragement. Through both his support and criticisms, he has made me a better scientist.

I would also like to thank my committee members, Professors Brian McCarry and Harald Stöver for their ideas and advice.

I am very grateful for the expertise of Marcia West in cryotoming and ESEM, and Professor Adam Hitchcock and Cynthia Morin for their STXM expertise.

To my lab-mates, past and present: thank you for allowing me to experience a productive, yet fun working environment. You have made this experience both enjoyable and educational. Thanks go to: Alicja, Marcus, Dave, Elena, Jinsheng, Lifang, Maggie, Antonin, Erica, Diane, and Kamillah.

Special thanks go to the Phoenix dwellers that help reach critical mass. No shop talk or you owe me one.

Finally, thanks to my friends and family. In particular, thanks to my Mom and Dad, my brother Ian (Baby E) and Denise for their patience, love and support over all these years.

Table of Contents

Chapter 2 - Formation and Characterization of Poly(acrylic acid-co-N,N'-methylenebisacrylamide) Pore-Filled Membranes

Chapter 3 - Hydrodynamic Permeability of Poly(Acrylic Acid) Pore Filled Membranes

List of Figures

List of Tables

List of Schemes

List of Abbreviations

Acronyms

AFM	Atomic force microscopy
ALS	Advanced Light Source
AMPS	2-amino-2-methylpropanesulfonic acid
BIS	N,N'-methylenebisacrylamide
CLSM	Confocal laser scanning microscopy
DABCO	1,4-Diazabicyclo[2,2,2]octane
DDB	2,2'-dihydroxy-4,4'-dimethoxybenzophenone
Diox	1,4-dioxane
DMF	N,N'-dimethylformamide
DMPA	2,2-dimethoxy-2-phenylacetophenone
EDX	Energy dispersive x-ray
ENP	Extended Nernst-Planck equation
ESEM	Environmental scanning electron microscopy
HEMA	2-hydroxyethylmethacrylate
IEC	Ion exchange capacity
MPD	*m*-Phenylenediamine
NEXAFS	Near edge x-ray absorption fine structure
NF	Nanofiltration
P-4VP	Poly(4-vinylpyridine)
PAA	Poly(acrylic acid)
PP	Polypropylene
PPD	*p*-Phenylenediamine
PSCF	Preferential sorption-capillary flow model

RO	Reverse Osmosis
SFPF	Surface force-pore flow model
STXM	Scanning transmission x-ray microscopy
TEM	Transmission electron microscopy
TFC	Thin film composite
TMC	Trimesoyl chloride
TMS	Teorell-Meyer-Sievers model
UV	Ultra violet
XL	Cross-linking

Symbols

α	Degree of ionization
$\alpha(E)$	Linear attenuation coefficient at energy E
$\Delta\pi$	Change in osmotic pressure
Δp	Pressure difference across membrane (Pa)
Δx	Membrane thickness (m)
ε, ε_s	Substrate porosity
η	Permeate viscosity at 25 °C (0.00089 Pa s)
ξ_{sp}	Correlation length of polymer
κ	Debye-Hückel parameter
σ_m	Reflection coefficient
τ	Tortuosity factor
$\mu(E)$	Energy-dependent mass absorption coefficient
v_2	The partial specific volume of the gel polymer (0.73 cm^3/g for poly(acrylic acid))

φ	Polymer volume fraction (PVF)
φ_{avg}, φ_D, φ_{ND}	Average PVF of membrane, PVF of draining region, PVF of non-draining region
φ_w	Water uptake
χ	Flory-Huggins polymer solvent interaction parameter
ω	Solute permeability
a	Bond length of the monomer unit (m)
A_k	Surface porosity
C_∞	Characteristic ratio
CD_E	Estimated charge density obtained from the extended Nernst-Planck equation (mol/m^3)
CD_M	Calculated membrane charge density (based on amount of incorporated polyelectrolyte (mol/m^3)
c_i	Concentration of ith ion in solution (mol/L)
c^m_1, c^m_2	Concentration of cation (i = 1) in membrane, concentration of anion (i = 2) in membrane (mol/L)
c_p, c_b	Concentration of salt in permeate (p), concentration of salt in bulk (b)
D_i	D_i is the diffusivity of the ion i in the membrane (m^2/s)
d_{pp}	Density of poly(propylene) (0.91 g/cm^3)
D_s	Generalized diffusivity defined in equation 4.7 (m^2/s)
d_w	Density of water (g/cm^3)
F	Faraday constant (= 96487 C/mol)
F_s, F_w	Driving forces for solute and water in hyperfiltration
J_i	The flux of the ith kind of ion (i = 1, cation, i = 2, anion) through the membrane
J_s	Solute flux defined by equation 4.5 (mol/m^2.s)

J_v	Volume flow across the membrane (m^3/s)
J_w	Pure water flux (m/s)
I	Attenuated intensity of x-ray beam
I_o	Intensity of the incident x-ray beam
k	Gel permeability (m^2)
k_m	Membrane permeability (m^2)
l	Contour length (m)
L	Membrane thickness (m)
l_b	Bjerrum length
L_e	Electrostatic persistence length
L_p	Pure water permeability (m^2)
m_M, $m_{m,dry}$	Total mass of the dried membrane with incorporated polyelectrolyte (kg)
$m_{m,wet}$	Mass of swollen membrane (kg)
m_s	Mass of substrate prior to polymerization
n	Number of bonds in the persistence length
n_t, n_p, n_e	Number of bonds in the total persistence length, bare persistence length and electrostatic persistence length
n_x	Equivalent number of the fixed charges in a membrane sample
OD	Optical density defined by equation 5.3
R	Radius of hard sphere (m) defined in equation 3.1
R	Gas constant (8.314 J/mol.K)
T	Temperature (K)
V_m, V_s, $V_{m,wet}$	Volume of swollen membrane (m^3)
V_n	Volume of nascent membrane (m^3)
v_{pe},	Volume of polyelectrolyte chains in pore

v^{ND}_{pe}, v^{D}_{pe}	Volume of polyelectrolyte chains in non-draining and draining regions
V_{pore}	Average pore volume of membrane
V_D, V_{ND}	Volume of the draining and non-draining regions
w	The three-body excluded volume parameter which is assumed to be zero in the marginal regime, defined in equation 3.2
z_i	The valence of the ith ion

Chapter 1

An Introduction to Pore-Filled Membranes

1 Introduction

A membrane acts as a barrier to flow, allowing selective passage of a particular species (solvent) while other species (solutes) are retained partially or completely.[1] Solute separation and permeate water (solvent) flux characteristics of membranes depend on the membrane material selection, the preparation procedures, and the structure of the membrane barrier layer.[1]

Polymeric membranes have been developed for a variety of industrial applications, examples of which include microfiltration, ultrafiltration, nanofiltration, reverse osmosis and gas separation. Each application imposes specific requirements on the membrane material and membrane structure. For example, for desalination, a reverse osmosis (RO) or nanofiltration (NF) membrane is required. The main difference between the two types of membranes lies in the pore size. The typical pore diameter can range from a few angstroms in RO to several nanometers in NF membranes.[2]

The focus of this thesis is on membranes designed for use in ultra-low pressure reverse osmosis,[1] or nanofiltration, as may be found in potable water treatment. These membranes use a pressure difference as the driving force for separation. In order to

describe nanofiltration membranes, it is also necessary to review reverse osmosis membranes, as they are very similar.

The largest amount of work on desalination membranes has focussed on reverse osmosis membranes, both from a preparative and from a theoretical point of view. The efficiency of desalination membrane-based separation can be judged in terms of two parameters: the permeate flux of the transport process and selectivity of the transport process.[3] The goal is to achieve both a very high rate of solvent flux and high selectivity. In reality, an acceptable balance must be found between flux and selectivity because these two parameters generally oppose each other.

1.1 RO/NF Membranes

1.2 Membrane Process Descriptions and Terminology

Osmosis is a natural phenomenon in which water passes through a semipermeable (no solute flow) membrane from the side with lower solute concentration to the higher solute concentration side (**Figure 1.1 A**) until equilibrium of solvent (water) chemical potential is restored (**Figure 1.1 B**). At equilibrium the pressure difference between the two sides of the membrane is equal to the osmotic pressure difference. To reverse the flow of water, a pressure difference is applied (**Figure 1.1 C**); as a result, separation of water from

solutions becomes possible. This phenomenon is termed *reverse osmosis*. It has also been termed *hyperfiltration*.

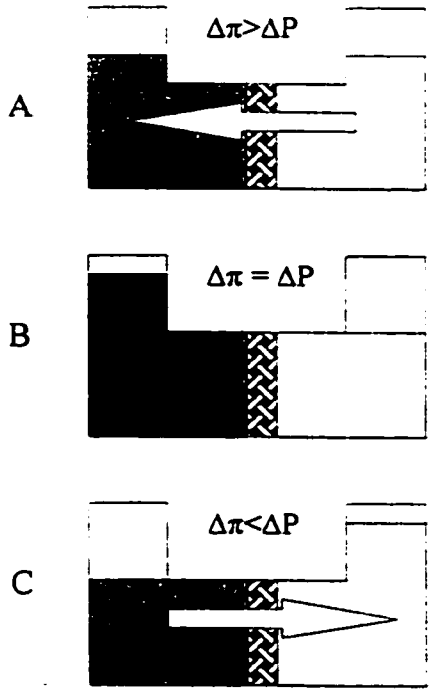

Figure 1.1: Schematic of reverse osmosis. A) Osmosis - solvent flux to concentrate side. B) Equilibrium - Osmotic pressure equals atmospheric or applied pressure. No solvent flux. C) Applied pressure greater than osmotic pressure - solvent flux to low concentrate side.

Reverse osmosis processes can be classified into three types: high pressure RO (5.6 to 10.5 MPa, such as seawater desalination), low pressure RO (1.4 to 4.2 MPa, such as brackish water desalination), and nanofiltration (<1.4 MPa, such as partial demineralization up to 80% NaCl rejection).

1.3 Development of RO/NF membranes

There are several ways to prepare polymeric membranes for desalination. The final morphology and performance of the membranes obtained will vary greatly, depending on the properties of the materials and the process conditions.

The practical application of polymer membranes as separation media for reverse osmosis started in the late 1950's with the discovery of Reid and Breton[4] that cellulose acetate can be an effective membrane material.[5] These symmetric membranes had low water fluxes, however, Loeb and Sourirajan[6] showed that the water flux can be increased if the membrane is made asymmetric, with a very dense, thin skin layer and a macroporous support layer.[5] In these membranes the selective skin layer and the underlying porous supporting structure were made of the same material.

These membranes have now been surpassed with the advent of extremely thin separating layers produced by interfacial condensation polymerization. Most commercial thin-film composite membranes are produced by the interfacial polymerization of reactive monomers.[7-12] The interfacial condensation polymerization method typically involves the reaction of a water soluble diamine monomer with an organic soluble monomer. The majority of patents have the aqueous phase initially fill the pores of the substrate, followed by subsequent application of an organic layer containing diacid chloride monomer on top of the substrate, with polymerization occurring at the interface to produce the thin film

membrane. Such processes are used by Ionics[8], Saehan Industries Inc.[9], Hydranautics[11-13] and the Exxon Research and Engineering Company[7].

Recently, commercial membranes manufactured by the interfacial polymerization technique have shown improved performance by controlling the morphology of the surface layer. The use of different multi functional amides can produce network polyamides that provide a wide variety of membrane surface structures.[14] With *m*-phenylenediamine (MPD) and trimesoyl chloride (TMC), the so-called ridge-and-valley structure is obtained,[15] while those formed from *p*-phenylenediamine (PPD) and TMC appear as dense, finely dispersed nodular structures resembling the surface of phase inversion membranes.[16] Quantitative analysis of the two polyamide films has shown that the average surface roughness of the MPD/TMC film is twice that of the PPD/TMC film.[16] It is typically found that an increase in surface roughness correlates into an increase in flux of the permeate with a decrease in rejection.[16,17]

Hirose and co-workers[18] have shown that the surface roughness of the barrier layer of polyamide TFC membranes can be enhanced by addition of *iso*-propanol to the amine solutions[18] or with a change in the chemical structure of the acid chloride used in the interfacial polymerization.[19] An increase of two orders magnitude in flux with a decrease in rejection was observed for the latter case.

1.4 Theory of Transport and Separation in Reverse Osmosis and Nanofiltration Membranes

In order too more fully understand the relationship between membrane properties on performance, a large number of models have been developed. The large amount of research done over the last four decades on RO/NF has resulted mainly in a phenomenological description of the relationships between properties of membrane materials and membrane performance.[5] Typically, the modelling of membrane transport does not involve a detailed description of the properties of the membrane and can be referred to as a "black box."[2] This does not allow one to gain further insight into the relationship between membrane characteristics and properties with membrane performance.

Several models have been developed to describe solute and solvent fluxes through RO membranes. Most models for reverse osmosis membranes assume diffusion or pore flow through the membrane while charged membrane theories include electrostatic effects.[1] For nanofiltration membranes, which are often negatively charged, Donnan exclusion models and extended Nernst-Planck models can be used to determine solute fluxes.[1] A brief description of some of the major transport models follows.

1.4.1 Solution-Diffusion Models

The solution-diffusion model was originally developed by Lonsdale, Merten, and Riley.[20] This model assumes both the solute and solvent dissolve in the nonporous and homogeneous surface layers of the membrane and then each diffuses across it in an uncoupled manner due to its own chemical potential gradient; this gradient is the result of concentration and pressure differences across the membrane.

According to this model,[20] based on pure diffusion, solvent flux (J_w) through the membrane is given by

$$J_w = \frac{P_w}{l}(\Delta p - \Delta \pi)$$

where $P_w = D_w c_{water} V_w / RT$, Δp is the pressure difference across the membrane, and $\Delta\pi$ is the osmotic pressure difference between the feed and permeate at the membrane surfaces. The solute flux, J_s, according to this model is given by[20]

$$J_s = \frac{P_s}{l}(c'_w - c'')$$

where $P_s = D_{sm} K_s$, c'_w is the concentration of solute in the feed solution at the membrane surface, and c'' is the concentration of solute in the permeate solution. In these equations, D_w and D_{sm} represent diffusivities of water and solute, respectively, c_{water} is the concentration of water in the membrane, V_w is the partial molar volume of water, K_s is the solute distribution coefficient, and l is the membrane thickness.

Rejection by the membrane depends on the solute distribution coefficient between the solution and membrane phase and the solute diffusivity in the membrane phase according to the following equation [20]

$$R' = \left(1 + \frac{P_s / l}{J_w}\right)^{-1}$$

This model is applicable to membranes with relatively small water content.

An extension of this model, the solution-diffusion-imperfection model recognizes that imperfections (pores) exist on the membrane surface through which solute and solvent can flow. The model includes both diffusion of solute and solvent and pore flow in the derivation.[21]

1.4.2 Pore Flow Models

Two existing pore flow models are the preferential sorption-capillary flow model (PSCF)[22] and the surface force-pore flow model (SFPF).[23] The PSCF model assumes the membrane to be microporous.[22] The model states that the membrane barrier layer has chemical properties such that it has preferential sorption for the solvent or preferential repulsion for the solutes of the feed solution.[22] As a result, a layer of almost pure solvent is found preferentially on the surface and in the pores of the membrane. Solvent from this layer is then forced through the membrane capillary pores under pressure.

The SFPF model is a quantitative description of the PSCF model and allows characterization and specification of a membrane as a function of pore size distribution (or average pore size) along with quantitative measure of surface forces arising between solute-solvent and the membrane wall inside the transport corridor.[23]

Mehdizadeh and Dickson[24] developed an improved version of the original SFPF model which included modified boundary conditions, potential function terms, material balance on the solute in the pore, and osmotic effect corrections.

1.4.3 Irreversible Thermodynamic Model

The thermodynamics of irreversible processes indicate that the flow of each component in a solution is related to the flows of other components. Kedem and Katchalsky[25] and later Spiegler,[3] developed relationships for flow in membranes using phenomenological equations of transport. In a non ideal membrane, there can be two fluxes, J_w and J_s, driven by forces F_w and F_s, respectively. By assuming both the solute and solvent flows are coupled, each flux is a function of both forces.[2]

$$J_w = L_{11}F_w + L_{12}F_s$$

$$J_s = L_{21}F_w + L_{22}F_s$$

There are four phenomenological coefficients, L, each depending on the conditions, but the Onsanger reciprocity relation[3,25] reduces the number of independent coefficients to three

$$L_{21} = L_{12}$$

From this analysis, the reflection coefficient, σ, the solute permeability, ω, and the hydraulic permeability L_p can be described.[2] With this choice of coefficients the following equations were derived for the two flows[3]

$$J_v = L_p(\Delta p - \sigma\Delta\pi) \qquad (1.1)$$

$$J_s = \omega\Delta\pi + (1 - \sigma)J_v c \qquad (1.2)$$

For the case of $\sigma = 1$, that is, in the absence of solvent and solute coupling, eqs. (1.1) and (1.2) can be reduced to the solution-diffusion model transport equations.[3]

1.4.4 Donnan Potential and Equilibrium Model

A dynamic equilibrium occurs when a charged membrane is placed in a salt solution. For example, if a cation exchange membrane is placed in a dilute solution of an electrolyte, a considerable difference in ion concentration exists between the membrane and the solution. The cation concentration will be higher in the membrane than in solution. The difference in ion concentration is a driving force for diffusion of the ions to attain an equilibrium concentration. However, such a process would disturb electroneutrality since the diffusion of cations out of the membrane would result in an accumulation of positive charge in solution, while diffusion of anions into the membrane would give a net negative charge in the membrane. The electric potential developed by the diffusion of ions serves to pull back the cations into the membrane, and anions back into solution. This is known as the Donnan potential.[2,26,27]

A result of the Donnan potential is that co-ions are repelled from the ion exchange membrane thus preventing the internal co-ion concentration from rising beyond an equilibrium value. This equilibrium value is usually much smaller than the concentration in the external solution. Co-ion uptake and electrolyte sorption are equivalent because of electroneutrality. Hence, the electrolyte is at least partially excluded from an ion exchange membrane.[27]

A potential also occurs when an applied pressure gradient forces water flow through the membrane. The effect of the Donnan exclusion is to repel the co-ion from the membrane, and because of electroneutrality requirements, the counter ion is also rejected. Because most RO membranes contain a fixed charge, the effect of Donnan exclusion must be considered in modelling of transport in the membranes.

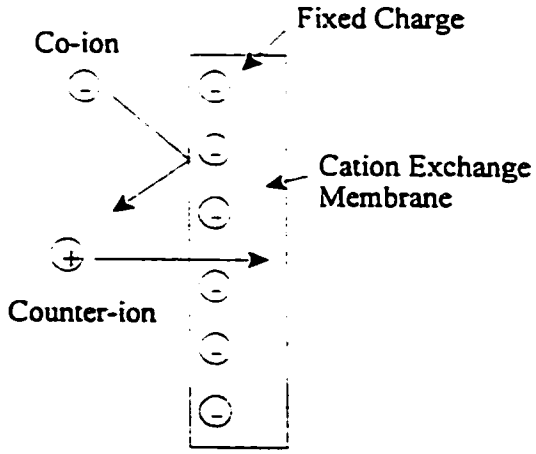

Figure 1.2. Donnan exclusion in a cation exchange membrane

Such a model, developed by Battacharyya and Cheng,[28] includes membrane charge density in the calculation and predicts that the membrane rejection is a function of the

membrane charge density, the feed solute concentration, and the charge of the ions. The model does not take into account diffusive and convective fluxes.

1.4.5 The Extended Nernst-Planck Equation

Several successful models for nanofiltration membranes are now based on the extended Nernst-Planck equation (ENP). The ENP consists of a diffusive, electrostatic and convective term. It has been used by Lakshminarayanaiah[29] and Dresner[30] to describe the flux of ions through a charged membranes, and can be described by the following equation

$$J_i = -D_i \frac{dc}{dx} + \frac{z_i F c_i D_i}{RT} \frac{dE}{dx} + c_i J_v$$

The ENP can be further modified to include boundary conditions or different electrostatic models. For example, Bowen[31,32] has included steric hindrance factors for both diffusion and convection. In this approach, the structural properties of the membranes, namely the effective pore radius, the ratio of membrane thickness over porosity, and the effective charge density are taken into account.

Kimura has numerically solved the ENP using the Teorell-Meyer-Sievers (TMS) model of ion exchange membranes.[33-36] The TMS model assumes that the membrane is homogeneous with a uniform distribution of charge density in the membrane volume and that ion transport may be quantified using bulk diffusivities. Steric hindrance factors may

be neglected if the pore size is much larger than the solute radius. This model was found to fit experimental data very well over a wide range of gel concentrations and is used to predict nanofiltration performance of membranes in this thesis.

1.5 A New Membrane Construct: Pore-Filled Membranes

Network polymers that lack sufficient mechanical strength to be used as membrane materials on their own can be anchored into a suitable host substrate that is mechanically stable. Such membranes can be referred to as "pore-filled".[37]

A pore-filled membrane receives its mechanical strength from the host substrate which is both physically and chemically stable and of sufficient porosity to accept an adequate amount of polymer. The pore filling material serves as the separation medium, possessing the chemical and physical properties required for the specific separation process. The average pore diameter of the supports is typically in the micron range and is much larger than the mesh dimension of the incorporated gels. As a result, molecular and viscous transport within the pores of the support as well as separation is determined by the properties of the pore-filling gels.[31,32,38-40] Depending on the nature of the gel, the basis of separation can range from molecular sieving (size exclusion), Donnan exclusion of co-ions by charged gels, or other specific interactions. An important feature of these composite membranes is that the microporous support provides mechanical strength and structural integrity. This means that the gel network can be optimized for a specific application

without sacrificing its functionality.

Various materials have been introduced into porous substrates including organic complexing agents[41] and polyelectrolytes.[42] One of the key issues in fabrication of pore-filled membranes is the manner in which the material is incorporated into the porous substrate. There are a variety of methods that have been used to introduce pore-filling materials into support membranes and they are reviewed in the following sections.

1.5.1 Physical Adsorption

Perhaps the simplest method of introducing materials into host supports is by physical adsorption. A solution containing the material to be introduced is brought into contact with the support membrane and the material then enters the pores of the membrane. The pore-filling material is held within the pores of the host membrane by van der Waals forces, dipole interactions or, if both the material to be incorporated and the host membrane are charged, electrostatic interactions.

Imato and coworkers[41] impregnated a microporous poly(propylene) film with a solution of tri-n-octylamine in 1-decanol to form a supported liquid membrane. The amine was used as a mobile carrier for the diffusion dialysis transport of organic and inorganic anions in acid solution. In general, supported liquid membranes are not stable due to loss of the pore-filling material during use.

Anderson and Kim prepared pore-filled membranes by adsorbing aqueous solutions

of poly(styrenesulfonate) into porous mica sheets.[42] The membranes were used to study the effects of adsorbed polymer layers on dextran transport through microporous membranes under pressure driven applications. The use of high molecular weight polymers as adsorbed pore-filling agents creates a more stable membrane than simple supported liquid membranes but long term stability was still a problem.

The Dow Chemical Company have patented the manufacture of reverse osmosis membranes by treating the surface of existing reverse osmosis membranes with polymers bearing carboxylic acid groups in order to improve performance.[43;44] The membranes have displayed enhanced salt rejection and/or increased water flux. This treatment is particularly useful for improving the membrane characteristics of cellulose acetate and polyamide membranes.

1.5.2 Grafting

A more robust method of anchoring materials in the pores of host membranes is the covalent attachment of the materials to the membrane. The creation of a covalent bond between the pore-filling material and the host substrate permanently "locks" the material in the membrane pores, such materials are said to be "grafted" onto the substrate. Technologies for modification of polymers using methods such as grafting have been of prime importance in polymer applications and have been reviewed in numerous articles and books over the past few years.[42;45-56] Two basic approaches are used to graft materials into

membranes, attachment of preformed polymers and graft polymerization of monomers within the membrane.

1.5.3 Attachment of Preformed Polymers

The method of coupling preformed polymers to a membrane illustrates the advantage of being able to control the characteristics of the grafted polymer, such as molecular weight and polydispersity, prior to attachment to the membrane. Mir and coworkers end-grafted poly(styrene) chains onto silicon and then sulfonated the aromatic rings to produce a negatively charged, grafted electrolyte.[57] Poly(ethyleneglycol) chains have been grafted onto functionalized poly(styrene) latex particles[58] and poly(sulfone) surfaces.[59] Other reports of grafting preformed polymers to surfaces are abundant.[60-63] One major disadvantage of the technique of grafting of preformed polymers is the lack of control over the density of the grafting.

1.5.4 Graft Polymerization

Examples of graft polymerization of monomers within membranes are numerous.[64-67] Two typical methods can be employed - ionizing radiation or chemical grafting.

Graft copolymers can be formed by plasma irradiation using noble, diatomic, carbon dioxide, ammonia, or hydrocarbon gas, as well as electron beam irradiation of

porous polymer substrates, followed by contacting a monomer solution. They can also be formed by plasma irradiation of chemical species[68,69] (namely monomers) in the gas phase in the presence of the substrate.

One of the drawbacks of this method is the formation of homopolymer rather than graft copolymers. Suppression of homopolymer formation has been achieved by using metal catalysts.[55,56] Casolaro and coworkers grafted poly(acrylic acid) onto cellulose membranes using free-radical mechanisms initiated by Ce(IV) salts and an oxygen plasma.[70]

Another disadvantage is degradation of the membrane after formation. Typically, modification of the surface of a membrane by plasma or ionizing radiation damages the substrate and changes the morphology of the existing substrate, usually by creating larger pores and providing sites for degradation of the formed membrane over time.

Chemical grafting methods have been applied to eliminate the effect of directly damaging the substrate by ionizing radiation. For example, Imaizumi and coworkers have photo-grafted acrylic acid onto poly(ethylene) films using benzophenone as a radical initiator.[71] The polyethylene film does not absorb UV radiation at the wavelength for initiation of benzophenone, but benzophenone can generate radicals on polyethylene by hydrogen abstraction to provide grafting sites for co-polymerization.

Membranes containing poly(vinylpyridine) have been prepared by grafting techniques.[71-75] Mika and coworkers have reported the preparation of poly(4-vinylpyridine) grafted membranes.[37,76,77] These membranes were prepared by absorbing 4-vinylpyridine

and a photoinitiator, benzoin ethyl ether, into the pores of a poly(propylene) or poly(ethylene) membrane followed by UV-initiated polymerization, **Scheme 1.1**.

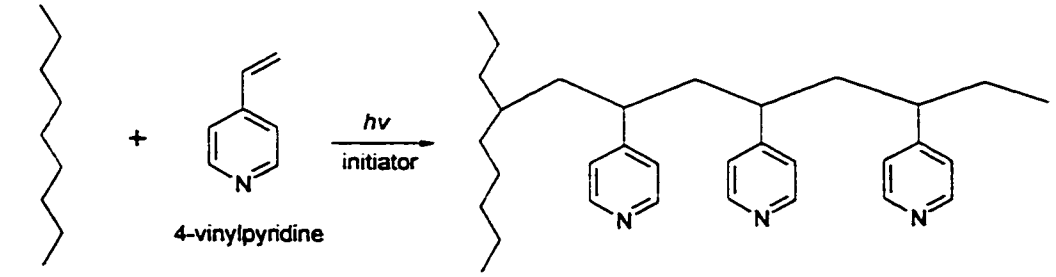

Scheme 1.1. Photo-grafting of 4-vinylpyridine onto a polyethylene membrane.

The Hoechst Celanese Corp. has fabricated pore filled membranes by radical polymerization of an acrylic acid monomer within an isotactic polypropylene.[78] The polypropylene substrates were wetted by a toluene solution containing acrylic acid and benzoyl peroxide and in some cases, a cross-linking agent. The wetted membranes were placed between glass plates or Teflon™ sheets to prevent evaporation and heated to affect graft polymerization.

1.5.5 Cross-linking of the Pore-Filling Polymer

In cases where there is concern about the presence of grafting (actual formation of a covalent bond between the substrate membrane and the incorporated material), and the

potential loss of the incorporated polymer, the addition of a cross-linking agent to the polymerization helps to improve the stability of the pore-filled membranes.

Mika and coworkers[79] have prepared poly(acrylic acid)-filled membranes using N,N'methylenebisacrylamide as a crosslinker for the *in-situ* polymerization. **Scheme 1.2** shows the formation of cross-linked poly(acrylic acid) resulting in a three-dimensional polymer gel.

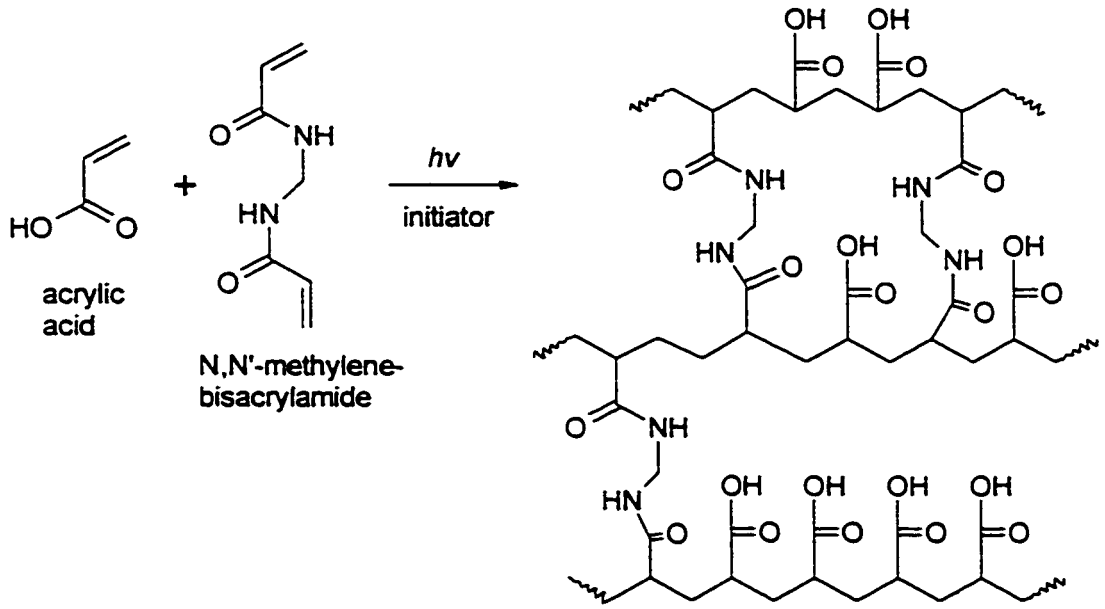

Scheme 1.2. Formation of Cross-linked Poly(acrylic acid)

A similar method was employed by Gabriel and Gillberg.[80] *In-situ* polymerization of acrylic acid monomer solutions (with cross-linker) were performed within the microporous structures of a polypropylene membrane, Celgard 2500. The hydrophilicity of these membranes was studied by the degree of wetting upon incorporation of poly(acrylic

acid). The membranes were not studied in terms of gel morphology on pressure driven performance.

When a cross-linking agent is used in the polymerization within a membrane, it is no longer necessary to rely on the formation of covalent bonds between the incorporated polymer and the porous substrate to anchor the gel within the membrane. Although grafting may still be occurring, the physical entanglement of the three dimensional, cross-linked polymer gel within the pores of the host substrate will assist in locking the pore-filling material in the membrane.

1.5.6 Cross-linking of Preformed Polymer

The necessity of grafting a polymer onto the host membrane in order to anchor the incorporated material can be completely avoided by cross-linking a preformed polymer within the pores of the substrate. A solution of preformed polymer and a cross-linking agent is absorbed into the membrane pores and the reaction of the crosslinker with the preformed polymer entangles and locks the polymer within the substrate. This technique has been used by Iijima and coworkers to incorporate poly(4-vinylpyridine) into poly(ethyleneterephthalate) films.[81;82]

This procedure has been also used by Mika to incorporate poly(4-vinylpyridine) into poly(ethylene) microporous membranes using dibromoalkanes as crosslinkers, as shown in **Scheme 1.3**.

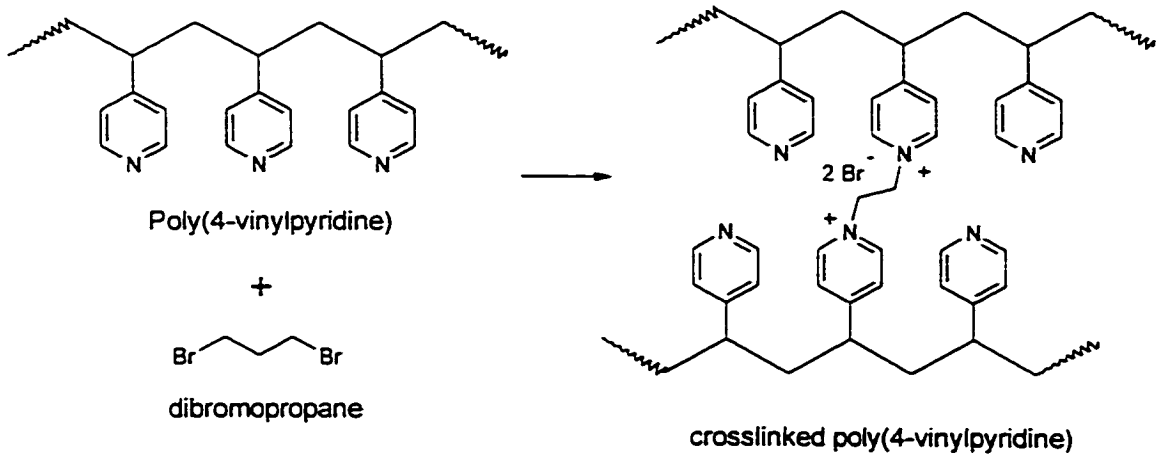

Scheme 1.3. Cross-linking of Poly(4-vinylpyridine) using Dibromopropane

Membranes produced by this technique yield stable anion exchange membranes upon alkylation of the pyridine sites without the need for covalent bonds (grafting) between the polyelectrolyte and the host membrane.

Another route to anion exchange membranes used by Childs and coworkers, shown in **Scheme 1.4**, is the reaction of poly(vinylbenzylchloride) with a crosslinker such as piperazine, within the pores of a poly(propylene) substrate[83].

Amination of the remaining benzylchloride groups yields a stable anion exchange membrane. One of the limitations of this technique is the amount of pore loading that can be achieved. A solvent must be used to insert the preformed polymer and crosslinker into the porous host, thus, the amount of material that can be introduced into the substrate is limited by the amount of polymer that can be dissolved in a given amount of solvent. By comparison, the *in situ* polymerization of monomers within the pores of the host does not require a solvent, hence a higher loading is possible.

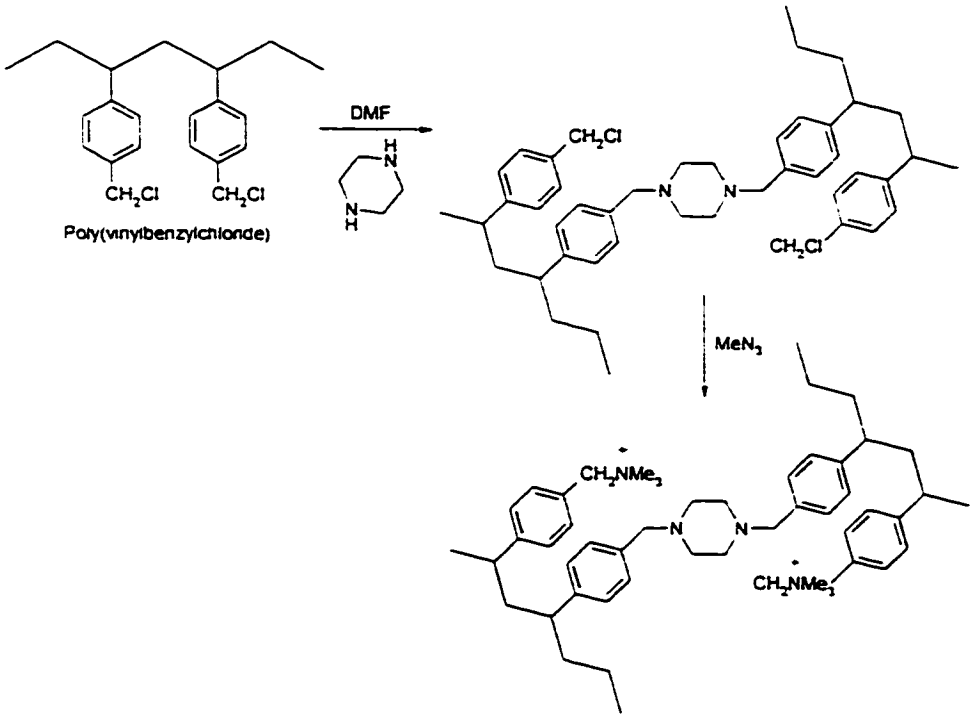

Scheme 1.4. Cross-linking of poly(vinylbenzylchloride) using piperazine

1.6 Properties of Pore-Filled Ion Exchange Membranes

1.6.1 The Host Substrate

As has been mentioned, the host membrane provides the majority of the mechanical strength of the final membrane. Thus, the host plays a role in determining the properties of the pore-filled membrane. If swelling of the membrane occurs, the water content will increase and this will affect the electrical resistance, permeability and selectivity of the membrane. Thus a host that has good tensile strength is desirable.

One of the critical factors regarding membrane use is the lifetime of the membrane under operating conditions. This calls into play the chemical and thermal stability of the host substrate. Having an incorporated polyelectrolyte with good stability is of no use if the support material is not stable.

1.6.2. Role of the Incorporated Polyelectrolyte

The choice of polyelectrolyte depends on the desired separation characteristics. For example, in acid recovery applications an anion exchange membrane is used since cations other than protons will be rejected. In this case a positively charged polyelectrolyte that is stable to an acidic environment is required. Conversely, for caustic recovery, a negatively charged polyelectrolyte that is stable to basic solutions is required. Water purification processes can use either anion or cation exchange membranes, the choice of which is determined based on the composition of the feed stream.

The area of pore-filled anion exchange membranes has been highly developed and a variety of symmetric anion exchange membranes involving poly(4-vinylpyridine) as the polyelectrolyte gel have been produced and studied. These pore-filled membranes have high ion-exchange capacities, up to 6 meq/g of dry membrane when the swelling of the pore-filled electrolyte is partially suppressed by cross-linking.[38] The water content in these membranes is very high (2-3 times higher than in commercial membranes) and can be controlled by cross linking. These polyolefin-based, pore-filled anion exchange membranes

have found many different applications. A few of these include acid recovery by diffusion dialysis[84] and ultra-low pressure (100 kPa) driven nanofiltration of salts.[85]

The area of cation exchange membranes based on the pore-filling concept has not been extensively studied and therefore warrants further investigation. Jiang[86] has fabricated pore filled membranes by sulfonation of polystyrene within a porous substrate. The membranes performance in terms of RO were very good; however the fluxes were very low mainly due to the fact that the degree of cross-linking was difficult to control during the sulfonation step.

Cation exchange membranes have also been prepared using poly(acrylic acid) as the polyelectrolyte fill. One technique used plasma activation of the membrane surface, followed by thermal initiation and polymerization of acrylic acid monomer. This technique was not found to be reproducible.[87]

The most successful attempts at formation of pore-filled cation exchange membranes were prepared by photo-initiated *in-situ* polymerization of acrylic acid with a cross linking agent.[79;88] To expand the area of cation exchange membranes and further understand the relationship between polyelectrolyte fill and performance, poly(acrylic acid) was chosen as the polyelectrolyte for the work in this thesis. The proven photo-polymerization system was chosen as the fabrication method.

1.7 Properties of the Gel Fill

The morphology of a gel produced by polymerization can vary depending on the process conditions used. Solution polymerization by radical initiation has been well studied,[89-96] and **Figure 1.5** shows schematically how the polymer structure can change with the degree of dilution, change in solvent quality and the content of the crosslinker in the polymerization mixture. In the following discussion radical cross-linking co-polymerization of mono and bis-unsaturated monomers is considered. If an inert good solvent is used in solution polymerization, the gel thus obtained will have a supercoiled (expanded) structure (**Gel B**). **Gel B** swells in good solvents much more than **Gel A** which is synthesized in bulk. If the amount of cross-linking divinyl monomer in the reaction mixture is increased while the amount of solvent remains constant, highly crosslinked networks are formed that cannot absorb all solvent molecules present in the reaction mixture and a heterogeneous structure is formed (**Gel C**). The same result occurs when the solvent quality is reduced. A part of the solvent separates from the gel phase during polymerization and the formed **Gel C** consists of two continuous phases, a gel and a solvent phase. In either case, if the amount of solvent is further increased, a critical point is passed at which the system becomes discontinuous because the amount of the monomer is not sufficient and the growing chains cannot occupy the whole available volume. Consequently, a dispersion of macrogel particles in the solvent results (**Gel D**). Increasing

the amount of solvent decreases the size of the gel particles. These gel particles are microgels, which are dissolved as a colloidal solution (**Gel E**).

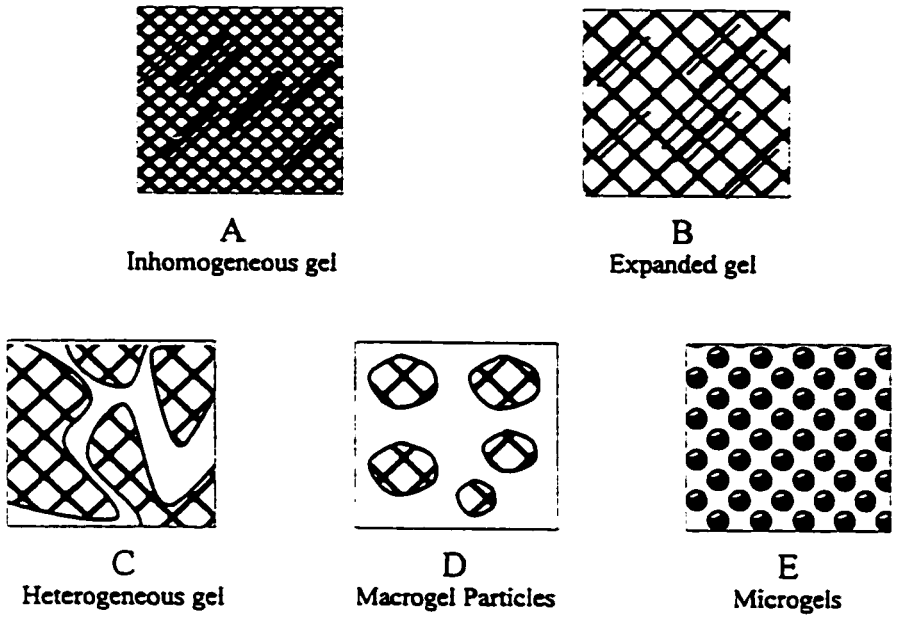

Figure 1.5: Various morphologies of gels produced by solution polymerization.

Osada and co-workers[97-99] have further shown that even the nature of the constricting walls has an effect on morphology. Gelation of 2-amino-2-methylpropanesulfonic acid (AMPS) sandwiched between two sheets, one hydrophobic (Teflon™) and one hydrophillic (glass), was shown to produce different morphology of gel at each interface.

1.8 Asymmetric Pore-Filled Membranes

As previously mentioned, the pore-filled membranes of Mika[79:85] show excellent performance in terms of nanofiltration versus commercial thin-film composite membranes. An approach for improvement of these types of membranes may be to create asymmetric membranes with a gel fill. It is well known that a thinner active layer contributes to effective separation while increasing membrane flux. A thinner layer usually holds with it the consequence of fragility, however, when formed as a composite with a rigid microporous host the integrity of the gel can be maintained while still conveying the properties of the imbedded polyelectrolyte. Stachera[100] and Ge[101] each have previously applied the pore-filling concept to the formation of asymmetric pore-filled membranes. Stachera diffused alkyl ammonium groups through one side of a symmetrically pore-filled poly(4-vinylpyridine) membrane, thereby creating a permanent gradient positive charge across the membrane. Ge used photo-initiated polymerization of 4-vinylpyridine and included a photo-blocker in the monomer solution to limit the penetration of photon depth into the membrane, thereby limiting polymerization to the surface exposed to the UV radiation source. The main drawback in the formation of these membranes was in the characterization of the degree of asymmetry. Environmental scanning electron microscopy coupled with energy dispersive x-ray analysis was used in both cases, but the resolution and reproducibility of the membranes were poor. Also, the start and finish of the edge of the membrane were difficult to determine. To the author's knowledge, there are no reports

of asymmetric pore-filled membranes formed by the photochemical polymerization route with a photoblocker.

1.9 Statements of Problem

It is clear that the process conditions used in the formation of gels can have a profound effect on the gel morphology. This in turn would affect the separating structure in a pore-filled membrane. This raises some basic fundamental questions concerning the concept of the McMaster pore-filled membranes. Namely, what effects do the process parameters have on gel morphology and distribution? What effects do the different gel morphologies or distributions have on membrane separation and performance?

1.10. Objectives

Three main objectives are designed to address the key questions involved:

1. To fabricate poly(acrylic acid) membranes and study the effects of monomer loading, reaction solvent and cross-linking on the morphology of gels formed within a host substrate;
2. To determine the effect of gel morphology on the performance of the pore-filled poly(acrylic acid) membranes in terms of hydrodynamic permeability and nanofiltration;

3. To fabricate and characterize asymmetric pore-filled poly(acrylic acid) membranes and evaluate them with respect to their symmetric counterparts.

Reference List

(1) Baker, R. W. *Membrane Technology and Applications*; McGraw-Hill: New York, 2000.

(2) Mulder, M. *Basic Principles of Membrane Technology*; Kluwer Academic Publishers: 1997.

(3) Spiegler, K. S.; Kedem, O. *Desalination* **1966**, *1*, 311-326.

(4) Reid, C. E.; Breton, E. J. *J.App.Polym.Sci.* **1959**, *1*, 133.

(5) Mika, A. M. and Childs, R. F. RO and NF membranes: The role of chemistry and morphology in membrane transport. 2001. A conference of the European Membrane Society. 9-9-2001.

(6) Loeb, S.; Sourirajan, S. *Adv.Chem.Sev.* **1962**, *38*, 117.

(7) Black, L. E. Interfacially polymerized membranes for the reverse osmosis separation of organic solvent solutions. (US5173191). 22-12-1992.

(8) Hodgdon, R. B. Polyamine-polyamide composite nanofiltration membranes for water softening. (US5152901). 6-10-1992.

(9) Koo, J.-Y. and Yoon, Y. S. Composite polyamide reverse osmosis membrane and method of producing same. (US6063278). 16-5-2000.

(10) Kumar, A. and Musale, D. Composite solvent resistant nanofiltration membranes. (US6113794). 5-9-2000.

(11) Tomaschke, J. E. Interfacially synthesized reverse osmosis membranes and processes for preparing the same. (US5246587). 21-9-1993.

(12) Tomaschke, J. E. and Ary, I. E. Interfacially synthesized reverse osmosis membranes and processesfor preparing same. (US5254261). 19-10-1993.

(13) Tomaschke, J. E. Amine monomers and their use in preparing interfacially synthesized membranes for reverse osmosis and nanofiltration. (US5922203). 13-7-1999.

(14) Cadotte, J. E. Evolution of composite reverse osmosis membranes; In *Material Science of Synthetic Membranes*; Lloyd, D. R., ed. American Chemical Society: Washington, 1985; p 273.

(15) Peterson, R. J.; Cadotte, J. E. Thin film composite reverse osmosis membranes; In *Handbook of Industrial Membrane Technology*; Porter, M. E., ed. Noyes Publications: Park Ridge, 1990; p 307.

(16) Kwak, S.-Y.; Jung, S. G.; Yoon, Y. S.; Ihm, D. W. *J.Polym.Sci.B., Polym.Phys.* **1999**, *37*, 1429.

(17) Kwak, S.-Y. *Polymer* 1999, *40*, 6361.

(18) Hirose, M.; Ito, H.; Kamiyama, Y. *J.Membrane Sci.* **1996**, *121*, 3671.

(19) Hirose, M.; Minamizaki, H.; Kamiyama, Y. *J.Membrane Sci.* **1997**, *123*, 151.

(20) Lonsdale, H.; Merten, U.; Riley, R. *J.App.Polym.Sci.* **1965**, *9*, 1341.

(21) Sherwood, T.; Brian, P.; Fisher, R. *Ind.Eng.Chem.Fundam.* **1967**, *6* , 2.

(22) Sourirajan, S. *Reverse Osmosis*; Academic Press: New York, 1970.

(23) Matsuura, T.; Sourirajan, S. *Ind.Eng.Chem.Process Des.Dev.* **1981**, *20*, 273.

(24) Mehdizadeh, H.; Dickson, J. *Ind.Eng.Chem.Res.* **1989**, *28*, 814.

(25) Katchalsky, A.; Kedem, O. *Trans.Faraday Soc.* **1963**, *59*, 1918.

(26) Davis, T. A.; Genders, J. D.; Pletcher, D. *Ion Permeable Membranes*; The Electrochemical Consultancy: Hant, 1997.

(27) Helfferich, F. *Ion Exchange*; McGraw-Hill Book Co. Inc.: Toronto, 1962.

(28) Battacharyya, D.; Cheng, C. *Separation of metal chelates by charged composite membranes*; CRC Press: Boca Raton, 1986; p 707.

(29) Lakshminarayanaiah, N.; *Transport Phenomena in Membranes*; Academic Press: New York, 1969.

(30) Dresner, L. *Desalination* **1972**, *10*, 27.

(31) Bowen, W. R.; Mukhtar, H. *J.Membrane Sci.* **1996**, *112*, 263-274.

(32) Bowen, W. R.; Mohammad, A. W.; Hilal, N. *J.Membrane Sci.* **1997**, *126*, 91-105.

(33) Tsuru, T.; Nakao, S.; Kimura, S. *J.Chem.Eng.Jpn* **1990**, *23*, 604-610.

(34) Tsuru, T.; Nakao, S.; Kimura, S. *J.Chem.Eng.Jpn* **1991**, *24*, 511-517.

(35) Tsuru, T.; Urairi, M.; Nakao, S.; Kimura, S. *J.Chem.Eng.Jpn* **1991**, *24*, 518-524.

(36) Wang, X.-L.; Tsuru, T.; Nakao, S.; Kimura, S. *J.Membrane Sci* **1995**, *103*, 117-133.

(37) Mika, A. M.; Childs, R. F.; Dickson, J. M.; McCarry, B. E.; Gagnon, D. R. *J.Membrane.Sci.* **1995**, *108*, 37-56.

(38) Mika, A. M.; Childs, R. F.; Dickson, J. M.; McCarry, B. E.; Gagnon, D. R. *J.Membrane .Sci.* **1997**, *135*, 81-92.

(39) Mika, A. M.; Childs, R. F.; Dickson, J. M. *J.Membrane Sci* **1999**, *153*, 45.

(40) Weiss, N.; van Vliet, T.; Silderberg, A. *J.Polym.Sci., Polym.Phys.Ed.* **1979**, *17*, 2229-2240.

(41) Imato, T.; Yabu, H.; Morooka, S. *J.Membrane Sci.* **1982**, *10*, 21-33.

(42) Kim, J. T.; Anderson, J. L. *Ind.Eng.Chem.Res.* **1991**, *30*, 1008-1016.

(43) Fibiger, R. F., Colucci, M. J., Forgach, D. J., Wessling, R. A., and Schmidt, D. L. Rejection enhancing coatings for reverse osmosis membranes. (US4909943). 20-3-1990.

(44) Fibiger, R. F., Colucci, M. J., Forgach, D. J., Wessling, R. A., and Schmidt, D. L. Rejection enhancing coatings for reverse osmosis membranes. (US4894165). 16-1-1990.

(45) Chan, C. M. *Polymer surface modification and characterization*; Hanser Publ.: New York, 1994.

(46) Dytnerskii, Y. I.; Dmitriev, A. A.; Mchedlishvili, B. V.; Potokin, I. L. *Russ. Coll.* **1983**, 1024-1028.

(47) Garbassi, F.; Morra, M.; Occhiello, E. *Polymer Surfaces*; John Wiley & Sons: New York, 1994.

(48) Hoffman, A. S. *Macromol.Symp.* **1996**, *101*, 443-454.

(49) Mattson, B.; Stenberg, B. *J.App.Polym.Sci.* **1993**, *50*, 1247-1259.

(50) Ogiwara, Y.; Torikoshi, K.; Kubota, H. *J.Poly.Sci.Poly.Lett.* **1982**, *20*, 17-21.

(51) Osada, Y.; Iriyama, Y. *Thin Film Solids* **1984**, *118*, 197-202.

(52) Poncin-Epaillard, F.; Chevet, B.; Brosse, J. C. *J.App.Polym.Sci.* **1994**, *53*, 1291-1306.

(53) Uyama, Y.; Kato, K.; Ikada, Y. *Adv.Polym.Sci.* **1998**, *137*, 1-39.

(54) Xu, G.; Lin, S. *J.M.S.-Rev.Macromol.Chem.Phys.* **1994**, *C34*, 555-606.

(55) Yamaguchi, T.; Nakao, S.; Kimura, S. *Macromol.* **1991**, *24*, 5522-5527.

(56) Yamaguchi, T.; Yamahara, S.; Nakao, S.; Kimura, S. *J.Membrane.Sci.* **1994**, *95*, 39-49.

(57) Mir, Y.; Auroy, P.; Avray, L. *Phys.Rev.Letters* **1995**, *75*, 2863-2866.

(58) Jayachandran, K. N.; Chatterji, P. R. *J.M.S.-Pure Appl.Chem.* **1998**, *A35*, 1971-1986.

(59) Thom, V.; Jankova, K.; Ulbricht, M. *Macromol.Chem.Phys.* **1998**, *199*, 2723-2729.

(60) Chen, G.; Ito, Y.; Imanishi, Y. *Macromolecules* **1997**, *30*, 7001-7003.

(61) Friej-Larsson, C.; Wesslen, B. *J.App.Polym.Sci.* **1993**, *50*, 345-352.

(62) Matsuda, T.; Sugawara, T. *Langmuir* **1995**, *11*, 2272-2276.

(63) Matsuda, T.; Sugawara, T. *Langmuir* **1995**, *11*, 2267-2271.

(64) Inagaki, N.; Kobayashi, N.; Matsushima, M. *J.Membrane Sci.* **1988**, *38*, 85-96.

(65) Kawakami, M.; Yamashita, Y.; Iwamoto, M.; Kagawa, S. *J.Membrane Sci.* **1984**, *19*, 249-259.

(66) Kita, H.; Sakamoto, T.; Tanaka, K.; Okomoto, K.-I. *Polymer Bulletin* **1988**, *20*, 349-354.

(67) Stancell, A. F.; Spencer, A. T. *J.App.Polym.Sci.* **1972**, *16*, 1505.

(68) Abeles, B. Plasma polymer membrane. (US5207909). 4-4-1993.

(69) Zhang, H., Anazawa, T., and Sakai, K. Asymmetric polymer membrane and preparation thereof. (US5236588). 17-8-1993.

(70) Casolaro, M.; Barbucci, R. *Colloids and Surfaces* **1993**, *77*, 81-89.

(71) Imaizumi, M.; Kubota, H.; Hata, Y. *Eur.Polym.J.* **1994**, *30*, 979-983.

(72) Dessouki, A. M.; Hegazy, E. A.; El-Dessouky, M. M. *Radiat.Phys.Chem.* **1985**, *26*, 157-163.

(73) El-Dessouky, M. M.; Hegazy, E. A.; Dessouki, A. M. *Radiat.Phys.Chem.* **1986**, *27*, 443-446.

(74) Hegazy, E. A.; Dessouki, A. M.; El-Dessouky, M. M. *Radiat.Phys.Chem.* **1985**, *26*, 143-149.

(75) Hegazy, E. A.; Dessouki, A. M. *Radiat.Phys.Chem.* **1986**, *28*, 273-279.

(76) Mika, A. M.; Childs, R. F.; West, M.; Lott, J. N. A. *J.Membrane.Sci.* **1997**, *136*, 221-232.

(77) Mika, A. M.; Childs, R. F. *J.Membrane Sci* **1999**, *152*, 129.

(78) Gillberg-LaForce, G. E. and Gabriel, E. M. Modified microporous structures. (US5049275). 17-9-1991.

(79) Childs, R. F.; Mika, A. M.; Pandey, A. K.; McCrory, C. T. C.; Mouton, S.; Dickson, J. M. *Sep.Purif.Technol.* **1999**, *22-23*, 507-517.

(80) Gabriel, E. M.; Gillberg, G. E. *J.App.Polym.Sci.* **1993**, *48*, 2081-2090.

(81) Makino, Y.; Hamada, K.; Iijima, T. *Polymer Journal* **1987**, *19*, 737-745.

(82) Nakanishi, T.; Usuda, Y.; Tak, T. *Polymer Commun.* **1985**, *26*, 300-303.

(83) Pandey, A. K.; Childs, R. F.; West, M.; Lott, J. N. A.; McCarry, B. E.; Dickson, J. *J.Polym.Sci.A.,Polym.Chem* **2001**, *39*, 807-820.

(84) Stachera, D. M.; Childs, R. F.; Mika, A. M.; Dickson, J. M. *J.Membrane.Sci.* **1998**, *148*, 119-127.

(85) Mika, A. M.; Childs, R. F.; Dickson, J. M. *Desalination* **1999**, *121*, 149-158.

(86) Jiang, W. Ph.D. Thesis: Preparation and Characterization of Pore-Filled Cation-Exchange Membranes. 1999. McMaster University.

(87) Chris McCrory. Formation of pore-filled poly(acrylic acid) membranes by plasma activation. 1998.

(88) Winnik, F. M.; Morneau, A.; Mika, A. M.; Childs, R. F.; Roig, A.; Molins, E.; Ziolo, R. F. *Can.J.Chem.* **1998**, *76*, 10-17.

(89) Dusek, K. Inhomogeneities Induced by Crosslinking in the Course of Crosslinking Copolymerization; In *Polymer Networks: Structure and Mechanical Properties*; Chompff, A. J., Newman, S., eds. Plenum Press: New York-London, 1971; pp 245-260.

(90) Horak, D.; Pelzbauer, Z.; Bleha, M.; Ilavsky, M.; Svec, F.; Kalal, J. *J.Appl.Polym.Sci* **1981**, *26*, 411-421.

(91) Kapur, V.; Charkoudian, J.; Anderson, J. L. *J.Membrane Sci* **1997**, *131*, 143.

(92) Lai, Y.-C.; Quinn, E. T. Photopolymeriztion: Fundamentals and Applications. ACS Symmposium Series 673; In *Photopolymeriztion: Fundamentals and Applications*; Scranton, A. B., Bowman, C. N., Peiffer, R. W., eds. American Chemical Society: Washington, 1997; pp 35-50.

(93) Righetti, P. G.; Caglio, S.; Sarachi, M.; Quaroni, S. *Electrophoresis* **1992**, *13*, 587-595.

(94) Righetti, P. G.; Gelfi, C. *Journal of Chromatography B* **1996**, *699* , 63-75.

(95) Svec, F.; Frechet, J. M. J. *Chem.Mater.* **1995**, *7*, 707-715.

(96) Svec, F.; Frechet, J. M. J. *Macromolecules* **1995**, *28*, 7580-7582.

(97) Gong, J. P.; Kii, A.; Xu, J.; Hattori, Y.; Osada, Y. *J.Phys.Chem.B* **2001**, *105*, 4572-4576.

(98) Kii, A.; Xu, J.; Gong, J. P.; Osada, Y.; Zhang, X. *J.Phys.Chem.B* **2001**, *105*, 4565-4571.

(99) Osada, Y.; Gong, J. P. Surface dynamic properties of polymer gels; American Chemical Society: Washington, 2000.

(100) Stachera, D. Ph.D. Thesis: Poly(4-vinylpyridine) membranes. 2000. McMaster University.

(101) Ge, J. and Childs, R. F. Unpublished work on asymmetric membranes. 2001.

Chapter 2

Formation and Characterization of Poly(acrylic acid-co-N,N'-methylenebisacrylamide) Pore-Filled Membranes

2.1 Introduction

Polymeric membranes have been developed for a variety of industrial applications, examples of which include microfiltration, ultrafiltration, nanofiltration, reverse osmosis and gas separation. Each application imposes specific requirements on the membrane material and membrane structure. For example, the solute permeability and solvent permeability determine the separation and flux of nanofiltration membranes.[1]

There are several ways to prepare porous polymeric membranes.[1-6] The final morphology of the separating structure will vary greatly depending on the properties of both the materials and the process conditions. A variety of porous structures, sizes and porosities can be constructed by manipulating the polymerization or gelation of the membrane. The performance of these membranes strongly depends on both the polymer distribution and morphology formed during synthesis.

Where the membrane relies on a gel as the separating medium, the performance of the membrane is determined by the characteristics of the gel. Gels produced by free radical polymerization can have very different morphologies depending on the

polymerization conditions used. Such change in morphology due to heterogeneity in non-ionic gels and gel-fills have been documented.[7-10] Osada and co-workers[11-13] have shown that even the nature of the interface with the monomer solution has an effect on morphology. Gelation of 2-acrylamido-2-methylpropanesulfonic acid (AMPS) sandwiched between two sheets, one hydrophobic (Teflon™) and one hydrophillic (glass) produces a non-uniform interference pattern throughout the gel. The interference pattern obtained close to each surface was completely different. Dusek and co-workers have shown that change of solvent or cross-linking create inhomogeneities within gels.[14,15] Lai and co-workers[16] have shown that the rate of polymerization, altered by changing photoinitiator or changing solvent, had a great impact on the mechanical properties of HEMA gels. Matsusaki,[17] Bansil,[18] and Hecht[19] have independently studied inhomogeneity in acrylamide gels by light scattering and found transitions from clear to opaque gels by increasing cross-link density or changing temperature. The work by Fréchet and/or Svec has led to the well defined and controlled morphology of polymer networks as porous beads[20-29] and monoliths,[30-32] both of which provide excellent chromatographic resolution, and further to the development of polymer sheets for use in high performance membrane chromatography.[33] Their work suggests that formation of polymer membranes of a wide variety of pore-sizes and morphologies can be achieved by free radical polymerization.

Recently, a new class of ion exchange membrane has been developed.[34] The membranes are based on the concept of taking a commercially available polyolefin

microporous membrane and filling the pores with a flexible ionic polymer. The area of pore-filled anion exchange membranes has been highly developed and a variety of membranes involving poly(4-vinylpyridinium salts) as the polyelectrolyte gel have been produced and studied.[35,36] These ion exchange membranes have found many different applications, including acid recovery by diffusion dialysis[37] and ultra-low pressure (100 kPa) driven nanofiltration.[38,39]

Cation exchange membranes are typically prepared by polymerization of monomers, in-situ cross-linking of preformed polymers or by chemical modification of substrates.[40-42] At the outset of this work, there were few examples of pore-filled cation exchange membranes. Moreover, the effects of the process conditions on the morphology of the incorporated gel in both cation and anion exchange membranes had not been examined. In this work, we prepare pore-filled poly(acrylic acid-co-N,N'-methylenebisacrylamide) cation exchange membranes and examine the effects of polymerization chemistry on the morphology of the polyelectrolyte gel formed within a porous host. Specifically, examination of monomer concentration, reaction solvent and cross-linking ratio on poly(acrylic acid) gels and gel-filled membranes were investigated.

2.2 Experimental

2.2.1 Materials

The porous substrate used in this study was a poly(propylene) microfiltration membrane (3M Company) produced by a thermally induced phase separation process. The polypropylene substrate had a bubble point pore diameter of 0.82 μm and a porosity of 80.5 vol-%, with an average thickness of 75 μm. The following chemicals were purchased and used without further purification: acrylic acid (Avocado Chemicals); *N,N*-methylenebisacrylamide (Aldrich); *N,N*-dimethylformamide; 1,4-dioxane (Caledon); 2,2-dimethoxy-2-phenylacetophenone (Aldrich).

2.2.2 Gel and Membrane Preparation

The preparation of pore-filled poly(acrylic acid) (PAA) membranes is similar to a procedure described elsewhere.[39] A sample of poly(propylene) substrate was soaked for a few minutes in a monomer solution containing acrylic acid, N,N'-methylenebisacrylamide (BIS) and 2,2-dimethoxy-2-phenylacetophenone (DMPA). The substrate sample was removed from the solution, sandwiched between two polyethylene or poly(ethylene terephthalate) films and placed on a glass plate. The excess solution and any air bubbles were squeezed out by application of a Teflon™ roll bar, and the substrate

was sealed between the sheets by taping them to a glass plate.

The remaining monomer solution, approximately 2ml, was charged into a cylindrical vial. The solution was not purged of oxygen. The vial was then capped and placed on the same glass plate as the membrane.

The sandwich and vial were irradiated at 350 nm in a UV system containing four parallel lamps (Southern N.E. Ultraviolet Co.) at a distance of 12 cm from the irradiated surface and a cooling fan. The irradiation was carried out for 60 min at room temperature. After polymerization, the membrane was thoroughly washed and placed in a water bath at 50 °C. The water was replaced each day with deionized water until the conductivity of the wash was below 1 μS. This typically took 3 days.

The prepared gels were removed from the vials and placed in a water bath at room temperature. The water was replaced every day until the conductivity of the wash was below 1 μS. This typically took 2 weeks.

2.2.3. Confocal Microscopy

For confocal microscopic analyses, thin slices of bulk gels samples were soaked in an aqueous solution of ethidium bromide dye (10^{-5} M, λ_{exc} = 510 nm, λ_{emmis} = 595nm) overnight (~16 h) at room temperature. The exterior of the samples were then washed with water and placed in deionized water for 24 hours. Wet samples were removed, cut thinly with a razor and placed on microscope slides with a cover slip. The samples were

viewed in a Carl Zeiss laser fluorescence confocal microscope (LSM 510, Carl Zeiss Corp., Germany). An argon laser of 488 nm was used to excite the fluorophore in the gel sample.

2.2.4. Characterization of Membranes

The pore-filled membranes were characterized by the concentration (mass gain or volume fraction) of the polyelectrolyte in the pores, ion-exchange capacity, water content, and volume. The mass of the incorporated gel was determined from the difference between the dry mass of a pore-filled membrane sample (dried in vacuum at room temperature to a constant mass) and that of the substrate. The gel concentration (volume fraction), ϕ, was calculated using

$$\phi = \frac{(m_{m,dry} - m_s)\upsilon_2}{V_s \varepsilon} \tag{2.1}$$

where $m_{m,dry}$ is the mass of a pore-filled sample (in a dry state), m_s is the mass of the substrate in the sample, υ_2 is the partial specific volume of the gel polymer, 0.73 cm^3/g for poly(acrylic acid),[43] V_s, is the substrate volume in the sample, and ε is the substrate porosity.

In case of any change in the volume of the pore-filled sample compared to the original volume of the substrate sample, the eq. (2.1) was modified to

$$\phi = \frac{(m_{m,dry} - m_s)\upsilon_2}{V_m - \frac{m_s}{d_{PP}}} \tag{2.2}$$

where V_m is the volume of the swollen sample and d_{PP} is the density of poly(propylene) (0.91 g/cm^3).

The ion-exchange capacity, X, of the membranes was calculated from the equivalent number of the fixed charges in a membrane sample, n_x, divided by the total mass of the dried polymerized membrane, according to

$$X = \frac{n_x}{m_{m,dry}} \tag{2.3}$$

The volume fraction of water in the membrane, ϕ_w, was calculated from the mass of water in the swollen sample, according to the following equation and assuming water density, d_w, equal to 1 g/cm^3:

$$\phi_w = \frac{m_{m,wet} - m_{m,dry}}{V_m d_w} \tag{2.4}$$

Membrane samples were cut as squares approximately 10 cm x 10 cm. The volume of the membrane samples were obtained by measuring the x-y dimensions with a ruler and thickness with a digital micrometer (Orion). Measurements of the x-y and thickness were taken at several random places on the membrane and averaged. Membranes were first immersed in deionized water for approximately 3 days until the pH

was equilibrated to 5.5 and the dimensions were determined. The membranes were converted to their sodium salt form by adding aliquots of 0.1 N NaOH to a beaker containing the membranes until the solution pH was 10.6. The beaker was sealed and left for two hours. Again, membranes were removed and dimensions measured.

$$V = \frac{V_{m,wet} - V_n}{V_n} \text{x}100\% \qquad (2.5)$$

2.3. Results and Discussion

Poly(acrylic acid) gels and membranes were synthesized by photo-initiated, free-radical co-polymerization of acrylic acid and N,N'-methylenebisacrylamide under a variety of process conditions. In order to reduce evaporation of the applied monomer solution, two solvents with boiling points greater than 100 °C were chosen, one as a good solvent for poly(acrylic acid), the other as a poor solvent for poly(acrylic acid). N,N'-dimethylformamide (DMF) and 1,4-dioxane (Diox) were chosen as they have boiling points of 152.8 and 101.3 °C,[44] respectively. They are also mutually miscible, and they dissolve acrylic acid, BIS and DMPA.

In order to determine the effect of polymerization chemistry on the morphology of poly(acrylic acid) pore-filled membranes, three series of gels and gel filled membranes were examined. In the first series, the monomer concentration in either DMF or 1,4-

dioxane was varied between 1.110 and 2.775 M, while keeping cross linking ratio (BIS) fixed at 5 mole percent relative to acrylic acid. In the second series, the total monomer concentration and cross linking ratio (BIS) was kept constant (2.775 M, 5 mol % XL) while different solvent mixtures ranging from 100% DMF to 100% 1,4-dioxane were used. Finally, in the third series, the total monomer concentration was fixed (2.775 M) and the degree of cross linking ratio was varied between 5 and 25 mole percent relative to acrylic acid.

2.3.1 Effect of monomer loading

The mass gain, water uptake and ion-exchange capacities (IEC) of membranes obtained with concentrations of the acrylic acid (AA) solution from 1.110 to 2.775 M, with 5 mol% XL, are shown in **Table 2.1.** The increase in monomer loading has similar effects on mass gain, IEC and water uptake, as membranes previously observed.[35,36,45]

With an increase in monomer loading there is a corresponding linear increase in mass gain within the membranes, in both DMF and 1,4-dioxane. Below 1.110 M, no mass gain was observed in the polymerization carried out in DMF. A mass gain of approximately 20% was observed at this concentration for membranes formed in 1,4-dioxane as reaction solvent.

The water uptake as a function of gel polymer volume fraction of membranes formed in either DMF or 1,4-dioxane is shown in **Figure 2.1.** With an increase in gel

volume of poly(acrylic acid) there is a decrease in water uptake within the membranes. At the same polymer volume fraction, membranes formed from DMF or 1,4-dioxane have the same water uptake, indicating that the water uptake depends only on the polymer volume fraction of poly(acrylic acid) and not on the reaction solvent used.

The IEC's for membranes formed in either DMF and 1,4-dioxane reaction solvents are shown in **Figure 2.2**. As the mass gain increases, the ion exchange capacity increases. The non-linear relationship of IEC with MG has been observed previously in our laboratory.[36,45] As observed in **Figure 2.2**, the IEC is the same for a given gel polymer volume fraction. This implies that the ion exchange sites are still equally accessible to deprotonation irrespective of the reaction solvent used for polymerization.

2.3.2 Effect of Reaction Solvent

The nature of the bulk gels formed in the different reaction solvents is illustrated in **Figure 2.3**. Monomer solutions polymerized in DMF as the reaction solvent produced clear space filling gels in the concentration range studied. Polymerization of monomer solutions with 1,4-dioxane as reaction solvent produced white, opaque gels. The figure shows that by increasing the volume percent of 1,4-dioxane in the DMF mixture at constant monomer concentration and cross-linking ratio, a transition occurs between 50 vol% and 75 vol% 1,4-dioxane whereby the gel becomes an opaque space-filling gel. Immersion of the bulk gels in deionized water showed no change in the nature of light

scattering over several months.

Images obtained by confocal laser scanning microscopy (CLSM) of bulk gels stained with ethidium bromide are shown in **Figure 2.4**. For gels synthesized in DMF, there is no observable microstructure with increase in monomer concentration and they appear clear. An image of a bulk gel with a monomer concentration of 2.775 M formed in DMF is shown in **Figure 2.4A**. The dark region is the edge of the gel, and was used as a reference for focusing. The gel is uniform, showing no surface roughness. However, a spherical morphology is revealed with bulk gels formed from 1,4-dioxane. With increase of monomer loading from 1.110 to 2.775 g/cm3 (**Figures 2.4 B - F**) there is an increase in the size of the spheres from approximately 0.2 to 10 μm, respectively.

Phase separation is the main reason for the formation of such inhomogeneities and it can be caused by the degree of XL[15,46] or by changes in polymer-solvent interactions.[14,26,47,48] During cross-linking polymerization of the vinyl-divinyl type, both effects are usually operative because the monomers act as a special kind of diluent and conversion of monomers into the polymer causes not only an increase in the cross-link density, but also a change of the composition of the polymerizing system. The fact that the translucence/opacity of the bulk gels do not visibly change upon swelling in water indicates that any large scale heterogeneities responsible for scattering light are now a permanent part of the structure of the gel filled membrane.

The globular structure observed by confocal microscopy for the poly(acrylic acid) bulk gels and membranes has been observed previously in heterogeneous gels.[45,46] It is

believed to be caused by the non solvating diluent, in this case 1,4-dioxane. The gel contains large agglomerates of microspheres which look like cauliflowers and each microsphere may also be an agglomerate of even smaller microgel or oligomeric nuclei.[47]

As can be seen in **Table 2.2**, the membrane mass gain is different depending on the reaction solvent used, even though the monomer concentration was the same. There is a difference in mass gain of almost 30% by changing reaction solvent from good (DMF) to poor (1,4-dioxane). An explanation for this observation could be the effect of diluents on the structure of the gel. In good solvents, the PAA microgel contains a larger, less dense extended network and allows escape of linear and branched PAA from the interstitial spaces of the membrane upon washing. The larger, more dense globular like structures formed in the 1,4-dioxane membranes are more likely to be "stuck" within some of the smaller membrane interstices.

2.3.3 Effect of Cross-linking

Pictures of bulk gels formed with increase in degree of cross-linking are shown in **Figure 2.5**. Clear space filling gels are observed between 5 and 15% cross-linking. The gels became increasingly opalescent at cross-linking ratios of 20 and 25%. As with bulk gels formed by different solvent, the immersion of these bulk gels in deionized water did not show any change in light scattering over several months.

The increase in cross-linking appears to create heterogeneous structures within the

gel, similar to the bulk gels synthesized in different reaction solvents. Again, phase separation is the main reason for the formation of such inhomogeneities[15,46] The light scattering from the bulk gels increases with increased cross-linking which implies that the light scattering structures are becoming larger. The creation of a microstructure within the gel network with increase of cross-linking ratio has been well documented by others in the formation of hydrogels.[7,9,10,15,35,49] The opalescent behaviour has been observed previously[16] and it has been suggested to arise from an aggregation of polymer and formation of heterogeneous structures. The heterogeneous structure of the highly cross-linked gels could not be observed by confocal microscopy in this work.

The effect of degree of cross-linking on mass gain, water uptake and IEC on membranes is shown in **Table 2.3**. Mass gain increases with increase in cross-linking even though the total monomer concentration was the same for this series of membranes. This is due to the fact that the BIS monomer has a molecular weight of 256 g/mol as opposed to acrylic acid with a molecular weight of 72.06 g/mol. With a constant monomer concentration, both the water uptake and IEC of the membranes decrease with an increase in cross-linking. Similar effects of the degree of cross-linking on water uptake have been reported,[17,50] and are suggested to be caused by restriction in swelling by the increase in cross-linking. The IEC decreases linearly with increase in XL ratio as the ionizable acrylic acid moieties are replaced by neutral BIS residues.

2.3.4. Swelling of Pore-Filled Membranes

The swelling of a neutral polymer network immersed in a good solvent is due to a balance of osmotic and elastic forces.[51] Ionic networks have an additional osmotic contribution to the swelling due to the higher concentration of mobile (non associated) ions within the network as a consequence of Donnan equilibrium.[52]

An increase in the number of mobile counter ions within the membrane, i.e. those counter ions free to be solvated and free to move a distance away from the fixed charge, will increase the observed osmotic forces in a gel.[51] In the case of a poly(acrylic acid) gel, this can be achieved by increasing the pH of the solution. This is confirmed for pore-filled membranes by the swelling data in **Table 2.1**. The initial swelling of the membranes in deionized water (pH 5.5) is due to the ionization of poly(acrylic acid). The pKa of poly(acrylic acid) is approximately 5.8,[53] and therefore the membrane would be half ionized. As the pH is increased from 5.5 to 10.6, an even larger increase in the degree of swelling is observed.

The data in **Tables 2.2** and **2.3** show that with either an increase in volume of poor solvent in the reaction mixture, or with increase in cross-link density, the swelling of the membranes decreases. As shown in **Figure 2.6**, the membranes formed in 1,4-dioxane increased in volume by more than 100% at high pH. The swelling was even greater, up to 178%, as the volume percent of DMF in the reaction solvent increased. This observation is rather interesting in light of the fact that the ion-exchange capacities of

membranes formed in either DMF or Diox were the same at the same polymer volume fraction. For membranes formed at 5 and 10% XL, no change in volume is observed at pH 10.6. Beyond 10 % XL the swelling decreases. Swelling data for 25% cross-linked membranes could not be obtained as the membranes were too fragile. At 25% XL, the membrane was destroyed when put in base.

These results can be understood in terms of the known effects that heterogeneity has on gel swelling. With an increase in heterogeneity, either through solvency or cross-linking, it has been suggested by Bansil[18] that the elastic forces arising when the gel swells are no longer evenly distributed over all subchains. The elastic forces have a complicated profile connected with the local cross-link density because of the induced inhomogeneity of the cross-linking process during the synthesis of the gel.[54] These effects alter the overall elastic modulus and therefore affects the swelling properties.

Khoklov *et al*[54] have suggested that an increase in heterogeneity of the polyelectrolyte gel will decrease the number of osmotically active counter ions and thus change the swelling properties of the gel. They utilize this polyelectrolyte effect to describe anomalous behaviour observed in swelling/deswelling networks. Their experimental data suggests that the fraction of osmotically passive counterions increases with increasing gel inhomogeneity, but the fraction is greater than that of Onsager-Manning condensation.[54] The local potential wells that are formed in the highly charged polymer rich regions additionally trap some of the counterions. As a result, the osmotic swelling pressure of counterions decreases, and the swelling ratio of an inhomogeneous

gel should be lower than that of a homogeneous one as is observed in **Tables 2.2** and **2.3**.

Oosawa[55] has described this effect for polyelectrolytes in solution. He suggests that in addition to having counter ions as holes at charged groups on the chain (**Figure 2.7-1**)and in a cylindrical valley along the chain (**Figure 2.7- 2**), a spherical trough in the apparent volume occupied by the macroion also contributes to binding counterions (**Figure 2.7- 3**). Counterions in these three regions are defined as bound to the macroion. They are mobile in the cylindrical potential valley and in the spherical potential trough but in effect are osmotically inactive. Counterions outside the spherical trough (**Figure 2.7- 4**) are considered to be free and contribute to osmotic swelling. A macroion in the extended conformation has no spherical trough, and thus would potentially have more osmotically active counterions. Polyelectrolyte chains in a gel, forced into this spherical conformation, for example by solvent induced effects, should in fact show a reduction in swelling as compared to more extended chains in a gel in gel produced in a good solvent.

The most interesting aspect of this is that while the swelling is different for both DMF and 1,4-dioxane membranes, the water uptake and ion-exchange capacity are the same with respect to polymer volume fraction, regardless of the reaction solvent used. This may impart some unique properties to the membranes in terms of performance. It has already been shown that with increase in the volume of poor solvent in the reaction mixture, the resistance of the membranes increases, as measured by impedance spectroscopy.[56]

2.4 Conclusion

It has been assumed by previous work in our laboratory that the polyelectrolyte and, indeed, any gel-filled membrane has a homogenous gel distribution within the pores. This is clearly an over simplification as these studies show that the monomer concentration, solvent and cross-linking ratio all have a direct effect on the morphology of the gel and gel fill. The question remains as to how these changes in gel morphology relate to the permeability and separation properties of the membranes. These topics are explored further in the next two chapters of this thesis.

Table 2.1. Effect of monomer loading on poly(acrylic acid) membranes formed in DMF and 1,4-dioxane.

Membrane	Monomer Concentration[a] (mol/L)	Reaction Solvent	Mass Gain (%, ± 5 %)	Water Uptake (%, ± 5 %)	IEC (meq/g, ± 0.2)	% Swelling of Membrane (± 12% in pH 5.5)	% Swelling of Membrane (± 14% in pH 10.6)
CTM 142	1.110	DMF	1.9	87.4	0.0	0	0
CTM 140	1.388	DMF	4.1	82.2	0.2	6	7
CTM 145	1.804	DMF	28.0	82.3	2.8	14	55
CTM 149	1.943	DMF	57.3	75.2	4.0	11	120
CTM 144	2.220	DMF	77.0	76.1	4.4	17	140
AR 03	2.498	DMF	94	70.2	5.2	21	160
CTM 121	2.775	DMF	122	65.8	5.6	17	175
CTM 171	1.665	1,4-Dioxane	35.4	76.82	2.98	-	-
CTM 170	1.943	1,4-Dioxane	45.7	75.6	3.8	-	-
CTM 169	2.220	1,4-Dioxane	59.6	73.8	4.3	-	-
CTM 168	2.498	1,4-Dioxane	107.8	68.1	5.8	-	-
CTM 167	2.775	1,4-Dioxane	148.5	71.2	6.0	-	-

A. Monomer concentration based on total monomer (AA plus 5 mol% BIS with respect to AA).

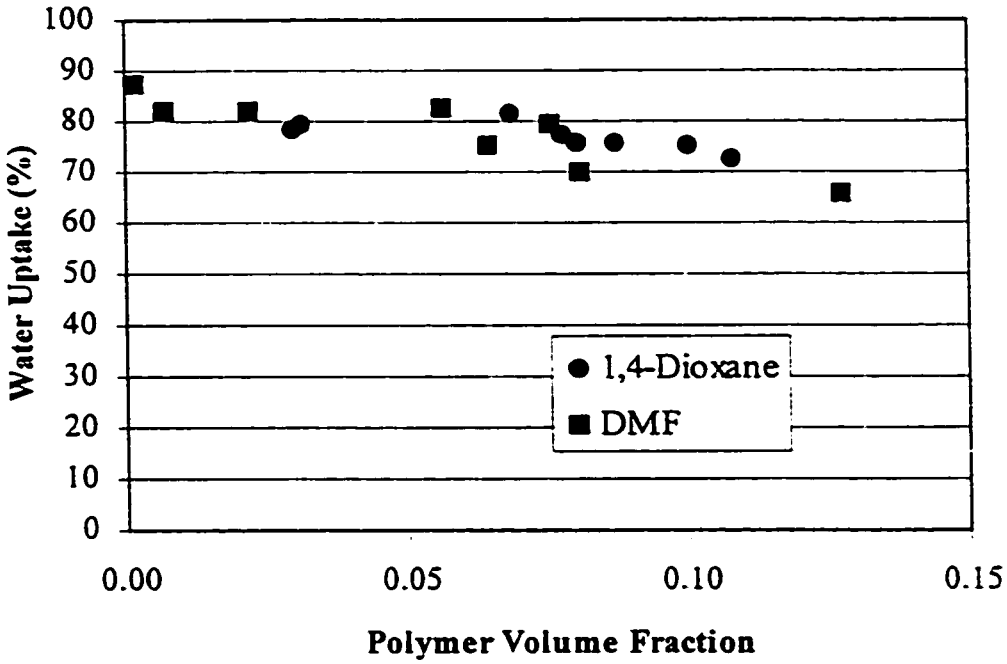

Figure 2.1. Percent water uptake, based on mass of water absorbed by hydrating vacuum dried membranes, in relation to the polymer volume fraction of gel within the membrane.

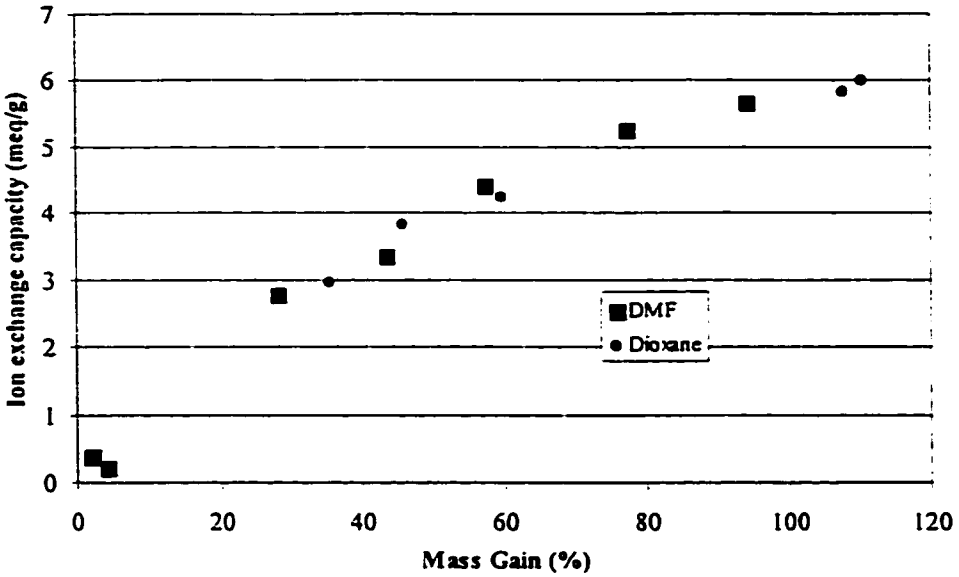

Figure 2.2. Ion exchange capacity of membranes formed from DMF and 1,4-dioxane with respect to mass gain.

Table 2.2. Effect of reaction solvent on poly(acrylic acid) pore-filled membranes.

Membrane	Reaction Solvent[a]	Mass Gain[b] (%, ± 5 %)	Water Uptake (%, ± 5%)	% Change in Volume (± 12% in pH 5.5,	% Change in Volume (± 14% in pH 10.6)
124	0	156	66	20	98
125	0.20	175	62	5	141
123	0.25	167	60	14	139
126	0.30	214	54	5	120
127	0.35	156	61	11	136
122	0.50	144	63	9	148
AR 03	0.75	141	64	14	160
121	1.0	122	66	17	175

A. Volume ratio of DMF/ 1,4-dioxane.
B. All membranes were synthesized using 2.775 M AA and 5 mol% BIS with respect to AA.

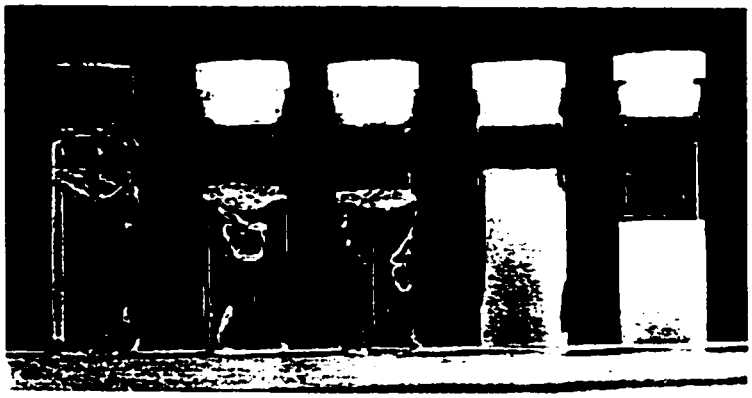

100 vol% DMF **25/75** **50/50** **75/25** **100 vol% 1,4-Dioxane**

Figure 2.3. Effect of polymerization conditions on bulk gels: Change in reaction solvent from good (DMF) to marginal (1,4-dioxane) on polymerization of acrylic acid and N,N'-methylenebisacrylamide (2.775 M AA, 5 mol % BIS with respect to AA).

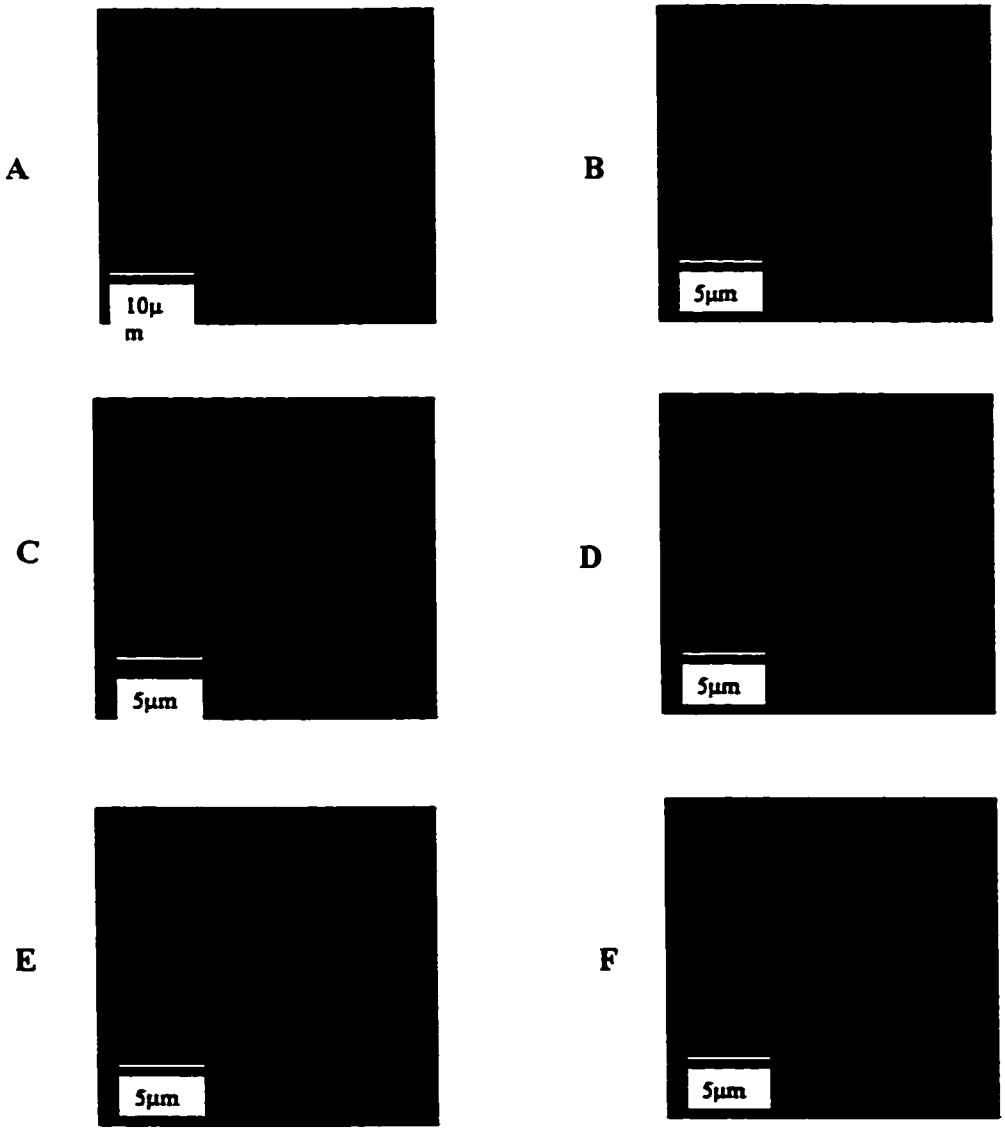

Figure 2.4: Confocal laser scanning microscopy of bulk gels showing change in morphology with change in reaction solvent and dilution. Gel **A)** was formed by co-polymerization of 2.775 M AA, with 5 mol% BIS relative to AA in DMF. Gels **B - F** were formed by polymerization of acrylic acid and N,N'-methylenebisacrylamide (5 mol% in 1,4-dioxane, with the following concentrations: **B)** 1.110 M; **C)** 1.665 M; **D)** 1.943 M; **E)** 2.220 M; **F)** 2.775 M. Gels were stained with an aqueous solution of 1×10^{-5} M ethidium bromide.

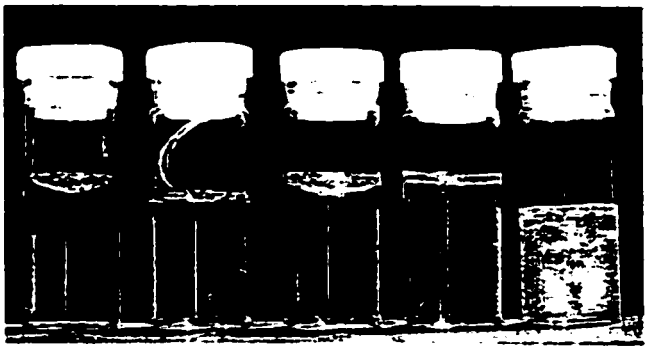

Figure 2.5. Effect of polymerization conditions on bulk gels: Effect of increasing degree of cross-linking (Total monomer concentration of acrylic acid and N,N'-methylenebisacrylamide: 2.775 M AA + BIS, DMF as reaction solvent).

Table 2.3. Effect of degree of cross-linking on poly(acrylic acid) pore-filled membranes.

Membrane	Reaction Solvent	Degree of Cross-linking (%)	Mass Gain [A] (%, ± 5 %)	Water Uptake (%, ± 5 %)	IEC (meq/g, ± 0.2)	% Change in Volume (± 12 %in pH 5.5)	% Change in Volume (± 12 % in pH 10.6)
CTM 121	DMF	5	122	66	5.6	17	175
CTM 129	DMF	10	141	66	5.6	35	164
CTM 131	DMF	15	153	60	4.9	22	154
CTM 132	DMF	20	166	53	4.5	17	131
CTM 133	DMF	25	176	50	4.3	11	N/A

A. Total Monomer Concentration 2.775 M (AA + x mol BIS, where x is the degree of cross-linking)

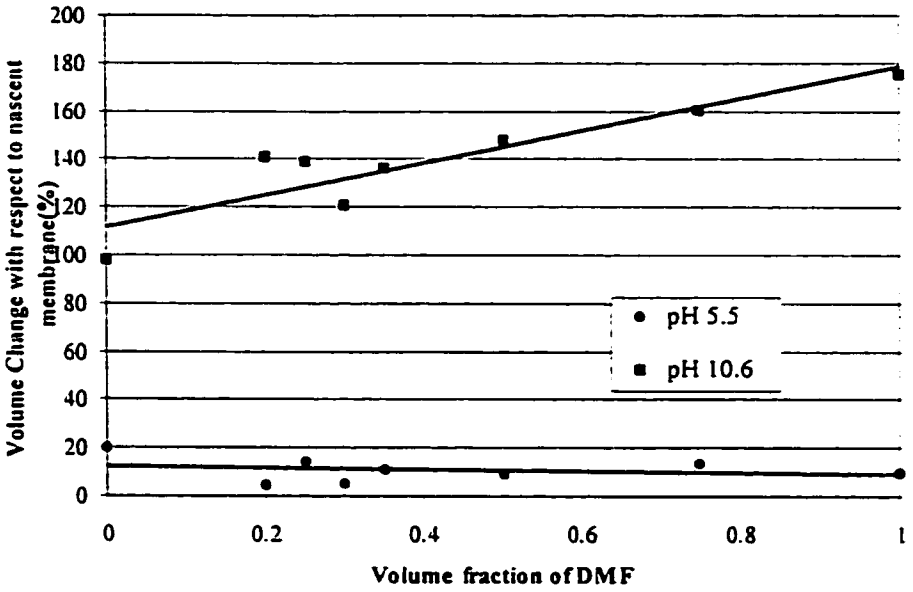

Figure 2.6. Change in volume of membranes of Table 2.2 in comparison with the volume ratio of DMF/1,4-Dioxane as reaction solvent. Membranes were first soaked in deionized water and left to equilibrate for 3 days where an equilibrium pH of 5.5 was achieved (•). The membranes were then placed in a 0.01 N NaOH bath for 3 days until a pH of 10.6 was achieved (■)

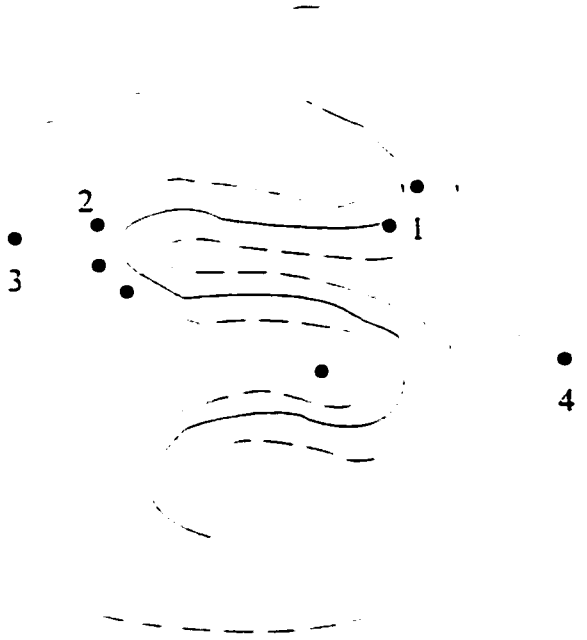

Figure 2.7. Three regions for counter ions bound in and around the macroion. (1) The potential hole at charged groups; (2) the potential valley along the cylindrical region apparently occupied by the macroion as a whole. The area marked by (4) is the outside region for free counter ions (from Oosawa, F. in *Polyelectrolytes*, Marcell Dekker, New York, 1971. pg 11)

Reference List

(1) Mulder, M. *Basic Principles of Membrane Technology*; Kluwer Academic Publishers: 1997.

(2) Kesting, R. E. *Synthetic Polymeric Membranes*; McGraw Hill: New York, 1985.

(3) Pusch, W.; Walch, A. *Angew.Chem.Int.Ed.Engl.* **1982**, *21*, 660.

(4) Strathmann, H.; Koch, K. *Desalination* **1977**, *21*, 241.

(5) Uragami, T.; Fujimoto, M.; Sugihara, M. *Angew.Makromol.Chem.* **1981**, *95*, 45-54.

(6) van de Witte, P.; Dijkstra, P. J.; van den Berg, J. W. A.; Feijen, J. *J.Mem.Sci.* **1996**, *117*, 1-31.

(7) Kapur, V.; Charkoudian, J.; Kessler, S. B.; Anderson, J. L. *Ind.Eng.Chem.Res.* **1996**, *35*, 3179.

(8) Kapur, V.; Charkoudian, J.; Anderson, J. L. *J.Membrane Sci* **1997**, *131*, 143.

(9) Weiss, N.; van Vliet, T.; Silderberg, A. *J.Polym.Sci., Polym.Phys.Ed.* **1979**, *17*, 2229-2240.

(10) Weiss, N.; van Vliet, T.; Silderberg, A. *J.Polym.Sci., Polym.Phys.Ed.* **1981**, *19*, 1505-1512.

(11) Gong, J. P.; Kii, A.; Xu, J.; Hattori, Y.; Osada, Y. *J.Phys.Chem.B* **2001**, *105*, 4572-4576.

(12) Kii, A.; Xu, J.; Gong, J. P.; Osada, Y.; Zhang, X. *J.Phys.Chem.B* **2001**, *105*, 4565-4571.

(13) Osada, Y.; Gong, J. P. Surface dynamic properties of polymer gels; American Chemical Society: Washington, 2000.

(14) Dusek, K.; Seidl, J.; Malinsky, J. *Collection Czech.Chem.Commun.* **1967**, *32*, 2766-2778.

(15) Dusek, K. Inhomogeneities Induced by Crosslinking in the Course of Crosslinking Copolymerization; In *Polymer Networks: Structure and Mechanical Properties*; Chompff, A. J., Newman, S., eds. Plenum Press: New York-London, 1971; pp 245-260.

(16) Lai, Y.-C.; Quinn, E. T. Photopolymeriztion: Fundamentals and Applications. ACS Symmposium Series 673; In *Photopolymeriztion: Fundamentals and Applications*; Scranton, A. B., Bowman, C. N., Peiffer, R. W., eds. American Chemical Society: Washington, 1997; pp 35-50.

(17) Sata, T.; Yamane, Y.; Matsusaki, K. *J.App.Polym.Sci.Part A: Polym.Chem.* **1998**, *36*, 49.

(18) Bansil, R.; Gupta, M. K. *Ferroelectrics* **1980**, *30*, 63-71.

(19) Hecht, A. M.; Geissler, E. *J.Phys.* **1978**, *39*, 631-638.

(20) Horak, D.; Pelzbauer, Z.; Bleha, M.; Ilavsky, M.; Svec, F.; Kalal, J. *J.Appl.Polym.Sci* **1981**, *26*, 411-421.

(21) Horak, D.; Pelzbauer, Z.; Svec, F.; Kalal, J. *J.App.Polym.Sci.* **1981**, *26*, 3205-3211.

(22) Horak, D.; Svec, F.; Ilavsky, M.; Bleha, M.; Baldrian, J.; Kalal, J. *Angew.Makromol.Chem.* **1981**, *95*, 117-127.

(23) Horak, D.; Svec, F.; Bleha, M.; Kalal, J. *Angew.Makromol.Chem.* **1981**, *95*, 109-115.

(24) Hradil, J.; Svec, F. *Angew.Makromol.Chem.* **1985**, *135*, 85-97.

(25) Hradil, J.; Svec, F. *Angew.Makromol.Chem.* **1985**, *130*, 81-90.

(26) Lukas, J.; Bleha, M.; Svec, F.; Kalal, J. *Angew.Makromol.Chem.* **1981**, *95*, 129-137.

(27) Smigol, V.; Svec, F.; Frechet, J. M. J. *Macromolecules* **1993**, *26*, 5615-5620.

(28) Svec, F.; Frechet, J. M. J. *Macromolecules* **1995**, *28*, 7580-7582.

(29) Wang, Q. C.; Svec, F.; Frechet, J. M. J. *J.Polym.Sci.A.,Polym.Chem* **1994**, *32*, 2577-2588.

(30) Peters, E. C.; Svec, F.; Frechet, J. M. J. *Chem.Mater.* **1997**, *9*, 1898-1902.

(31) Svec, F.; Frechet, J. M. J. *Chem.Mater.* **1995**, *7*, 707-715.

(32) Xie, S.; Svec, F.; Frechet, J. M. J. *Chem.Mater.* **1998**, *10*, 4072-4078.

(33) Svec, F.; Jelinkova, M.; Votavova, E. *Angew.Makromol.Chem.* **1991**, *188*, 167-176.

(34) Mika, A. M., Childs, R. F., and Dickson, J. M. Patent Pending. 1996.

(35) Mika, A. M.; Childs, R. F.; Dickson, J. M.; McCarry, B. E.; Gagnon, D. R. *J.Membrane Sci.* **1997**, *135*, 81-92.

(36) Mika, A. M.; Childs, R. F.; West, M.; Lott, J. N. A. *J.Membrane Sci.* **1997**, *136*, 221-232.

(37) Stachera, D. M.; Childs, R. F.; Mika, A. M.; Dickson, J. M. *J.Membrane Sci.* **1998**, *148*, 119-127.

(38) Mika, A. M.; Childs, R. F.; Dickson, J. M. *Desalination* **1999**, *121*, 149-158.

(39) Childs, R. F.; Mika, A. M.; Pandey, A. K.; McCrory, C. T. C.; Mouton, S.; Dickson, J. M. *Sep.Purif.Technol.* **1999**, *22-23*, 507-517.

(40) Winnik, F. M.; Morneau, A.; Mika, A. M.; Childs, R. F.; Roig, A.; Molins, E.; Ziolo, R. F. *Can.J.Chem.* **1998**, *76*, 10-17.

(41) Yamaguchi, T.; Nakao, S.; Kimura, S. *Macromolecules* **1991**, *24*, 5522-5527.

(42) Yamaguchi, T.; Yamahara, S.; Nakao, S.; Kimura, S. *J.Membrane Sci.* **1994**, *95*, 39-49.

(43) *Polymer Handbook*; John Wiley & Sons: New York, 1999.

(44) Hawley, G. G. *The condensed chemical dictionary*; Van Nostrand Reinhold Company: New York, 1977.

(45) Mika, A. M.; Childs, R. F.; Dickson, J. M.; McCarry, B. E.; Gagnon, D. R. *J.Membrane Sci.* **1995**, *108*, 37-56.

(46) Dotson, N. A.; Macosko, C. W.; Tirrel, M. Cyclization During Crosslinking Free-Radical Polymerizations; In *Synthesis, Characterization, and Theory of Polymeric Networks and Gels*; Aharoni, S. M., ed. Plenum Press: New York, 1992; pp 319-336.

(47) Guyot, A. Synthesis and Structure of Polymer Supports; In *Syntheses and Separation using Functional Polymers*; Sherrington, D. C., Hodge, P., eds. John Wiley & Sons: New York, 1988; pp 1-42.

(48) Takeshita, H.; Kanaya, T.; Nishida, K.; Kaji, K. *Macromolecules* **1999**, *32*, 7815-7818.

(49) Mijnlieff, P. F.; Jaspers, W. J. M. *Trans.Faraday Soc.* **1971**, *67*, 1837.

(50) Hwang, G. J.; Ohya, H. *J.Membrane Sci.* **1998**, *140*, 195-203.

(51) Saunders, B. R.; Crowther, H. M.; Vincent, B. *Macromolecules* **1997**, *30*, 482-487.

(52) Helfferich, F. *Ion Exchange*; McGraw-Hill Book Co. Inc.: Toronto, 1962.

(53) Budd, P. M. Polymers and water: an overview; In *Industrial water soluble polymers*; Finch, C. A., ed. The Royal Society of Chemistry: Cambridge, 1996; pp 1-9.

(54) Zeldovich, K. B.; Khoklov, A. R. *Macromolecules* **1999**, *32*, 3488-3494.

(55) Oosawa, F. *Polyelectrolytes*; Marcel Dekker: New York, 1971.

(56) McCrory, C. T. C. and Childs, R. F. Polyelectrolyte pore-filled membranes: Control of membrane resistance through control of gel morphology, manuscript in preparation. 2001.

Chapter 3

Hydrodynamic Permeability of Poly(acrylic acid) Pore-Filled Membranes

3.1 Introduction

The morphology of the polymeric material has been shown to be a crucial element in separations using functional polymers.[1] This is well established and understood in porous beads and related structures, where pore size and surface area greatly affect separation.[1] Work by Fréchet and Svec *et al* has led to the well defined and controlled formation of porous polymer beads[2-11] and monoliths,[12-14] both of which provide excellent chromatographic resolution, and the development of polymer sheets for use in high performance membrane chromatography.[15] Their work suggests that formation of polymer membranes of a wide variety of pore-sizes and distributions, by free radical polymerization, can be achieved by using the same principles as in the formation of polymer beads and monoliths.

However, the morphology of soft gels also appears to be a factor affecting separation and permeability of these materials. For example, by introducing heterogeneity in polyacrylamide gels through porogenic substances, Righetti could control the size of DNA fragments migrating during gel electrophoresis.[16,17] Weiss *et al*[18,19] have shown that there is an increase in permeability with an increase in the cross-linking ratio of

polyacrylamide gels.

Anderson[20] also observed differences in hydrodynamic permeability and separation of different types of proteins by poly(acrylamide) gel-filled membranes. The differences in performance were attributed to the presence of microstructures within the gel.

Recent studies have demonstrated that robust membranes containing soft polyelectrolyte gels can be made by a "gel in a shell"[21] or "pore-filling" approach.[20,22-25] In this construct, the gel is formed inside the pores of a microporous substrate. The host provides the structural framework which constrains the gel. The gel acts as the separating component and the morphology of the gel would be expected to affect the properties of the membrane.

As described in **Chapter 2**, the morphology of the poly(acrylic acid) gels and gel-filled membranes can be controlled by monomer loading, reaction solvent and degree of cross linking. This chapter involves a study of the effect of the gel morphology on the hydrodynamic permeability of the poly(acrylic acid) pore-filled membranes. **Chapter 4** will deal separately with the issue of nanofiltration using these membranes.

Mika and Childs [26] have recently developed a model to successfully predict the permeability of poly(vinyl-pyridine) gel filled membranes. The model was modified and used to predict the permeability of poly(acrylic acid) pore-filled membranes used in this work.

3.2. Theoretical Model

The model developed by Mika for predicting permeability of gels and gel filled membranes has already been described elsewhere.[26] A summary of the theory underlying the model will be briefly presented.

From a hydrodynamic point of view, the approach taken is to assume that the polymer gel is a homogeneous assemblage of spheres. The Happel model for viscous flow through the assemblage can then be applied to obtain the gel permeability, k [27]

$$k = \frac{2R^2}{9\phi}\left[3 - \frac{(9/2)\phi^{1/3} + (9/2)\phi^{5/3} - 3\phi^2}{3 + 2\phi^{5/3}}\right] \tag{3.1}$$

where R is the radius of the hard sphere occupying the volume fraction φ in a spherical cloud.

In order to calculate the diameter of the spheres, R, it is assumed that the confined gels are semidilute polymer solutions of the same polymer concentration (volume fraction).[26] The correlation length in the solution is taken as R. The correlation length of polymers in solution is estimated using scaling methods,[28] and Schaefer's model of the polymeric structure in semidilute solutions,[29]

$$\xi_p = \frac{n^2 a}{\left[n(1-2\chi)\phi + wa^{-6}\phi^2\right]^{1/2}} \tag{3.2}$$

where n is the total number of bonds in the persistence length, a is the bond length, χ is the Flory-Huggins interaction parameter and w is the three-body excluded volume parameter which is assumed to be zero in the marginal regime. The electrostatic interactions in the gel are accounted for by increasing the number of bonds in the total persistence length to

$$n_t = n_p + n_e \tag{3.3}$$

where $n_p = C_\infty/6$ is the number of bonds in the persistence length and $n_e=(0.83)^2L_e/3a$ is the number of bonds in the electrostatic persistence length. The electrostatic persistence length in a salt-free polyelectrolyte solution is given by[30,31]

$$L_e = \frac{l_B}{4\kappa^2 A^2} \tag{3.4}$$

where $l_B = q_e^2/Dk_BT$ is the Bjerrum length (D is the dielectric constant of the solvent and k_BT is the Boltzmann factor) and κ is the Debye-Hückel parameter in salt free solution.[38] For a wormlike polyelectrolyte chain of contour length l with bare persistence length L_p, bearing P elementary charges (q_e), the charges are separated by a contour distance $A=lP^{-1}$.

This Happel model accounts for the Darcy permeability of a gel. The membrane permeability, k_m is obtained by correcting the gel permeability for the substrate porosity, ε_s, and the pore tortuosity τ through the so-called tortuosity factor ε_s/τ:[32]

$$k_m = k(\varepsilon_s / \tau) \tag{3.5}$$

The tortuosity τ was estimated as $\tau = K_s/K^* = 2.5$ where K_s is the Kozeny constant ($K_s \approx 5$ for porosity ≈2/3) and $K^* = 2$ is the Kozeny constant for parallel capillary pores of circular cross-section.[32]

3.3. Experimental

3.3.1. Materials, Membrane Preparation and Characterization

The materials and method for membrane production has been described previously in **Chapter 2**.

3.3.2. Pressure Tests

The flux measurements were carried out in a dead-end cell with a membrane active area of 38.50 cm^2. The cell was fitted with a thermocouple to measure temperature of the feed solution and a sample port so that the composition of the feed could be determined during the course of experiment. The feed solution was stirred at the rate of 250-300 rpm. Permeate samples were collected over a given period and then weighed.

The flux (kg/m^{2}h), corrected for the temperature to 25°C, was calculated from the mass of permeate divided by time and the membrane active area.[26]

The experimental hydraulic permeabilities, k_m, of the membranes were determined from the flux-pressure measurements and calculated according to the equation:

$$k_m = \frac{\eta J_v}{\Delta P / L} \tag{3.6}$$

where J_v is the volume flow across the membrane (m^3/s), L is the membrane thickness (m), η is the permeate viscosity at 25 °C (0.00089 Pa s), and ΔP is the trans-membrane pressure (Pa). The permeabilities of the membranes were derived from the slopes of the straight lines obtained by plotting $J_v\eta$ as a function of $\Delta P/L$.

3.4. Results

The series of membranes were prepared by photopolymerizing an applied monomer solution containing acrylic acid and N,N'-methylenebisacrylamide within the pores of a microporous polypropylene host. Full details of these membranes are given in **Chapter 2**. The pure water fluxes of the membranes were measured at various pressures. The fluxes were linear up to 300 kPa for all membranes. The permeabilities were determined using **equation 3.6** with the linear portion of the flux/pressure data.

Table 3.1 contains selected characterization data for membranes synthesized with increasing monomer concentration, along with hydrodynamic permeability. The data for

membranes formed with different reaction solvents are given in **Table 3.2**. **Table 3.3** shows the data for membranes formed with 2.775 M AA, but different degrees of cross-linking.

Figure 3.1 shows the effect of gel polymer volume fraction on membrane permeability. Two series of data are shown, one for the membranes synthesized in a DMF reaction solvent and one for the membranes synthesized with 1,4-dioxane as solvent.

Figure 3.2 shows the membrane permeability as the reaction solvent used in membrane formation is modified from good to poor. **Figure 3.3** shows the relationship between permeability and increase of cross-linking ratio. Although the 25% XL membranes could be synthesized, they were very fragile even when wet and were damaged when placed under pressure.

3.5 Discussion

3.5.1 Effect of Monomer Loading

An increase in the polymer volume fraction of the PAA gel fixed in the membrane after polymerization results in a decrease in membrane permeability, **Table 1** and **Figure 3.1**. This decrease is expected. Thus, considering **equation 3.2**, an increase in the polymer volume fraction of gel would decrease the correlation length of the semi-dilute polymer solution, and result in a smaller sphere size, according to **equation 3.1**. This will

result in a decrease in gel permeability and membrane permeability. Similar effects have been observed independently by Mika and Childs [26] and Kapur *et al*[32] on gel and membrane permeabilitiy.

3.5.2 Effect of Reaction Solvent

As described in **Chapter 2**, microheterogeneous structures can be formed in the gel fill with change of the reaction solvent or by increasing the degree of cross-linking. Bulk gels formed in DMF at 5% XL were clear. Gels formed in 1,4-dioxane reaction solvent were opaque, and white in colour. The transition from DMF to 1,4-dioxane created white gels between 50-75 vol.% 1,4-dioxane in the polymerization mixture. The causes of this were attributed to phase separation and formation of microstructures within the space filling gel.

The use of marginal or non solvent to form heterogeneous structures in the formation of polymeric separation media to change their separation properties has been previously reported. Work by Kun and Kunin[33] show that by using porogenic solvents, macroporous styrenic beads contain agglomerates of microspheres (100-200 nm) and individual microspheres are composed of even smaller nuclei (10-30 nm). Thin film composite membranes by Hirose[34] were shown to coarsen and form globular structures at the membrane surface by the addition of a non solvent such as isopropyl alcohol to the water mixture for the interfacial polymerization. Svec has also shown that use of marginal

or non solvents could increase the average pore size diameter of polymer beads and monoliths.[2,4,5,12,14]

The permeabilities of poly(acrylic acid) pore-filled membranes synthesized from different solvents are shown in **Figures 3.1** and **3.2**. An increase in permeability is observed with increase in the volume fraction of the poor solvent in the reaction mixture. Despite a 30% higher mass gain , the permeability of the 1,4-dioxane membrane (CTM 124) is almost 9 times higher in permeability than its counterpart formed in DMF (CTM 121). An increase in membrane permeability is observed even at 25 vol. % dioxane (**Figure 3.2**), and permeability increases further as the solvency of the mixture decreases.

In order to understand the relationship between a polymer gel and its permeability, it is important to consider more deeply the factors which affect permeability.[26] The solid line in **Figure 3.1** for DMF membranes was obtained using **equation (3.1)** over the gel polymer volume fraction range of $0.005 \leq \phi \leq 0.200$, with the following literature values: characteristic ratio of PAA, $C_\infty = 11.3$,[35] and $\chi = 0.39$.[36] The calculated values of the correlation length, ξ_p, changed from 50.7 Å ($\phi = 0.005$) to 2.1 Å ($\phi = 0.200$). The model matches well with the experimental permeability data, for membranes formed using DMF as a solvent, by using literature data for PAA. No fitting parameters were used in the model.

However, the model does not match the data for membranes formed from 1,4-dioxane. Although the polymer volume fraction and water uptake are identical for both sets of membranes, the permeability deviates from that of a homogeneous gel fill such as

that formed in DMF. The membrane permeability deviates more as the reaction solvent becomes poorer.

As shown in **Chapter 2**, with increase in poor solvent content in the reaction solvent, there is an increase in heterogeneity in the gel. Weiss has referred to heterogeneous poly(acrylamide) gels as gels that contain regions which are draining and non-draining.[18,19] The draining regions are considered as polymer poor and the non-draining regions are polymer rich. The decrease in the gel concentration within the polymer poor area could effectively result in an increase in permeability of a gel filled membrane. However, this type of gel fill is not homogeneous and therefore the Mika model used previously,[26] which assumes a homogeneous gel, does not hold for these systems.

However, the Mika model can be modified in order to test the formalism of draining and non-draining regions within the gel, and account for the enhancement in permeability for heterogeneous poly(acrylic acid) membranes observed in this work.

The average polymer volume fraction of gel in the membrane pores can be defined as

$$\phi_{avg} = \frac{v_{PE}}{V_{Pore}} = \frac{v_{PE}^{ND} + v_{PE}^{D}}{V_{Pore}} \qquad (3.7)$$

where $v_{PE} = v^{ND}_{PE} + v^{D}_{PE}$. v_{PE} is the volume of polyelectrolyte in the pore volume V_{pore}. The variables v^{ND}_{PE} and v^{D}_{PE} are the volumes of polyelectrolyte chains in non-draining and draining regions, respectively. The polymer volume fraction in the polymer rich region,

ϕ_{ND}, and polymer poor region, ϕ_D regions can be defined as

$$\phi_{ND} = \frac{v_{PE}^{ND}}{V_{ND}} \qquad \phi_D = \frac{v_{PE}^{D}}{V_D}$$

where V_{ND} and V_D are the volume of the non-draining and draining regions, respectively.

Assuming that the volume of the non-draining pore is much smaller than the draining pore

$$V_{ND} \ll V_D, \text{ then } V_D \sim V_{pore}$$

and

$$\phi_D \approx \frac{v_{PE}^{D}}{V_{pore}} \qquad (3.8)$$

With this in mind, we can use **equation 3.1** to calculate the gel polymer volume fraction of the draining region, ϕ_D, assuming the solvent only flows through the draining regions of the gel. Using **equation 3.8**, the volume of the polymer in the draining region, v^D_{PE}, can be calculated, and we can now obtain the volume of polymer in the non-draining region v^{ND}_{PE} with **equation 3.7**.

The estimated polymer volume fractions of the draining regions, for membranes synthesized in different solvents, are listed in **Table 3.4**. As the volume of 1,4-dioxane increases in the monomer mixture, the gel volume fraction of the draining region decreases. The ratio of v^{ND}_{PE}/v^{D}_{PE} is also shown in **Table 3.4**. A ratio less than one would

indicate that the volume of the draining region is larger than the volume of the non-draining region.

According to the Mika model,[26] the volume of the non-draining region increases as the reaction solvent becomes poorer. The gel in the membrane synthesized in DMF is considered wholly as draining. The volume of the draining region for AR 011 is ten times larger than that of the non-draining region. The modified model can be considered valid for this membrane. However, the volume of the non-draining region increases to where it can no longer be considered as much less than the draining region for membranes CTM 122, 123 and 124. For these membranes, the model does not hold and the volume of the non-draining region must be taken into account. At the moment it is not possible to directly obtain the volume of polymer in the non-draining regions of the gel.

3.5.3 Effect of Cross-linking

The series of bulk gels formed with increasing degree of cross linker were clear at 5-15% XL, and became increasingly opalescent to 25%. It has been shown by light scattering that inhomogeneity occurs in gels even though it is not visible to the naked eye.[37] Higher cross linking ratios have been observed to create opalescence in poly(acrylamide) gels,[37] similar to that observed with the bulk poly(acrylic acid) gels found in this work. It was suggested by Bansil[37] that aggregates of the BIS residues can occur and that these local concentration fluctuations not only scatter light, but provide

larger draining pores. In fact, the increase in permeability of gels with increase in cross-linking has been observed by Weiss,[18] however, this was not correlated with observations of bulk gels or gel filled membranes.

An increase in permeability is observed for the poly(acrylic acid) membranes with an increase in the degree of cross linking, as shown in **Figure 3.3**. Between 5-15% cross-linking, the PAA membrane exhibits an increase in permeability, even though the space filling gels are clear (**Chapter 2, Figure 2.5**). This indicates that it is not necessary to have microstructures large enough to scatter light within the gel in order to increase the membrane permeability. At 20% XL, the onset of light scattering is observed in the gels, and the membrane shows the highest permeability of the series of membranes.

The overall effect of the increase in degree of cross-linking of poly(acrylic acid) membranes is an increase in the heterogeneity of the poly(acrylic acid) membranes, which results in the observed increase in membrane permeability. The increase in degree of cross-linking seems to have a similar effect on permeability as did the change in reaction solvent. Regions of polymer rich and polymer poor may be produced with increased cross-link density, creating dense non-draining and open draining pores. This effect would be responsible for the enhancement in permeability of the membrane.

3.6 Conclusions

The morphology of the gel in a pore-filled membrane is a major factor in

determining the permeability of the membrane. A poly(acrylic acid) gel filled membrane, formed from DMF as the reaction solvent, provides a gel which can be considered homogeneous. Increasing the volume fraction of poor solvent in the monomer solution, or increasing in the degree of cross-linking, incorporates heterogeneity in the gel. The formalism of draining and non-draining regions within a heterogeneous gel can account for the enhancement in permeability using the Mika model. However, the Mika model only holds when the non-draining volume is small. With formation of larger, non-draining regions in the gel, the volume of the polymer rich regions can no longer be neglected.

Table 3.1. Characterization data for poly(acrylic acid) pore-filled membranes formed in DMF solvent.

Membrane	Degree of Cross-linking (%)	Mass Gain (%, ± 5%)	Polymer Volume Fraction	Percentage Water Uptake (± 5 %)	Hydrodynamic Permeability (m^2, ± 3%)
CTM 142	5	1.9	0.002	87	4.06 e-14
CTM 140	5	4.1	0.006	82	5.35 e-14
CTM 149	5	28	0.056	82	3.31 e-18
CTM 144	5	44	0.065	82	-
CTM 145	5	57	0.081	75	5.47 e-19
AR 03	5	94	0.127	70	-
CTM 121	5	122	0.144	66	1.69 e-19

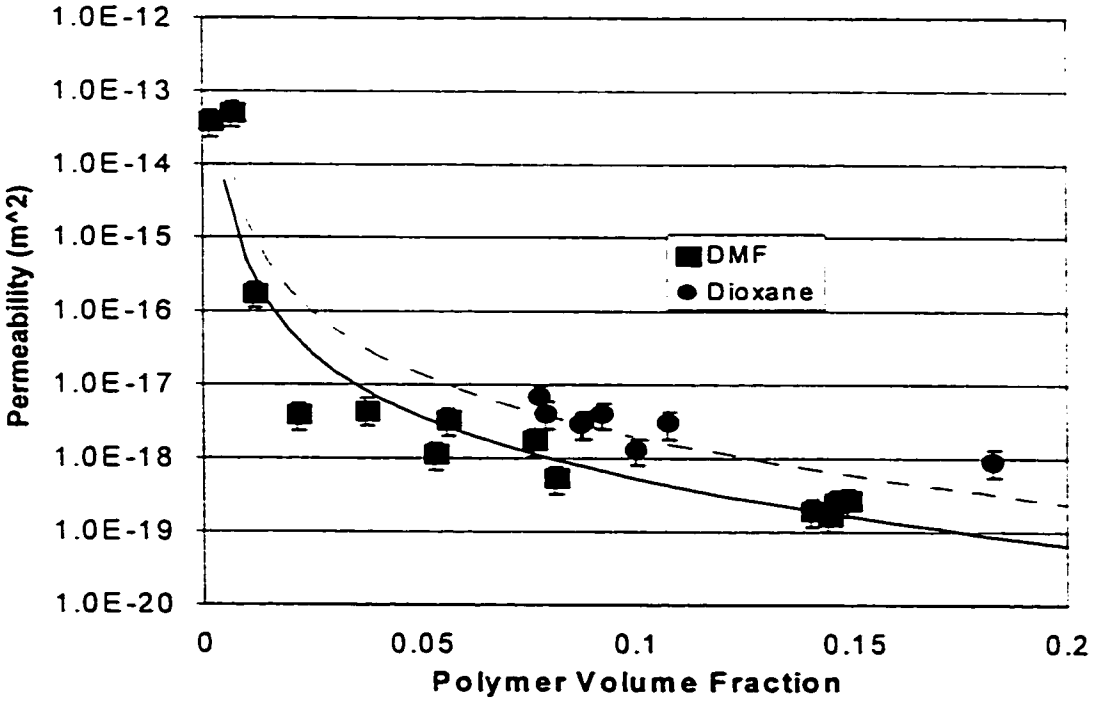

Figure 3.1. Hydrodynamic permeability of poly(acrylic acid) pore-filled membranes for different gel polymer volume fraction. (■) Membranes synthesized using DMF as the reaction solvent. (•) Membranes formed using 1,4-dioxane as reaction solvent. (–) modeled permeability using χ=0.39.

Table 3.2. Data for membranes synthesized by polymerization of 2.775 M AA, 5 % XL, in different reaction solvents.

Membrane	Reaction Solvent	Thickness (μm, ± 4 μm)	Polymer Volume Fraction	Hydrodynamic Permeability (m^2, ± 3%)
124	100% Dioxane	98	0.183	9.08×10^{-19}
123	75% Dioxane	94	0.149	2.68×10^{-19}
122	50% Dioxane	85	0.14	1.95×10^{-19}
AR 11	25% Dioxane	90	0.145	1.39×10^{-19}
121	100% DMF	82	0.144	1.11×10^{-19}

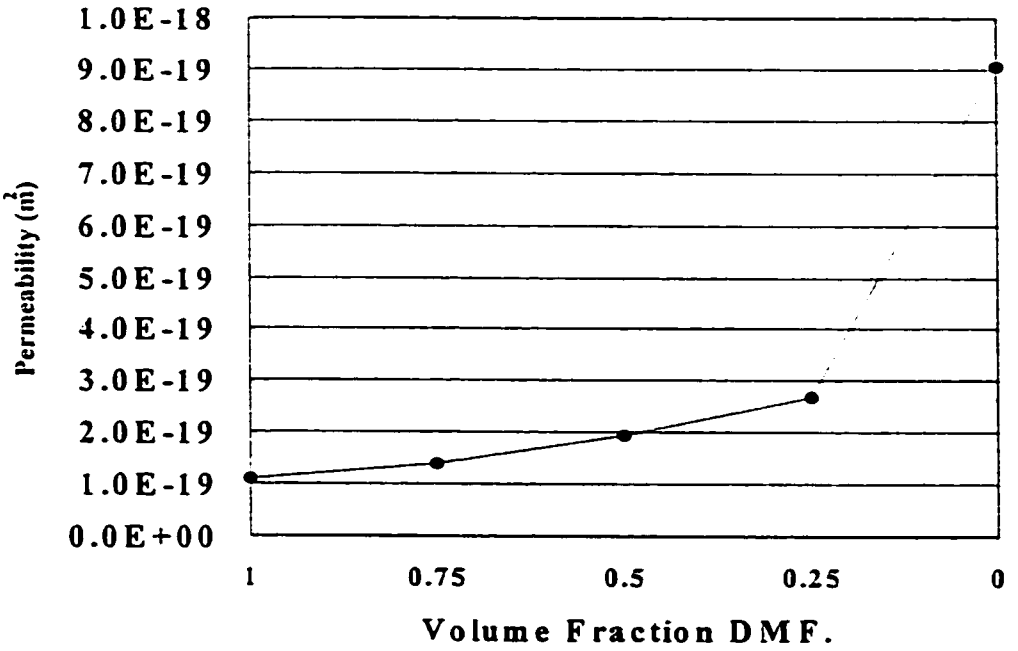

Figure 3.2. Hydrodynamic permeability of poly(acrylic acid) pore-filled membranes in relation to the reaction solvent used for polymerization. Membranes were synthesized using the same monomer concentration (2.775 M AA, 5 mol % BIS with respect to AA) and in DMF, 1,4-dioxane, or mixtures thereof.

Table 3.3: Data for series of membranes with increasing degree of cross-linking. Membranes were synthesized by polymerization of 2.775 M AA, plus x % XL. (where x = degree of cross-linking) in DMF.

Membrane	Degree of Cross-linking (%)	Mass Gain (%, ± 5%)	Water Uptake (%, ± 5%)	IEC (meq/g, ± 0.2)	Hydrodynamic Permeability ($m^2 * 10^{-19}$, ± 3%)
CTM 121	5	122	66	5.6	1.09×10^{-19}
CTM 129	10	141	66	5.6	1.68×10^{-19}
CTM 131	15	153	60	4.9	2.43×10^{-19}
CTM 132	20	166	53	4.5	3.35×10^{-19}

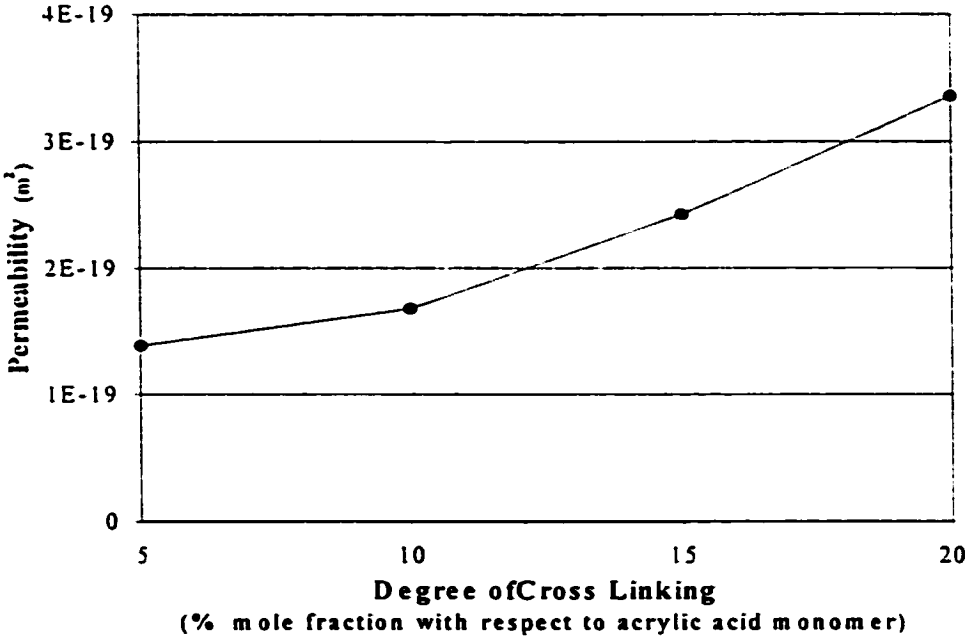

Figure 3.3. Hydrodynamic permeability of poly(acrylic acid) pore-filled membranes in relation to the degree of cross-linking. Membranes were formed using 2.775 M monomer solutions in DMF, and the molar ratio of acrylic acid to N,N'-methylenebisacrylamide varied.

Table 3.4: Estimated polymer volume fractions of the draining regions, ϕ_D, and ratio of volume of non-draining to draining regions in poly(acrylic acid) membranes formed in different reaction solvents.

Membrane	Reaction Solvent	Total Polymer Volume Fraction	φ_D	v_{ND}/v_D
124	100% Dioxane	0.183	0.036	4.8
123	75% Dioxane	0.149	0.086	0.83
122	50% Dioxane	0.14	0.104	0.35
AR 11	25% Dioxane	0.145	0.127	0.1
121	100% DMF	0.144	0.144	0

Reference List

(1) Guyot, A. Synthesis and Structure of Polymer Supports; In *Syntheses and Separation using Functional Polymers*; Sherrington, D. C., Hodge, P., eds. John Wiley & Sons: New York, 1988; pp 1-42.

(2) Horak, D.; Pelzbauer, Z.; Bleha, M.; Ilavsky, M.; Svec, F.; Kalal, J. *J.Appl.Polym.Sci* **1981**, *26*, 411-421.

(3) Horak, D.; Pelzbauer, Z.; Svec, F.; Kalal, J. *J.App.Polym.Sci.* **1981**, *26*, 3205-3211.

(4) Horak, D.; Svec, F.; Ilavsky, M.; Bleha, M.; Baldrian, J.; Kalal, J. *Angew.Makromol.Chem.* **1981**, *95*, 117-127.

(5) Horak, D.; Svec, F.; Bleha, M.; Kalal, J. *Angew.Makromol.Chem.* **1981**, *95*, 109-115.

(6) Hradil, J.; Svec, F. *Angew.Makromol.Chem.* **1985**, *135*, 85-97.

(7) Hradil, J.; Svec, F. *Angew.Makromol.Chem.* **1985**, *130*, 81-90.

(8) Lukas, J.; Bleha, M.; Svec, F.; Kalal, J. *Angew.Makromol.Chem.* **1981**, *95*, 129-137.

(9) Smigol, V.; Svec, F.; Frechet, J. M. J. *Macromolecules* **1993**, *26*, 5615-5620.

(10) Svec, F.; Frechet, J. M. J. *Macromolecules* **1995**, *28*, 7580-7582.

(11) Wang, Q. C.; Svec, F.; Frechet, J. M. J. *J.Polym.Sci.A.,Polym.Chem* **1994**, *32*, 2577-2588.

(12) Peters, E. C.; Svec, F.; Frechet, J. M. J. *Chem.Mater.* **1997**, *9*, 1898-1902.

(13) Svec, F.; Frechet, J. M. J. *Chem.Mater.* **1995**, *7*, 707-715.

(14) Xie, S.; Svec, F.; Frechet, J. M. J. *Chem.Mater.* **1998**, *10*, 4072-4078.

(15) Svec, F.; Jelinkova, M.; Votavova, E. *Angew.Makromol.Chem.* **1991**, *188*, 167-176.

(16) Righetti, P. G.; Caglio, S.; Sarachi, M.; Quaroni, S. *Electrophoresis* **1992**, *13*, 587-595.

(17) Righetti, P. G.; Gelfi, C. *Journal of Chromatography B* **1996**, *699* , 63-75.

(18) Weiss, N.; van Vliet, T.; Silderberg, A. *J.Polym.Sci., Polym.Phys.Ed.* **1979**, *17*, 2229-2240.

(19) Weiss, N.; van Vliet, T.; Silderberg, A. *J.Polym.Sci., Polym.Phys.Ed.* **1981**, *19*, 1505-1512.

(20) Kapur, V.; Charkoudian, J.; Anderson, J. L. *J.Membrane Sci* **1997**, *131*, 143.

(21) Boschetti, E. *J.Chromatography A* **1994**, *658*, 207.

(22) Mika, A. M.; Childs, R. F.; Dickson, J. M.; McCarry, B. E.; Gagnon, D. R. *J.Membrane Sci.* **1995**, *108*, 37-56.

(23) Mika, A. M.; Childs, R. F.; Dickson, J. M.; McCarry, B. E.; Gagnon, D. R. *J.Membrane Sci.* **1997**, *135*, 81-92.

(24) Mika, A. M.; Childs, R. F.; Dickson, J. M. *Desalination* **1999**, *121*, 149-158.

(25) Stachera, D. M.; Childs, R. F.; Mika, A. M.; Dickson, J. M. *J.Membrane Sci.* **1998**, *148*, 119-127.

(26) Mika, A. M.; Childs, R. F. *Ind.Eng.Chem.Res.* **2001**, *40*, 1694-1705.

(27) Happel, J. *AIChE J.* **1958**, *4*.

(28) de Gennes, P. G. *Scaling Concepts in Polymer Physics*; Cornell University Press: Ithica, 1979.

(29) Schaefer, D. W. *Polymer* **1984**, *25*, 387.

(30) Odijk, T. *J.Polym.Sci., Polym.Phys.Ed.* **1977**, *15*, 477.

(31) Skolnick, J.; Fixman, M. *Macromolecules* **1977**, *10*, 944.

(32) Kapur, V.; Charkoudian, J.; Kessler, S. B.; Anderson, J. L. *Ind.Eng.Chem.Res.* **1996**, *35*, 3179.

(33) Kun, K. A.; Kunin, R. *J.Polym.Sci. A1* **1968**, *6*, 2689.

(34) Hirose, M.; Ito, H.; Kamiyama, Y. *J.Membrane Sci.* **1996**, *121*, 3671.

(35) *Polymer Handbook*; John Wiley & Sons: New York, 1999.

(36) Horkay, F.; Tasaki, I.; Basser, P. J. *Biomacromolecules* **2000**, *1*, 84-90.

(37) Bansil, R.; Gupta, M. K. *Ferroelectrics* **1980**, *30*, 63-71.

Chapter 4

Nanofiltration Using Poly(acrylic acid) Pore-Filled Membranes

4.1 Introduction

A wide variety of polymeric membranes have been developed for various water treatments. The main difference between each membrane lies in the relative size of the pores. For example, low-pressure types of nanofiltration membranes, which have been recently developed and are commercially available, have an intermediate pore size between ultrafiltration and reverse osmosis membranes. In the case of pore-filled membranes, the transition from ultrafiltration to reverse osmosis membranes can be controlled by modifying the amount of gel introduced into the pore of the host membrane.

In order to understand the separation characteristics of nanofiltration membranes it is important to have a suitable model to predict performance. A variety of models have been proposed, but few predict separation over a wide range of polymer concentrations.[1] "Black box" models are available, but as they do not take into account pore structure or charge, they do not allow an understanding of the effect of membrane chemistry on performance.[2]

Kimura *et al*[3,4] numerically solved the extended Nernst-Planck equation and incorporated the effect of charge with the Teorell-Meyer-Sievers (TMS) model. The TMS

model has several simplifying assumptions which include: the membrane is homogeneous; ion transport is accounted for by bulk diffusivities; and the fixed charge distribution is uniform throughout the membrane. The model does not take into account any steric hindrance, assuming that the pore size is much larger than the solute size. This fixed charge model has recently been used successfully over a wide concentration range to predict nanofiltration of a variety of monovalent salts by poly(vinylbenzyl ammonium salt) pore-filled membranes.[5]

The purpose of this study is to determine the effect of gel morphology on nanofiltration with poly(acrylic acid) pore-filled membranes. Nanofiltration experiments with sodium chloride were performed and the extended Nernst-Planck equation was applied to analyze the experimental results in terms of effective charge density.

4.2 Teorell-Meyer-Sievers (TMS) Model

The TMS model assumes that both ion concentration and electric potential have a uniform distribution within a membrane. The model has been applied to reverse osmosis membranes containing a fixed charge [3,6,7]. According to Kimura *et al*,[4] the extended Nernst-Planck equation, which includes the contribution of volume flux to ion flux, is expressed by **equation 4.1**

$$J_i = -D_i \frac{dc_i^m}{dx} + \frac{z_i F c_i^m D_i}{RT} \frac{dE}{dx} + c_i J_v \qquad (4.1)$$

where J_i is the flux of the ith kind of ion ($i = 1$, cation, $i = 2$, anion) through the membrane and the terms on the right-hand side represent transport due to diffusion, electric field gradient and convection respectively. D_i is the diffusivity of the ion i in the membrane, c^m_i is the concentration of ion i in the membrane, z_i is the valence of the ion, and J_v is the volume flux. The no electric current condition is expressed as

$$I = \sum_i (z_i J_i) = 0 \qquad (4.2)$$

Electroneutrality in the membrane and the external solution is expressed, respectively, as follows

$$\sum_i (z_i c_i^m) - X = 0 \qquad \text{(Inside membranes)}$$

$$\sum_i (z_i c_i) = 0 \qquad \text{(External solution)} \quad (4.3)$$

where X is the charge density based on volume of capillary pore, and c_i is the concentration of ion i in solution. A Donnan equilibrium is assumed to exist at the interface between the membrane and external solution and is stated by the following equation.

$$\exp\left(-\frac{F}{RT}\Delta\Phi^D\right) = \left(\frac{c_i^m}{c_i}\right)^{1/z_i} \qquad (4.4)$$

For 1-1 type electrolytes, combining **equation 4.3** with **equation 4.4** and using $J_1 = J_2 = J_s$ leads to

$$J_s = -\frac{D_1 c_1^m \cdot D_2 c_2^m}{D_1 c_1^m + D_2 c_2^m}\frac{d}{dx}\ln(c_1^m c_2^m) + \frac{D_1 + D_2}{D_1 c_1^m + D_2 c_2^m} c_1^m c_2^m J_v \qquad (4.5)$$

Integrating **equation 4.5** from the feed side ($c = c_b$) to the permeate side ($c = c_p$)with **equations 4.3** and **4.4**, yields

$$\frac{J_v \Delta x}{A_k} = -\frac{1}{2} D_s \left[\ln \frac{Z(c_p)^2 - 2c_p Z(c_p) + A}{Z(c_b)^2 - 2c_p Z(c_b) + A} + \frac{c_p}{B} \ln \frac{Z(c_p) - c_p - B}{Z(c_p) - c_p + B} \cdot \frac{Z(c_b) - c_p + B}{Z(c_b) - c_p - B} \right] \qquad (4.6)$$

where

$$A = 2(1 - 2\alpha(D))c_p X - X^2$$

$$B = [(X - c_p)^2 + 4\alpha(D) X c_p]^{0.5}$$

$$Z(c) = (4c^2 + X^2)^{0.5}$$

$$\alpha(D) = D_1 / (D_1 + D_2)$$

$$D_s = 2D_1 D_2 / (D_1 + D_2) \qquad (4.7)$$

and Δx is the thickness of the membrane (m).

The reflection coefficient is a phenomenological parameter associated with all desalination membranes.[8] A value of $\sigma = 1$ is an ideal semi-permeable membrane where all solute is rejected, while $\sigma = 0$ indicates the membrane is completely permeable to solute. Hoffer and Kedem[6] derived the reflection coefficient, σ, by assuming that the membrane parameters were determined at the feed boundary condition of the membrane.

$$\sigma_m = 1 - \frac{D_1 + D_2}{D_1 c_1^m + D_2 c_2^m} \frac{c_1^m c_2^m}{c} \qquad (4.8)$$

4.3 Experimental

4.3.1. Materials, Membrane Preparation and Characterization

The materials and methods for membrane production have been described previously in **Chapter 2**. Sodium chloride and sucrose were obtained from BDH Chemical and used without purification. The concentrations for both solutes were 5 mM.

4.3.2. Pressure Tests

The flux and separation experiments were carried out in a dead-end cell with a membrane active area of 38.50 cm^2. The cell was fitted with a thermocouple to measure temperature of the feed solution and a sample port so that the composition of the feed could be determined during the course of experiment. The feed solution was stirred at the rate of 250-300 rpm. Permeate samples were collected over a given period and weighed. Samples were taken at 100, 300 and 500 kPa. The flux (kg/m^2h) for a given pressure, was calculated from the mass of permeate divided by time and the membrane active area, and

was corrected to 25°C. The salt concentrations in feed and permeate were determined by conductivity (Model 105, Orion). The sucrose concentrations in the feed and permeate were determined with an O-I Analytical total organic carbon analyzer. The solute rejections were calculated as the percentage of the solute removed from the feed solution (the ratio of the difference between the solute concentration in the feed and permeate to the feed concentration). Each measurement was repeated three or more times. The reproducibility of the measurements was ± 3%. The pH of the feed solutions was 5.7 ± 0.2.

4.3.3 Membrane Charge Density

The charge densities of the membranes were required for the analysis of the factors affecting membrane performance. The poly(acrylic acid) pore-filled membranes contain weak carboxylic acid groups whose degree of ionization will be pH dependent. The apparent ionization constant, pK_a, is a function of the degree of ionization, α. According to the literature, the pK_a of poly(acrylic acid) at a degree of ionization α=0.5 is approximately 5.8 in pure water.[9] For the purposes of this work, the poly(acrylic acid) membranes are assumed to be approximately 50% ionized under the test conditions (pH of feed = 5.7 ± 0.2). The membrane charge densities, CD_M, for the membranes containing poly(acrylic acid) gels were calculated based on the following equation:

$$CD_M = \frac{IEC \times m_m \times \alpha}{V_m}$$

where IEC is the number of titrated sites per kilogram of membrane, m_m is total mass of the dried membrane (kg), V_m is the swollen membrane (m^3) and the degree of ionization, α, is assumed to be 0.5. The IEC values for the membranes used in these studies are given in **Chapter 2.**

4.4 Results and Discussion

Three series of membranes were prepared by photopolymerizing an applied monomer solution containing acrylic acid and N,N'-methylenebisacrylamide within the pores of a microporous polypropylene host. In the first series, the monomer concentration, in either DMF or 1,4-dioxane was varied between 1.110 and 2.775 M while keeping the cross linking ratio (BIS) fixed at 5 mol.% relative to acrylic acid. In the second series, the total monomer concentration and degree of cross linking (BIS) was kept constant (2.775 M, 5 mol. % BIS) while different solvent mixtures ranging from 100% DMF to 100% 1.4-dioxane were used. Finally, in the third series, the total monomer concentration was fixed (2.775 M) and the degree of cross linking was varied between 5 and 25 mol.% BIS relative to acrylic acid. The properties of these membranes are fully described in **Chapter 2** and briefly summarized in this chapter in **Tables 4.1 - 4.3.**

As shown in **Chapter 2**, the poly(acrylic acid) (PAA) containing membranes were shown to have the gel polymer evenly distributed throughout the thickness of the membranes. Increase in the total monomer concentration resulted in a corresponding increase in gel-polymer incorporated (Series 1). An increase in heterogeneity was observed in the gel fill by either changing the reaction solvent from good to poor (Series 2) or increasing the degree of cross-linking (Series 3). The increase in heterogeneity resulted in an increase in permeability.

4.4.1 Sucrose Separation

The maximum rejection of sucrose by any of the membranes was 4%. The very low rejection implies that the membranes do not provide any major steric hindrance toward solute rejections of components smaller in size than sucrose. This means that rejection of sodium and chloride ions should be strictly by a Donnan exclusion mechanism and not by sieving.

4.4.2 Salt Separation

All of the membranes in Series 1, 2 and 3 were capable of rejecting NaCl under pressure. The membranes were stable over the test period and the measured rejections and fluxes were reproducible.

4.4.2.1 Effect of Monomer Concentration (Series 1)

The separation/flux relationships with 5 mM sodium chloride solutions for the PAA membranes with increasing mass gain are shown in **Figure 4.1**. The nanofiltration data were modeled with the extended Nernst-Planck equation using the effective charge density, CD_E, as a fitting parameter. The solid lines in **Figure 4.1** represent the modeled nanofiltration data. Selected data for membranes of Series 1, including membrane charge density, effective charge density and reflection coefficient (**equation 4.8**), are found in **Table 4.1**.

In **Chapter 3**, it was proposed that homogeneous gels were formed in the membranes when DMF was used as the polymerization solvent. This suggestion was supported by the fit of the hydrodynamic permeabilities to the model.[10] As a result, the membranes formed from DMF should have a homogenous distribution of charge within the membrane. This means that the assumption of a uniform charge distribution in the TMS model are valid for the pore-filled membranes in Series 1.

The results presented in **Table 4.1** show that for the poly(acrylic acid) membranes in Series 1, an increase in gel concentration within the host membrane results in an increase in the membrane charge density. Thus, membrane CTM 155, with a mass gain of 39%, has a calculated membrane charge density, CD_M, of 37 mol./m^3, whereas CTM 121, with a mass gain of 122%, has a membrane charge density of 83 mol./m^3.

A similar increase in the estimated CD_E with increase in mass gain is also observed. For example, CTM 155 has an effective charge density of 30 mol./m^3 while CTM 121 has an effective charge density of 115 mol./m^3. Qualitatively the same trends in CD_M and CD_E are observed, however, the values obtained of CD_M differ from those for CD_M, particularly at high mass gain. Bowen has recently shown that the membrane charge densities obtained by the extended Nernst-Planck equation are typically overestimated.[11] It is interesting that in the results obtained here, at lower mass gain the charge densities appear to be underestimated.

According to **equation 4.6**, for a membrane with a homogeneous distribution of charge, an increase in effective charge density should result in an increase in rejection at constant flux. Conversely, at constant rejection, it is expected that the flux will increase with decrease in membrane charge density. Also, at constant membrane charge density, as the flux increases, so too should the rejection increase. These effects are clearly evident in the data obtained for the Series 1 membranes.

As shown in **Figure 4.1** for each of the membranes in Series 1, there is an increase in separation as the flux (pressure) is increased. At constant flux, there is an increase in rejection with increase in mass gain. Moreover, it can be shown in **Figure 4.1** at essentially constant rejection, the membrane flux increases as the membrane mass gain decreases. Membranes of 39, 43, 57, and 77 % mass gain exhibit approximately 40, 60, and 70 % rejection at 100, 300 and 500 kPa, respectively. Membrane CTM 121, with a mass gain of 122%, has approximately 30, 60, and 70 % rejection at 100, 300 and 500

kPa, respectively. These results are consistent with our earlier findings that as the flux for pore-filled membranes synthesized in good solvents increase with decreasing gel concentration, the rejection remains constant.[12] The overall trends in separation/flux obtained with the Series 1 membranes confirm the hypothesis that the gel formed using DMF as the reaction solvent is homogeneous.

With increasing mass gain of the poly(acrylic acid) pore-filled membranes, there is also an increase in the reflection coefficient. A membrane with 122% MG has a reflection coefficient of 0.93 while a 37% MG membrane has a reflection coefficient of 0.74. **Table 1** shows the reflection coefficient calculated using **equation 4.8**. The membranes of high mass gain consistently have a higher reflection coefficient than membranes of low mass gain, under the same test conditions.

4.4.2.2 Effect of Reaction Solvent (Series 2)

The relationship between separation and flux for Series 2 membranes with 5 mM sodium chloride is shown in **Figure 4.2**. The solid lines in **Figure 4.2** are again calculated using **equation 4.6** with the effective charge density as a fitting parameter to the nanofiltration data. Selected membrane data, including membrane charge densities, effective charge densities and reflection coefficients (**equation 4.8**) for membranes of Series 2 are given in **Table 4.2**.

Within the error limits, there is no difference in membrane charge densities for all of the membranes in Series 2. This can be seen from the data given in **Table 4.2**. As a result, it would be expected that these membranes should behave very similarly in nanofiltration, with very similar flux at a constant rejection. However, as shown in **Figure 4.2**, at similar level of rejection the fluxes are not similar and increase significantly in the order 121 < 122 < 123 < 124. This order corresponds to increasing relative volume of the poor solvent in the reaction mixture. At 500 kPa, CTM 124 has over two times the flux of CTM 121, with a flux of 2.2×10^{-6} m/s as opposed to 1.1×10^{-6} m/s. At pressures of 100, 300 and 500 kPa, NaCl rejections of approximately 30, 60 and 70 % are found for membranes CTM 121 to 123, respectively. However, the rejections for membrane CTM 124, are approximately 40, 68 and 75 % at 100, 300 and 500 kPa, respectively. Clearly, the membranes do not behave as expected, and vary quite markedly depending on the reaction solvent used during the polymerization step.

It has been shown in **Chapter 2** that with change in reaction solvent there was a change in gel morphology. The membranes formed in DMF contain a homogenous gel. However, with increasing volume of poor solvent in the reaction mixture, the gels become heterogenous and draining (polymer poor) and non-draining (polymer rich) regions (**Chapter 3**). The nanofiltration model, based on the extended Nernst-Planck equation and TMS model, assumes that the charge distribution within the membrane is uniform throughout the gel. A heterogeneous gel containing draining (polymer poor) and non-draining (polymer rich) regions would give rise to areas of different charge

concentrations. The draining regions would have a low fixed charge concentration while the non-draining regions would have a high fixed charge concentration. With heterogeneity in the gel, the assumptions of the TMS model no longer would be expected to hold.

Khoklov[13] has suggested that increase in heterogeneity of a polyelectrolyte gel will increase the number of osmotically inactive (bound) counterions and thus change the swelling properties of the gel. Their experimental data suggests that the fraction of osmotically passive (bound) counterions increases with increasing gel inhomogeneity, to an extent that exceeds the Onsager-Manning condensation.[13] A local potential well is formed in the highly charged polymer rich regions, which additionally binds more counterions. The increase in bound counterions also serves to decrease the effective charge density of the charged polyelectrolyte in the dense regions.

A similar decrease in swelling with heterogeneity as seen in Khoklov's work has been observed for poly(acrylic acid) pore-filled membranes in **Chapter 2**. This work has shown that the fixed charge sites of the acid moieties are still accessible within the membrane regardless of reaction solvent used. However, with an increase in heterogeneity of the poly(acrylic acid) gel fill, the membranes decrease their swelling capacity. This may indicate, that although the mass of the polyelectrolyte within the membranes formed from different solvent are similar, the effective charge density, CD_E, decreases with increase in heterogeneity.

If we assume that the gel within the draining region is homogeneous and that the fixed charge associated with the non-draining region does not contribute to the effective charge density in nanofiltration, the TMS/ENP model should give an estimate of the charge density of the draining regions. The estimated values for the effective charge densities of the draining regions of membranes formed from different solvents are shown in **Table 4.2**. Using the data in **Table 4.1**, we can extrapolate further and obtain an estimate of the polymer volume fractions of poly(acrylic acid) within the draining regions based on the effective charge densities in the draining regions. This leads to the estimated polymer volume fractions in the draining regions of the membranes formed from different solvent, as shown in **Table 4.2**.

As mentioned previously, the membrane charge density calculated from mass gain does not change, within error, with change in reaction solvent. The effective charge density, CD_E, decreases as the reaction solvent becomes poorer with addition of 1,4-dioxane. The effective charge density of membrane CTM 121 is 115 mol./m^3, while the effective charge density of CTM 124 is 60 mol./m^3, **Table 4.2**. With an increase in volume of poor solvent in the reaction mixture, the effective polymer volume fraction of poly(acrylic acid) within the draining regions decreases. In the most heterogeneous case, membrane CTM 124, this translates into an effective polymer volume fraction of 0.081 in the draining regions as opposed to $\varphi = 0.183$ for the gel within the entire membrane.

The reflection coefficient decreases slightly with increasing heterogeneity, as shown in **Table 4.2**. CTM 121 has a reflection coefficient of 0.93, while CTM 124, has a

reflection coefficient of 0.86. The observed reflection coefficient is consistent with a membrane with a polymer volume fraction of 0.081.

4.4.2.3 Effect of Cross-linking (Series 3)

Full characterization data for membranes in Series 3 are given in **Chapter 2.** **Table 4.3** contains selected data for membranes formed with the same monomer concentration, but different degrees of cross-linking. The membrane with 25 % cross-linking was too fragile for use in pressure testing.

It was shown in **Chapter 2**, that the number of ionizable sites in the poly(acrylic acid) pore-filled membranes decreases with an increase in the degree of cross-linking. Also, the swelling of the membrane decreases with increase in degree of cross-linking. Overall, as the degree of cross-linking increases, the membrane charge density increases from 83 mol./m^3 at 5% XL, to 110 mol./m^3 at 20% XL, **Table 4.3**.

The increase in membrane charge density (**Table 4.3**) for Series 3 membranes should result in a decrease in flux, at constant rejection. **Figure 4.3** shows the relationship between separation and flux for a 5 mM sodium chloride solution. At pressures of 100, 300 and 500 kPa, the rejections are approximately 30, 60 and 70 %, respectively, for all degrees of cross-linking. As expected, with the increase of charge density of the membranes, at constant rejection, the flux decreases with increased cross-linking.

Previous chapters have clearly shown that the pore-filling gels within a membrane are heterogenous with increase in cross-linking. The concept of draining and non-draining regions (**Chapter 3**) in heterogenous gels is not necessary to analyze the nanofiltration data for membranes in Series 3. This is suspicious considering that, with the Series 2 membranes, an increase in heterogeneity leads to a non-uniform distribution of charges, and the TMS/ENP model is no longer valid without the assumption of draining and non-draining regions within the gel. The concept that the charge distribution is homogeneous within the gel of membranes of Series 3 may not be valid, and other factors occurring with increase in cross-linking may be the cause of the observed performance.

One factor originates from the water content in the membrane. Stachera[14] and Pandey[15] have each shown that with a decrease in water content in the membranes, there was an increase in the fixed charge concentration for poly(alkylated-vinylpyridine) and poly(vinylbenzyl ammonium salt)-filled membranes, respectively. The decrease in water content in the membrane also had the effect of increasing the tortuosity of the membrane.[14] An increase in tortuosity would affect nanofiltration by increasing the effective thickness in **equation 4.6**.

The Series 2 membranes have been shown to have the same water uptake, (**Chapter 2**). They also have been shown to have the same diffusion coefficients, within error, and thus the tortuosity of this series of membranes is likely the same.[16] However, the water contents of the Series 3 membranes have been shown to decrease with increase in degree of cross-linking (**Chapter 2**). The increase in cross-linking would result in an

increase in tortuosity of the membranes, and thus may also be responsible for the observed decrease the flux in **Figure 4.3**.

4.5 Conclusions

The Mika model, extended Nernst-Planck equation and the heterogeneity model work remarkably well in describing the morphology and performance of gel-filled membranes. Polyelectrolyte-filled membranes formed by polymerization in good solvents can be considered as having a homogeneous distribution of gel, and therefore, a uniform distribution of charge throughout the membrane. Changing the morphology of the polyelectrolyte gel, by changing the reaction solvent, serves to create draining and non-draining regions within the gel. This picture is consistent with hydrodynamic permeability data given in **Chapter 3** and separation performance of the membranes discussed in this chapter. The polymer volume fraction of gel in a draining region decreases with increasing heterogeneity induced by the reaction solvent, and only a portion of the total titratable fixed charge in the membrane is responsible for salt rejection.

However, the picture of morphology of a highly cross-linked gel-filled membrane is very complex and further study is warranted. Factors such as water content and membrane tortuosity should be taken into account. These could be measured directly by diffusion experiments.

The pKa for the poly(acrylic acid) gels in this work was assumed to be 5.8.[9] This value is for salt free solutions, and it is well known that the pKa will change with addition of salt to the polymer system.[9] Also, the immobilization of a polyelectrolyte gel within a porous polypropylene substrate has been shown to effect pKa.[17] Determination of the number of ionizable sites of the poly(acrylic acid) membranes at the test feed pH and salt concentration can be achieved through titration methods. Electrochemical methods such as streaming potential and impedance spectroscopy may also provide better values of membrane charge density under the same test conditions as for nanofiltration.

At a recent conference, Bowen[11] proposed a new model for prediction of nanofiltration. The model closely matches calculated membrane charge density with the observed effective charge density. It would be interesting to see if this model could help further understand the pore-filled membranes. However, the new Bowen model does not take into account non-uniform charge distribution. Ideally, a model that incorporates non-uniform charge density would provide further insight into the morphological effects of the gel within pore-filled membranes.

Table 4.1. Summary of selected data for membranes synthesized by polymerization of 2.775 M AA, 5 % XL, in DMF (Series 1).

Membrane	Mass Gain (%, ± 5 %)	Polymer Volume Fraction	Membrane Charge Density (CD_M) (Mol./m^3, ± 10 %)	Effective Charge Density (CD_E) (Mol./m^3)	Reflection Coefficient
121	122	0.144	83	115	0.93
144	77	0.065	70	44	0.82
149	57	0.056	58	37	0.78
154	43	0.053	42	35	0.77
155	39	0.037	37	30	0.74

Table 4.2. Selected data for membranes formed by polymerization of 2.775 M AA, 5 % XL, but different reaction solvent (Series 2).

Membrane	Reaction Solvent	Mass Gain (%, ± 5 %)	Polymer Volume Fraction	Membrane Charge Density (CD_M) (mol/m³, ± 10 %)	Effective Charge Density (CD_E) (mol./m³)	Effective Polymer Volume Fraction	Reflection Coefficient
124	100% Dioxane	156	0.183	76	60	0.081	0.86
123	75% Dioxane	167	0.149	90	80	0.109	0.89
122	50% Dioxane	144	0.14	87	87	0.119	0.9
121	100% DMF	122	0.144	83	115	0.144	0.93

Table 4.3. Selected data for membranes synthesized by polymerization of 2.775 M AA, x % XL (where x = degree of cross-linking) in DMF (Series 3).

Membrane	Degree of Cross-linking (%)	Mass Gain (%)	Water Uptake (%)	Membrane Charge Density (CD_M) (mol./m^3, ± 10 %)	Effective Charge Density (CD_E) (mol./m^3)	Reflection Coefficient
CTM 121	5	122	66	83	115	0.93
CTM 129	10	141	66	89	130	0.93
CTM 131	15	153	60	99	143	0.92
CTM 132	20	166	53	110	178	0.92

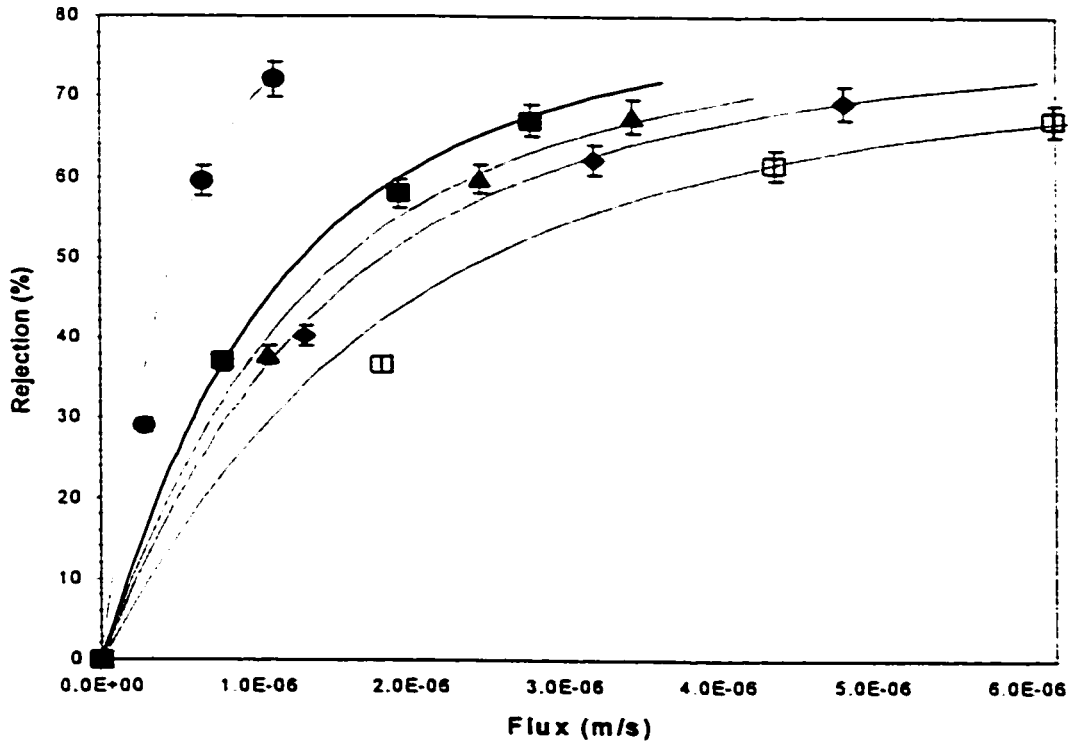

Figure 4.1. Nanofiltration of 5 mM NaCl using poly(acrylic acid) membranes synthesized from DMF, and 5% XL: (•) 122 % Mass Gain; (■) 77 %; (▲)57 %; (♦)43 %; (□)39 %. Solid lines are calculated by equation 4.6. The estimated charge densities are found in **Table 4.1.** Red, blue and black data points represent the test pressures of 100, 300 and 500 kPa, respectively.

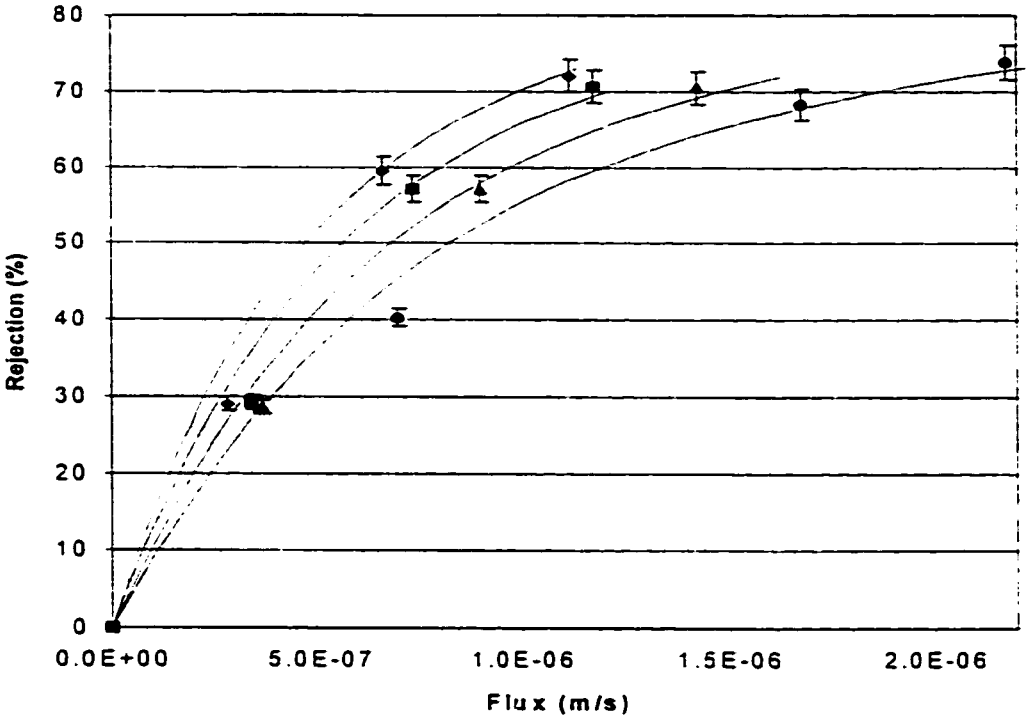

Figure 4.2. Nanofiltration of 5 mM NaCl for membranes synthesized by polymerization of 2.775 M AA with 5% XL, but different reaction solvent: (♦) DMF (CTM 121); (■) 50/50 DMF/Dioxane (CTM 122); (▲) 25/75 DMF/Dioxane (CTM 123); (•) 1,4-Dioxane (CTM 124). The solid lines are calculated by using equation 4.6. The estimated charge densities are found in **Table 4.2**. The red, blue and black data point represent the test pressures of 100, 300 and 500 kPa, respectively.

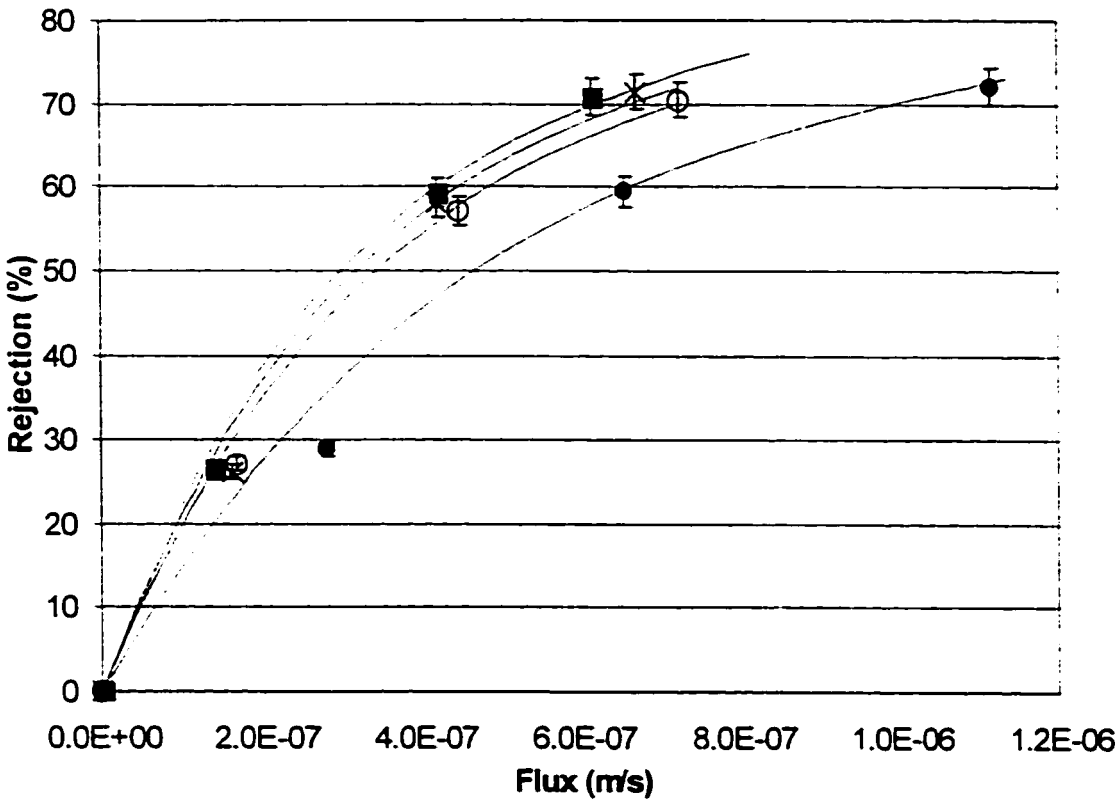

Figure 4.3. Nanofiltration of 5 mM NaCl using poly(acrylic acid) pore filled membranes synthesized from the same monomer concentration, but different degree of cross-linking with N,N'-methylenebisacrylamide: (•) 5% XL; (○) 10 %; (×) 15 %; (■) 20 %. The solid lines are calculated using equation 4.6. The estimated charge densities are found in **Table 4.3.** The red, blue and black data points represent the test pressures of 100, 300 and 500 kPa, respectively.

Reference List

(1) Garcia-Aleman, J. M.Eng. Thesis: Mathematical modeling of the pressure-driven performance of nanofiltration membranes: mixed electrolyte systems. 1998. McMaster University.

(2) Mika, A. M.; Childs, R. F.; Dickson, J. M. *Desalination* **1999**, *121* , 149-158.

(3) Tsuru, T.; Nakao, S.; Kimura, S. *J.Chem.Eng.Jpn* **1991**, *24*, 511-517.

(4) Wang, X.-L.; Tsuru, T.; Nakao, S.; Kimura, S. *J.Membrane Sci* **1995**, *103*, 117-133.

(5) Mika, A. M. Unpublished work. 2001.

(6) Hoffer, E.; Kedem, O. *Desalination* **1967**, *2*, 25.

(7) Tsuru, T.; Urairi, M.; Nakao, S.; Kimura, S. *J.Chem.Eng.Jpn* **1991**, *24*, 518-524.

(8) Mulder, M. *Basic Principles of Membrane Technology*; Kluwer Academic Publishers: 1997.

(9) Budd, P. M. Polymers and water: an overview; In *Industrial water soluble polymers*; Finch, C. A., ed. The Royal Society of Chemistry: Cambridge, 1996; pp 1-9.

(10) Mika, A. M.; Childs, R. F. *Ind.Eng.Chem.Res.* **2001**, *40*, 1694-1705.

(11) Bowen, W. R. and Welfoot, J. S. Predictive modelling of membrane nanofiltration - achievements and challenges. Luque, S. and Alvarez, J. R. 2, 222-227. 2001. Servicio de Publicaciones. Proceedings of Engineering with membranes.

(12) Childs, R. F.; Mika, A. M.; Pandey, A. K.; McCrory, C. T. C.; Mouton, S.; Dickson, J. M. *Sep.Purif.Technol.* **1999**, *22-23*, 507-517.

(13) Zeldovich, K. B.; Khoklov, A. R. *Macromolecules* **1999**, *32*, 3488-3494.

(14) Stachera, D. Ph.D. Thesis: Poly(4-vinylpyridine) membranes. 2000. McMaster University.

(15) Pandey, A. K.; Childs, R. F.; West, M.; Lott, J. N. A.; McCarry, B. E.; Dickson, J. *J.Polym.Sci.A.,Polym.Chem* **2001**, *39*, 807-820.

(16) McCrory, C. T. C. and Childs, R. F. Polyelectrolyte pore-filled membranes: Control of membrane resistance through control of gel morphology, manuscript in preparation. 2001.

(17) Mika, A. M.; Childs, R. F. *J.Membrane Sci* **1999**, *152*, 129.

Chapter 5

Synthesis, Characterization and Performance of Asymmetric Poly(Acrylic Acid) Pore-Filled Membranes

5.1 Introduction

The effect of gel heterogeneity on the performance of a poly(acrylic acid) pore-filled membranes has been presented in Chapters two and three. A 9-fold increase in hydrodynamic permeability of a membrane was observed when a poorer solvent was used in the formation step and a 4-fold increase in permeability with an increase in cross linking. These results were explained by formation of regions that were draining and non draining due to the microheterogeneity in the gel. The separation properties of membranes with homogeneous poly(acrylic acid) gels were good. The salt rejection was found to be practically constant, at constant pressure, over a wide range of gel concentrations. However, questions arise as to whether their performance could be enhanced.

There are potentially several other ways to modify the performance of the pore-filled membranes. One of these is to decrease the thickness of the active layer of the membranes. The membranes as currently made in this thesis have more or less an even distribution of the incorporated polyelectrolyte gel through the thickness of the membrane. This means that the active layer in these membranes is at least as thick as the

membranes by Loeb and Sourirajan.[4] These consist of a very dense top layer or skin with a thickness of 0.1 to 0.5 μm supported by a porous sublayer with a thickness of about 50 to 150 μm. These cellulose acetate membranes combined the high selectivity of a dense membrane with the high permeation rate of a very thin membrane.

In the past two decades a number of methods have been developed to create anisotropic membranes with performances which surpass those of the original cellulose acetate films. The majority of asymmetric membranes can be covered by four categories: phase separation membranes;[4-10] interfacial composite membranes;[11-21] solution-coated composite membranes;[22-24] and specialized anisotropic membranes.[25-28] Most anisotropic membranes are produced by phase separation, solution coating, or interfacial polymerization, with the later membranes dominating the nanofiltration market.[1] A number of other techniques, such as plasma graft polymerization,[29,30] can be used to form membranes. but these are not used on a large scale.

5.1.1 Asymmetric Pore-filled membranes

There is a fundamental difference in membrane construction between thin film and pore-filled membranes. The separating or active layer in thin film membranes is typically a dense layer that is formed on the top of a support membrane.[7] This dense layer faces the feed solution. In pore-filled membranes we are using a low density, cross-linked polyelectrolyte gel as the separating 'layer'. Because of the nature of the gel, it has to be

(13) Zeldovich, K. B.; Khoklov, A. R. *Macromolecules* **1999**, *32*, 3488-3494.

(14) Stachera, D. Ph.D. Thesis: Poly(4-vinylpyridine) membranes. 2000. McMaster University.

(15) Pandey, A. K.; Childs, R. F.; West, M.; Lott, J. N. A.; McCarry, B. E.; Dickson, J. *J Polym.Sci.A.,Polym.Chem* **2001**, *39*, 807-820.

(16) McCrory, C. T. C. and Childs, R. F. Polyelectrolyte pore-filled membranes: Control of membrane resistance through control of gel morphology, manuscript in preparation. 2001.

(17) Mika, A. M.; Childs, R. F. *J.Membrane Sci* **1999**, *152*, 129.

Chapter 5

Synthesis, Characterization and Performance of Asymmetric Poly(Acrylic Acid) Pore-Filled Membranes

5.1 Introduction

The effect of gel heterogeneity on the performance of a poly(acrylic acid) pore-filled membranes has been presented in Chapters two and three. A 9-fold increase in hydrodynamic permeability of a membrane was observed when a poorer solvent was used in the formation step and a 4-fold increase in permeability with an increase in cross linking. These results were explained by formation of regions that were draining and non draining due to the microheterogeneity in the gel. The separation properties of membranes with homogeneous poly(acrylic acid) gels were good. The salt rejection was found to be practically constant, at constant pressure, over a wide range of gel concentrations. However, questions arise as to whether their performance could be enhanced.

There are potentially several other ways to modify the performance of the pore-filled membranes. One of these is to decrease the thickness of the active layer of the membranes. The membranes as currently made in this thesis have more or less an even distribution of the incorporated polyelectrolyte gel through the thickness of the membrane. This means that the active layer in these membranes is at least as thick as the

NOTE TO USERS

Page(s) not included in the original manuscript and are unavailable from the author or university. The manuscript was microfilmed as received.

This reproduction is the best copy available.

UMI

membranes by Loeb and Sourirajan.[4] These consist of a very dense top layer or skin with a thickness of 0.1 to 0.5 μm supported by a porous sublayer with a thickness of about 50 to 150 μm. These cellulose acetate membranes combined the high selectivity of a dense membrane with the high permeation rate of a very thin membrane.

In the past two decades a number of methods have been developed to create anisotropic membranes with performances which surpass those of the original cellulose acetate films. The majority of asymmetric membranes can be covered by four categories: phase separation membranes;[4-10] interfacial composite membranes;[11-21] solution-coated composite membranes;[22-24] and specialized anisotropic membranes.[25-28] Most anisotropic membranes are produced by phase separation, solution coating, or interfacial polymerization, with the later membranes dominating the nanofiltration market.[1] A number of other techniques, such as plasma graft polymerization,[29,30] can be used to form membranes. but these are not used on a large scale.

5.1.1 Asymmetric Pore-filled membranes

There is a fundamental difference in membrane construction between thin film and pore-filled membranes. The separating or active layer in thin film membranes is typically a dense layer that is formed on the top of a support membrane.[7] This dense layer faces the feed solution. In pore-filled membranes we are using a low density, cross-linked polyelectrolyte gel as the separating 'layer'. Because of the nature of the gel, it has to be

prevented from swelling in contact with water by the physical constraint imposed upon it by the microporous host. As a result, in pore-filled membranes we seek to avoid having surface layers but try and ensure that the polyelectrolyte is held within the pores of the host, **Figure 5.2**. Thus while in both cases the approach to improving performance is to make the active layers as thin as possible, the way of achieving this has to be fundamentally different.

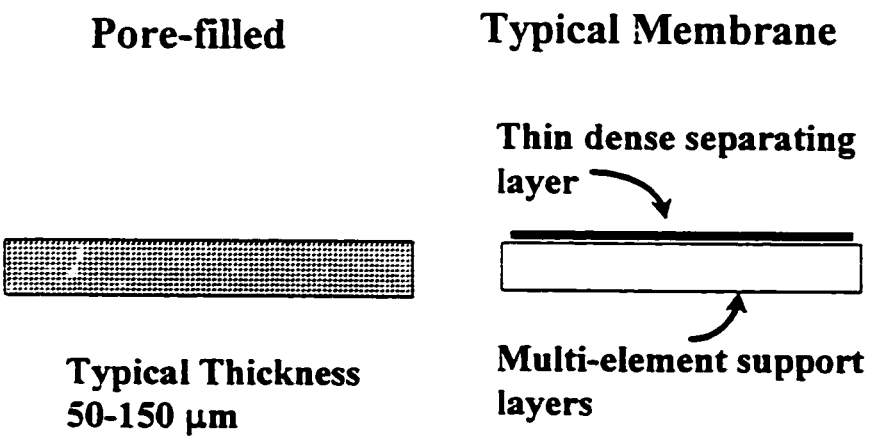

Figure 5.2. Comparison of the construct of a pore-filled membrane versus a typical thin film membrane.

One obvious route to making the active layers in the pore-filled membranes thinner is to start with thinner microporous host membranes. This approach has been used previously [3] with poly(ethylene) microporous hosts supplied by both 3M Canada and DSM (Holland), however, the resulting membranes are very fragile. Lamination of these thin membranes onto a support membrane is a possible way of overcoming this fragility.

A second route is to construct a membrane in which there is an even distribution

of gel, but where asymmetry is provided by altering the chemistry of the gel across the thickness of the membrane. For example, Yeom *et al*[31] have cast symmetric poly(vinyl alcohol) membranes, and diffused glutaraldehyde from one side of the membrane to obtain membranes with a gradient cross-link density. Stachera[32] has formed a symmetric pore-filled poly(4-vinylpyridine) substrate to which he diffused halogenated hydrocarbons, such as methyl bromide, on one side of the membrane. The result is a pore-filled membrane with a gradient of positive charge across the thickness of the membrane.

Another route is to partially fill a thicker microporous host membrane, as illustrated in **Figure 5.3**.

Symmetric Loading Asymmetric Loading

Figure 5.3. Schematic of the gradient gel in an asymmetric pore-filled membrane as compared to a symmetric fill.

Asymmetrically filled porous membranes of this construct have been prepared by plasma induced graft polymerization. In particular, Yamaguchi has described the introduction of grafted poly(acrylic acid)[29,30] or poly(methylacrylate) into a microporous high density poly(ethylene) membrane (0.02 μm averaged pore size). These workers concluded that the thickness of the grafted polymer depended on a balance between

monomer diffusivity and reactivity throughout the membrane. Work in our laboratories has shown that it is very hard to control the location of the grafted polymer using plasma activation techniques. Mass loadings of poly(acrylic acid) were not reproducible by this method and EDX analysis showed little, if any, asymmetry in the gel fill.[33] This may be due to the fact that the average pore size of the polypropylene base substrate in our work is approximately 40x larger (0.8 μm) than the substrate used in Yamaguchi's work. The diffusion of monomer through the 0.8 μm pore size polypropylene substrate would be expected to be much faster than the smaller pore size substrate and may not confine polymerization to surface layers of the membrane. It should be noted that the grafted polymers introduced by the plasma method were not cross-linked.

Ge[34] has used an evaporation method to create asymmetrically pore-filled membranes. A dilute solution of a polymer and suitable cross-linking agent was used to fill the pores of a microporous membrane. The membrane was then allowed to stand with the surface exposed to an airflow in a fume-hood for a period of time. After this evaporation step the membrane was covered with a poly(ethyleneterephthalate) sheet, sandwiched between two glass plates, and allowed to stand for 12 hours to complete the *in-situ* cross-linking.

Ge[34] has also formed asymmetrically gel-filled membranes by use of a UV photoblocker in the photopolymerization of poly(4-vinylpyridine) and cross-linker. This resulted in an asymmetric gel fill distributed across the thickness of the substrate. To the author's knowledge, there are no reports on the synthesis of asymmetric membranes by

photochemically filling a structurally rigid, porous support with a polyelectrolyte gel in an asymmetric manner.

The membranes studied in this chapter were prepared by photopolymerizing acrylic acid within the pores of a microporous poly(propylene) host.[35] Under the conditions used the incident light intensity was attenuated through the thickness of the membrane in a manner that was thought could lead to an asymmetric distribution of poly(acrylic acid) across the membrane. A practical goal of this work was to determine the effect of a photoblocker, 2,2'-dihydroxy-4,4'-dimethoxybenzophenone (DDB), on the gradient gel morphology within a porous substrate, and further determine the effects of the asymmetric gel fill on performance of the poly(acrylic acid) pore-filled membranes.

Although both Stachera and Ge have demonstrated the formation of asymmetric pore-filled membranes, the quantitative determination of the asymmetric gel fill by ESEM/EDX was difficult because of the limitations of this technique. Therefore, the use of a relatively new technique for polymer characterization, X-ray microscopy,[36] was proposed to try to quantitatively map the distribution of poly(acrylic acid) in the pores across the full width of the polypropylene membrane.

5.1.2 Characterization of Asymmetric Pore-Filled Membranes

In terms of understanding the properties of these membranes and further improving their performance, it is critical to know the distribution of the polyelectrolyte

gels within the microporous host. In this work we demonstrate that soft x-ray spectromicroscopy imaging, combined with appropriate data analysis techniques, can quantitatively analyse the composite polymer membrane structure, and in particular, determine the spatial distribution of the polyelectrolyte gel relative to the membrane.

5.1.3 NEXAFS/STXM

X-ray absorption spectroscopy has advanced rapidly in the last decades, particularly with synchrotron radiation-based techniques.[36] This chapter describes one of these techniques, scanning transmission x-ray microscopy (STXM)[37-39] combined with near edge x-ray absorption fine structure (NEXAFS), and illustrates its usefulness as a tool for characterization of asymmetric pore-filled membranes. Analytical soft x-ray microscopy has been developed and applied to a wide range of materials[40-42] including polymers[43-46] and authoritative reviews of STXM have been published which stress materials[40,41] and biological[42] applications.

5.1.4 Near Edge X-ray Absorption Fine Structure

As an x-ray passes through matter, it is absorbed to an extent which depends on the nature of the substance, the thickness of the sample, and the density of the sample. The absorbed photons cause excitation of the inner shell electrons of the atoms in the

substance. These excited inner shell (core) electrons can be promoted to unoccupied energy levels to form a short lived excited state or they can be removed completely to form an ionized state. Traditionally, X-ray absorption spectroscopy was described in terms of absorption edges which are the onsets of inner-shell ionization.[36] There is an absorption edge associated with each inner shell energy level of an atom, such that all elements have an X-ray absorption edge in the soft X-ray energy range (100-1200 eV). The amount of a particular element can be determined quantitatively from the difference in the x-ray absorption just above and just below its absorption edge.

Near-edge x-ray absorption fine structure, or NEXAFS,[36] can identify and quantitate the chemical structure of the element from the fine scale details of the absorption spectrum that occurs at each edge. These features correspond to electronic excited states in which an inner-shell electron has been excited to unfilled molecular orbitals or conduction bands. As the x-ray energy is increased throughout an absorption edge, first there is structure associated with excitation to the lowest unoccupied molecular orbital, which is a π^* orbital for unsaturated molecules (double or triple bonds), followed by structures associated with higher energy unoccupied molecular orbitals, typically of σ^* character associated with saturated (single) chemical bonds, and then direct inner-shell ionization. The unoccupied electronic structure and thus the inner-shell excited states are determined by the geometric and electronic (bonding) structure of the sample. NEXAFS spectra differ significantly even for rather similar molecular structures. This means that the NEXAFS spectrum of each polymer can be used as a fingerprint. In many cases,

enough is known about how chemical structure and X-ray absorption spectral features are related to allow one to identify unknown species from measured NEXAFS spectra. Individual spectral features, particularly the low energy p* features, are often sufficient for qualitative identification in reasonably well characterized systems, and they can serve as useful energies for selective chemical contrast in X-ray microscopy. There is characteristic NEXAFS structure at the absorption edge of each element in a sample. Thus combined studies of C 1s, N 1s and O 1s NEXAFS is a very powerful tool in polymer analysis. Finally, comparison with NEXAFS spectra of pure standards provides a means to derive quantitative composition maps of the components of a complex material from a series of X-ray microscopy images.

5.1.5 Scanning Transmission X-ray Microscope (STXM): Simple Description and Operation

A simplified view of STXM is shown in **Figure 5.4**. A Fresnel zone plate focuses mono energetic X-rays provided by a suitable monochromator beamline mounted on a suitable, bright synchrotron source. The focal point is typically 50 nm in diameter over a 3-10 mm waist. An image is generated by monitoring the X-ray signal transmitted through a thin section of a specimen as it is raster-scanned at the focus of the x-rays. Micro-spectra are measured by holding the beam at the spot of interest on the sample while the photon energy is scanned. The sample in a STXM can be mounted sandwiched

between two X-ray transparent silicon nitride windows.

5.1.6 Singular Value Decomposition Methodology

When an x-ray beam with energy E passes through a material, the intensity I is exponentially attenuated, according to:

$$I = I_0 e^{-\alpha(E)t} \qquad (5.1)$$

where t is the thickness of the material, α is the linear attenuation coefficient at energy E, I_0 is the intensity of the initial beam, and I is the intensity of the beam transmitted through the sample. Tabulations of x-ray absorption data usually give the energy-dependent mass absorption coefficient $\mu(E)$, where

$$\alpha(E) = \mu(E)\,\rho \qquad (5.2)$$

and ρ is the density of the material.

For quantitative image analysis, the transmitted signal is converted to an optical density (OD) according to

$$OD(E) = \ln (I_0/I) \qquad (5.3)$$

The optical density is linearly related to the sample properties by

$$OD(E) = \mu(E).\rho.x \qquad (5.4)$$

where $\mu(E)$ is the mass absorption coefficient at x-ray energy E, ρ is the density and x is the path through the sample or the sample thickness. If the energy-dependent mass

absorption coefficient μ is in cm^2/g and density ρ is in g/cm^3, one obtains the relative path through each of the components in cm.

The *OD* of a sample containing *j* non-interacting components is then given by

$$OD(E) = \mu(E)_1 \rho_1 t_1 + \mu(E)_2 \rho_2 t_2 + \ldots + \mu(E)_j \rho_j t_j \quad (5.5)$$

where t_j is the 'relative path' through each of the constituent with mass absorption coefficient μ_j and density ρ_j. (Note 'relative path' is used to encompass cases where the components are not in pure phases, but rather are mixed such that a column of the material has two or more components through its thickness.) If one knows the energy-dependent mass absorption coefficients μ_j and one measures the *OD* for different energies *E*, one can use linear algebra to convert the images into component maps $\rho t(x,y)$, by solving the above equation system for every pixel (x,y) of the image set. After correction for density, the vertical scale of the derived component maps is the 'relative path' of each component that is required to reproduce the total optical density *OD* at each pixel in the region sampled.

Although the details of the near edge x-ray fine structure provide the basis for distinguishing the components, the reference spectra must be placed on an absolute mass absorption scale in order to achieve quantitative analysis. The mass absorption coefficients are derived from measurements of the NEXAFS spectra of the pure components. In some cases (as in this work), reference spectra can be recorded from regions of the sample known to be pure in one of the components. In practice, spectra are obtained by first recording an energy scan *I* from the spot of interest and subsequently the

incident flux I_o measured with the same detector and optical path but with the sample out of the beam. The spectra are converted to *OD* by using **equation 5.3** and subsequently converted to a mass absorption scale by matching the signal in the pre-edge and post-edge regions to the sum of tabulated atomic mass absorption coefficients[47] for the elemental composition of the pure component (C_3H_6 for polypropylene and $C_3H_4O_2$ for poly(acrylic acid)).

The result of applying SVD to a sequence of X-ray images is a set of component maps, each of which is a plot of the density-thickness product (density-weighted 'relative path') for a given component. Accordingly, after correction for density, these maps provide component distributions in the thin section.

The X-ray photoabsorption response of a multi-component sample is a superposition of the response of each compound present in the column, weighted by its mass absorption coefficient at the photon energy employed, as described by the classical Beer-Lambert optical absorption law. Because of the linear relationship between spectral response (absorption or optical density) and concentration, the spatially resolved X-ray absorption signal can be used for quantitation. In order to carry out quantitative analyses the NEXAFS spectra of the pure components are recorded and converted to an absolute mass absorption scale by normalising to the atomic response outside of the fine structure at the core excitation threshold[47].

5.2 Experimental

5.2.1 Membrane materials and synthesis

The materials for membrane production have been described previously in **Chapter 2**, with exception of the photoblocker. The photo blocker, 2,2'-dihydroxy-4,4'-dimethoxybenzophenone (Aldrich) has a λ_{max} at 350nm of ε = 12,187 L/cm.mol. The method of membrane synthesis has been slightly modified and is outlined below.

The porous substrate used in this study was a poly(propylene) [PP] microfiltration membrane (3M Company) produced by a thermally induced phase separation process.[48] The PP substrate had an average porosity of 80.5% and average thickness of 72 μm. The general preparation of pore-filled poly(acrylic acid) (PAA) membranes is similar to a procedure described elsewhere.[35] A sample of poly(propylene) substrate was soaked for a few minutes in an N,N'-dimethylformamide solution containing 2.775 M acrylic acid, 5 mol. % N,N'-methylenebisacrylamide, 2 mol % of 2,2-dimethoxy-2-phenylacetophenone (DMPA) and 0 - 0.144 M 2,2'-dihydroxy-4,4'-dimethoxybenzophenone (DDB).

The substrate sample was removed from the solution, sandwiched between two polyethylene films and placed on a glass plate. The excess solution and any air bubbles were squeezed out by application of a Teflon™ roll bar, and the substrate was sealed between the sheets by taping them to a glass plate.

Two sets of membranes were prepared with varying concentrations of DDB. One

set was used for STXM analysis, while the second set prepared under identical conditions, was used for permeability and nanofiltration measurements. The concentrations of DDB used in membrane preparation are described in **Table 5.1**.

The sandwich and vial were irradiated at 350 nm in a UV system containing four parallel lamps (Southern N.E. Ultraviolet Co.) at a distance of 12 cm from the irradiated surface and a cooling fan. The irradiation was carried out for 60 min at room temperature. After polymerization, the membrane was thoroughly washed and placed in a water bath at 50 °C. The water was replaced each day with clean water until the conductivity of the wash was below 1 μS. This typically took 3 days.

Characterization methodologies for mass gain, water uptake and ion exchange capacity of the membranes are described in **Chapter 2**.

5.2.2 STXM sample preparation

A section of the wet membrane was frozen at -120°C and cryo-microtomed, to provide a cross-section of approximately 300 nm thickness. While frozen, the cross-section was laid flat on a 250μm x 250μm silicon nitride window and a second silicon nitride window was placed on top. The sample was warmed to room temperature to create the wet sample, which was analyzed at room temperature.

5.2.3 STXM Analysis

The C 1s images were recorded with beam line 7.0 STXM at the Advanced Light Source (ALS). The transmitted x-ray photon flux is measured on single photon counting basis using a scintillation converter and a high-performance photomultiplier tube (Hamamatsu 647P). To avoid any absorption by the air, the microscope chamber is completely filled with helium at atmosphere pressure after the sample is installed. Typical count rates are about 2 $x10^7$ photons/s transmitted through the helium at 300 eV, with the ALS storage ring running at 1.9 eV, 400 mA. Counting periods (dwell times) of 0.2 ms per pixel are typically used for analytical imaging. Currently the best spatial resolution of the microscope is about 100 nm, mainly due to mechanical vibration, rather than the zone plate, which has a diffraction-limited resolution of about 50 nm. The entrance and exit slits of the monochromator were set to obtain an energy resolution of about 100 meV in the carbon 1s region ($E/\Delta E$ ~3000).

Images were recorded at selected energies through the carbon edge region. Images at a photon energy particularly sensitive to radiation damage were recorded after each image sequence to monitor damage. Post acquisition image alignment[49] was used to correct for drift of the field of view associated with lateral run-out of the zone plate as it is moved along the optical axis to maintain focus.

The reference mass absorption coefficient signal for the poly(acrylic acid) gel was derived from regions of a separately recorded image sequence[49] as well as from the set of

images recorded for this SVD analysis. As we show below, the latter is preferred for quantitative analysis of the poly(acrylic acid) gel distribution. The reference mass absorption coefficient signal for polypropylene was obtained from a spectrum of pure polypropylene recorded at the ALS STXM. The incident flux signal used to convert the measured transmission intensity to optical density was recorded through the wet cell structure adjacent to the membrane. Thus there was no need to explicitly account for water or the Si_3N_4 window absorption in the quantitative analysis.

5.2.4 Performance testing of Asymmetric Pore-Filled Membranes

The procedure for determination of hydrodynamic permeability of the asymmetric membranes is the same as the procedure described for symmetric membranes in **Chapter 3.** The procedure for nanofiltration of 5 mM NaCl solutions is the same as the procedure described in **Chapter 4.**

5.3 Results and Discussion

Poly(acrylic acid) pore-filled membranes were synthesized by photo-initiated, free-radical co-polymerization of acrylic acid and N,N'-methylenebisacrylamide, with or without a photoblocker. We chose to use 2,2'-dihydroxy-4,4'dimethoxybenzophenone (DDB) as the photo-blocker. This compound has a strong absorption at 350 nm, the

wavelength of radiation of the UV lamps used for photo-initiation by DMPA. The absorption of radiation by DDB is reversed thermally meaning that the starting DDB is not depleted on irradiation but converts the photochemical energy into heat. DDB is not expected to interfere or become involved in the polymerization reactions induced by the initiator DMPA. It sole function is to compete for the incident photons that would otherwise be captured by the DMPA.

The addition of 2,2'-dihydroxy-4,4'-dimethoxybenzophenone, a photo-absorber, will limit the depth of penetration of the incident UV radiation. The intensity of the UV radiation should decrease as one goes further into the bulk of the substrate, with the lowest intensity of light at the other surface of the membrane. Using the Beer Lambert law, one can calculate the concentration of photoblocker required to obtain a desired gradient of UV light through the membrane. Assuming that the Beer Lambert law holds at high concentrations of DDB, we calculated the concentration of DDB required to absorb 1/10th, 1/100 and 1/10000 of the incident light for the membrane thickness. These concentrations are described in **Table 5.1** and were used in the experiments described below. The light intensity profiles calculated with these DDB concentrations are shown in **Figure 5.5.**

The porous substrate serves to act as a reservoir of monomer, and the distribution of monomer within the substrate is assumed to be uniform. The rate of initiation is dependent on the intensity of UV radiation.[50] A membrane without photoblocker should have the same initiation rate throughout the thickness of the membrane and would thus

lead to a symmetric, gel filled membrane. However, as the UV intensity is attenuated in the thickness of the substrate containing photoblocker, there should be a gradient in the initiation rate depending on the depth within the membrane. The highest rate of initiation will be at the closest surface exposed to the radiation, with the lowest rate of initiation furthest from the source. This gradient in rate of polymerization is expected to have the effect of producing an asymmetric gel within the membrane.

Assuming very little diffusion of monomer and that the irradiations are not carried out for an infinite time, a gel profile similar to the intensity profile of **Figure 5.5** would be expected. An increase in DDB concentration should further decrease the penetration depth of UV radiation, and should serve to produce an even greater asymmetry of the gel fill.

However, this picture is not likely as longer polymerization times will produce a monomer concentration gradient, and the monomer would be expected to diffuse to areas of depleted monomer (i.e. the areas with highest rate of polymerization) in response to the concentration gradient. An asymmetric gel fill is expected, but with a higher gel density at the membrane surface than predicted by the light curves shown in **Figure 5.5**. In other words, this diffusional process serves to enhance the asymmetry of the membranes.

5.3.1 Characterization - Mass Gain, Water Uptake and Ion-exchange capacity

Two sets of membranes were prepared with varying concentrations of DDB. Membranes CTM 008, 009 and 010 were used for STXM analysis. Membranes A012,

A013, and A014 (prepared under identical conditions to first set) were used for permeability and nanofiltration tests. All membranes were examined in terms of the physical properties, such as mass load, thickness, ion exchange capacity, and water uptake. These results were compared with CTM 121, a symmetric pore-filled membrane described in **Chapter 2**. The results and comparison are given in **Table 5.1.**

The mass gains, ion exchange capacities and water uptake are the same for asymmetric membranes in **Table 5.1**, and are also the same within error, to CTM 121. This indicates that the amount of monomer polymerized within the gel is the same and that mass of gel incorporated within the sets of membranes is the same. This result strongly supports the monomer diffusional model outlined above. It is interesting to note that the thickness of the membranes increased with the addition of DDB to the monomer solution.

5.3.2 STXM Analysis - Determination of degree of asymmetry

The spectroscopic basis for distinguishing the polymer components is presented in **Figure. 5.6**, where C 1s NEXAFS spectra of polypropylene and poly(acrylic acid) gel in mass absorption units are given. The figure also shows the calculated elemental absorption curves[47] which were used to convert both spectra to mass absorption units. The polypropylene spectrum is dominated by a strong broad transition at 287.9 eV which is attributed to C 1s – $\sigma^*_{C\text{-}H}$ transitions. The broad peak at 292 eV is associated with $\sigma^*_{C\text{-}C}$

resonances. The C 1s spectrum of the acrylic acid gel is dominated by the C 1s - $\pi^*_{C=O}$ transition at 288.5 eV. There are also signals at ~288 eV (shoulder), 292 eV and ~305 eV, corresponding to σ^*_{C-H} , $\sigma^*_{C=O}$ and σ^*_{C-C} resonances.

Membrane samples of CTM 121, CTM 008, CTM 009 and CTM 010 were analysed by STXM. A STXM image at 300 eV of a microtomed section of the hydrated CTM 010 membrane section sandwiched between two Si_3N_4 windows is given in **Figure 5.7**. Images similar to this were recorded at 11 different energies (287.6 to 289 eV in 0.2 eV steps and from 289 to 295 eV in 1.5 eV steps) from the sub-region indicated. Note the large mass of poly(acrylic acid) gel formed at the surface of CTM 010.

Two of these images (recorded at 287.6 and 288.6 eV on membrane CTM 010) are plotted in **Figure 5.8**. At 287.6 eV, the black area is due mainly to absorption of x-rays by polypropylene, and the pore structure of the membrane is clear. At 288.6 eV, the PAA also absorbs and it is clear that the PAA gel fills the pores of the polypropylene substrate (grey areas in **Figure 5.8**). The SVD analyses presented in **Figure 5.8** clearly show the poly(acrylic acid) is distributed asymmetrically across CTM 010. In contrast, the polypropylene distribution is relatively uniform, apart from the bottom region of the imaged area (**Figure 5.8**) where the polypropylene pores have been enlarged presumably due to the swelling of the poly(acrylic acid) gel.

In order to use these measurements to determine the asymmetric loading of the gel in membrane, it is necessary to quantitatively characterize the distribution of the gel across the membrane. Given the photochemical generation of the asymmetric loading it is

appropriate to model this distribution with a combination of an exponential fit. The results of this analysis applied to the gel component maps derived from the SVD for membranes CTM 008, CTM 009, and CTM 010 are presented in **Figure 5.9**. In order to reduce the sensitivity to the random distribution of the polypropylene pores, the STXM analysis is performed on an average across the full membrane width (2 μm) sampled.

It appears in **Figure 5.9** that as the concentration of DDB in the monomer mixture increases, the distribution of poly(acrylic acid) gel across the polypropylene substrate becomes more asymmetric in the order CTM 121 < CTM 008 < CTM 009 < CTM 010. Since the total mass of polyelectrolyte incorporated into the substrate is essentially the same for each of these membranes, the gel must be becoming more dense as the gel thickness becomes thinner with increase in DDB concentration. This indicates again that the monomer is diffusing along a concentration gradient to the surface of the membrane and the resulting mass of incorporated gel is the same for the series of poly(acrylic acid) membranes. It appears in **Figures 5.7** and **5.9** that the densest gel area is at the surface exposed to the UV radiation, while the least dense is furthest away.

5.3.3 Permeability Measurements

The flux versus pressure relationships were linear up to 500 kPa for all membranes. The results of the hydrodynamic permeability of the poly(acrylic acid) membranes are shown in **Table 5.1**. The membrane permeability decreases in the order

CTM 121 > A012 > A013 > A014, or, in the order of increasing DDB concentration. A 13% reduction in permeability is observed going from membrane CTM 121 (1.69×10^{-19} m^2) to A014 (1.47×10^{-19} m^2).

The average mass of polymer in these membranes is very similar. However, the asymmetry in gel distribution means that the gel polymer density must be increasing as the gel layer becomes thinner. This results in a dense gel fill in the thin layer, as confirmed by the STXM results (**Figure 5.9**). However, in **Chapter 3** it was shown that with an increase in gel polymer volume fraction (mass gain), there was a decrease in permeability. Therefore, while the reduction in gel layer thickness should increase membrane permeability, the increase in polymer volume fraction of the thinner gel layer will act to reduce membrane permeability. The density of the gel layer is the dominant factor in determining membrane permeability.

5.3.4 Nanofiltration Measurements

The data for nanofiltration of 5 mM NaCl by the membranes is given in **Table 5.2**. **Figure 5.10** shows the separation/flux relationships for the series of membranes with increasing photoblocker concentration. The rejection remains constant at a given pressure for all membranes in **Table 5.2**, within error. The flux of the membranes at constant rejection decreases in the order CTM 121 > A012 > A013 > A014. The results of **Chapter 4** showed that with an increase in mass of gel within the membrane, there was a

decrease in flux at constant rejection. The results are similar to the nanofiltration results for the membranes in **Table 5.2.**, and the observed decrease in membrane flux with increase in gel asymmetry is due to the increase in gel density in the thinner layer.

5. 4 Conclusions

The imaging results presented for these membranes illustrate a number of important advantages of the STXM technique for quantitative chemical mapping relative to other approaches. First, it is important to be able to study the material in the wet state since it is the distribution of the poly(acrylic acid) gel in the wet state that is critical to filtration membrane performance in actual applications. Electron beam-based microscopies, while providing potentially superior spatial resolution, cannot carry out studies in the presence of liquid water.

The chemical quantitation is based on the intrinsic spectroscopic properties of the constituents of the sample, and does not require any fluorescence or heavy atom labelling to achieve differentiation. The latter approaches, while certainly very powerful, raise questions about potential sample modification from the labelling chemistry.

The technique is able to sample the full width of the membrane at high spatial resolution in an efficient manner. The component map of the gel is based on a balanced sampling through the full thickness of the sample section (~0.3 μm), and thus the derived gel distribution is representative of the full membrane, not just the top or bottom portion.

This is in contrast to highly surface sensitive techniques such as X-ray photoelectron spectroscopy (XPS) or AFM, which are only able to sample the outermost surface of a sample. Given the extremely heterogeneous porous nature of these membranes, this is a critical advantage.

The photoblocker technique, coupled with photopolymerization, is an effective method to achieve asymmetric gel distribution within a porous substrate. The results demonstrate that asymmetry can be controlled by changing the concentration of photoblocker in the polymerization mixture, resulting in thinner, more dense membranes. To further increase the asymmetry of the membrane, one could simply increase the concentration of photoblocker in the solution.

We have only studied one variable affecting the morphology of the gel fill in the pore-filled membranes, namely photoblocker concentration. There are two other variables which should be studied in the photopolymerization technique: polymerization time; and monomer concentration.

There are two effects that can result from a long polymerization time. The first is a depletion of monomer in the region of high initiation rate, and a diffusion of monomer from the bottom of the substrate to the surface. This would give rise to a dense gel fill at the top of the membrane, with a sparse (or none) fill at the bottom. The second is that even though the initiation rate at the bottom of the membrane is low compared to the top of the membrane, over a one hour period a significant degree of polymerization can occur. Decreasing the time of polymerization, followed by quenching of the reaction, should

serve to limit the diffusion of monomer to the surface, and thus reduce the gel mass, and even thickness, at the surface.

With a long polymerization time, the density of the gel fill seems to rely on the diffusion of the monomer in solution. At long polymerization times, a decrease in the monomer concentration in the "membrane reservoir" would limit the density of polymer achieved. This seems to be the more practical and easier method to control asymmetry. Moreover, there should be little waste of monomer and one does not have to worry about quenching the reaction when a high monomer concentration is within the membrane at short polymerization times.

Table 5.1. Characterization of asymmetric poly(acrylic acid) pore-filled membranes.

Membrane	Concentration of DDB (mol/L)	Mass Gain (%, ± 5 %)	Water Uptake (%, ± 5 %)	IEC (meq/g, ± 0.2)	Thickness[a] (μm, ± 4)	Hydrodynamic Permeability (m^2)
CTM 121	0	122	66	5.6	83	1.69×10^{-19}
A012	4.74×10^{-3}	131	62	5.8	103	1.59×10^{-19}
A013	2.44×10^{-2}	125	65	5.3	103	1.53×10^{-19}
A014	1.44×10^{-1}	127	65	5.5	107	1.47×10^{-19}
CTM 008	4.74×10^{-3}	120	69	5.3	99	-
CTM 009	2.44×10^{-2}	123	64	5.4	105	-
CTM 010	1.44×10^{-1}	125	66	5.4	105	-

a. Thickness of swollen membrane in deionized water.

Table 5.2. Nanofiltration of 5 mM NaCl at various pressures.

	CTM 121		A012		A013		A014	
Pressure (kPa)	Flux (kg/m2.hr)	Rejection (%)	Flux (kg/m2.hr)	Rejection (%)	Flux (kg/m2.hr)	Rejection (%)	Flux (kg/m2.hr)	Rejection (%)
100	1	29	1	31	0.8	31	0.6	30
300	2.4	60	2.3	58	1.9	56	1.8	57
500	4	72	3.8	71	3.4	71	3	69

Note the error in flux is ± 0.2 kg/m^2.hr and the error in separation is ± 3%.

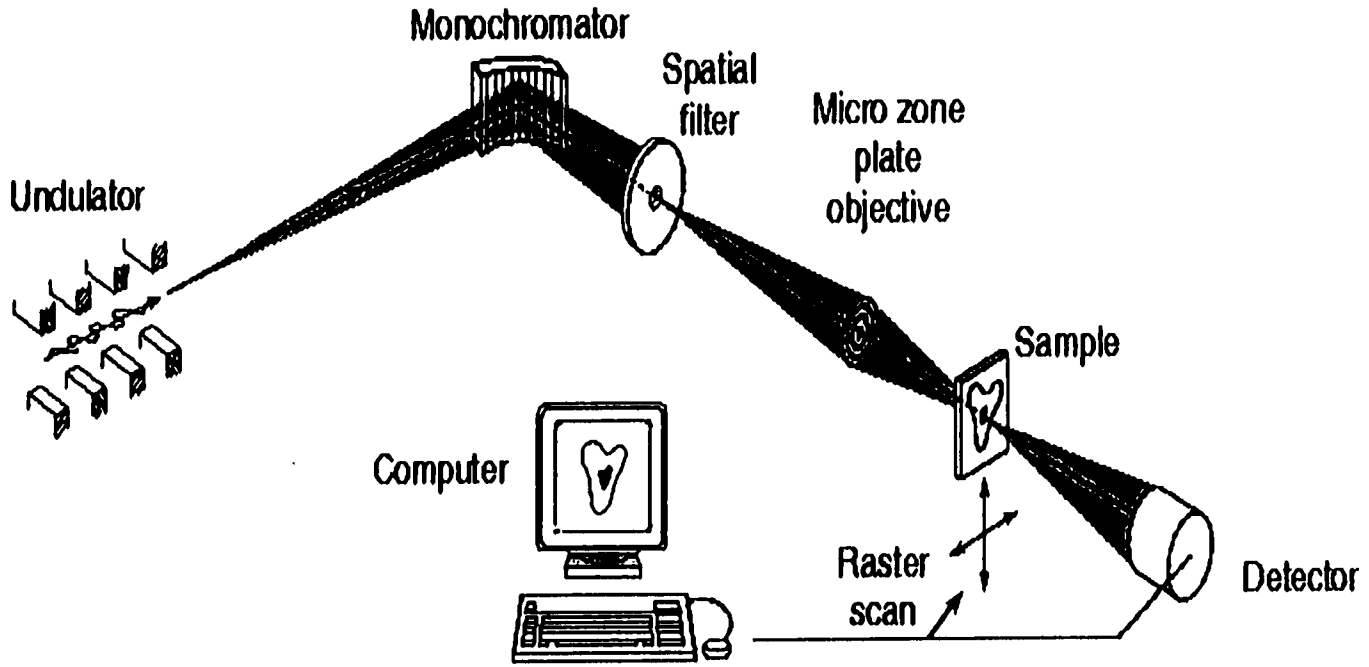

Figure 5.4. A simplified view of the scanning transmission x-ray microscope.

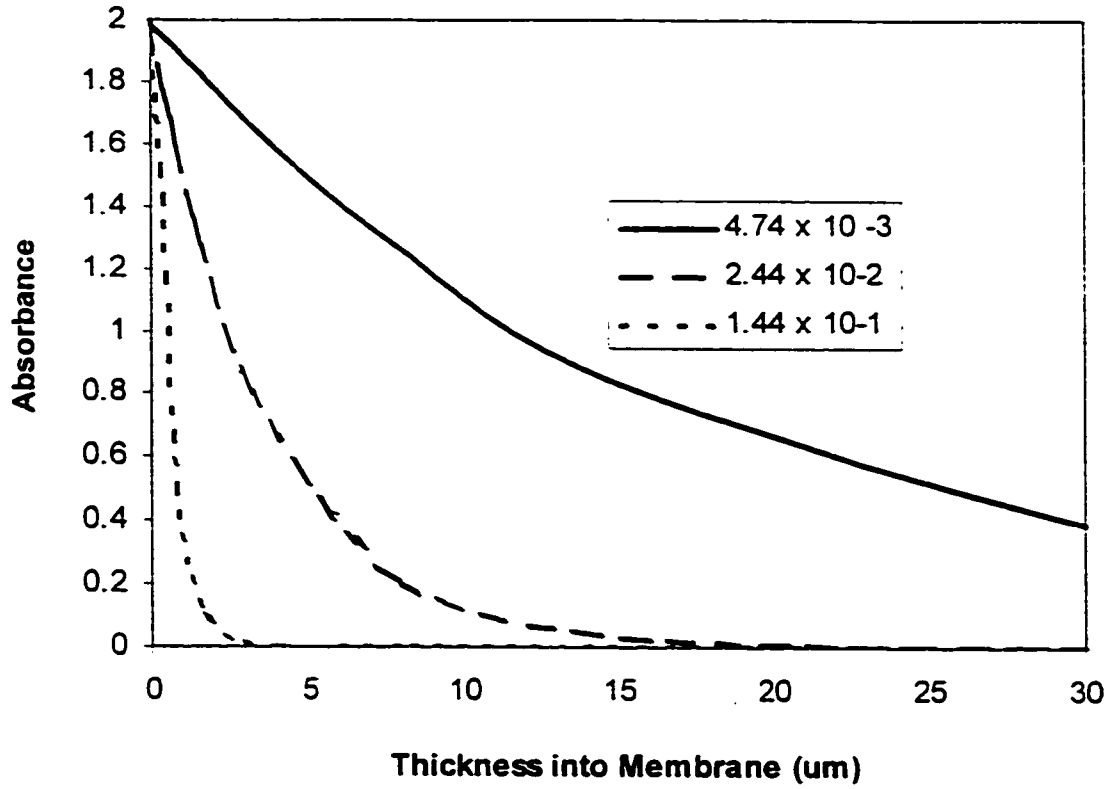

Figure 5.5 Calculated attenuated UV light, based on the concentration of DDB (concentrations are given in legend), across the first 30 microns of the membrane. Calculations were performed using the Beer-lambert equation for a typical membrane of 70 μm.

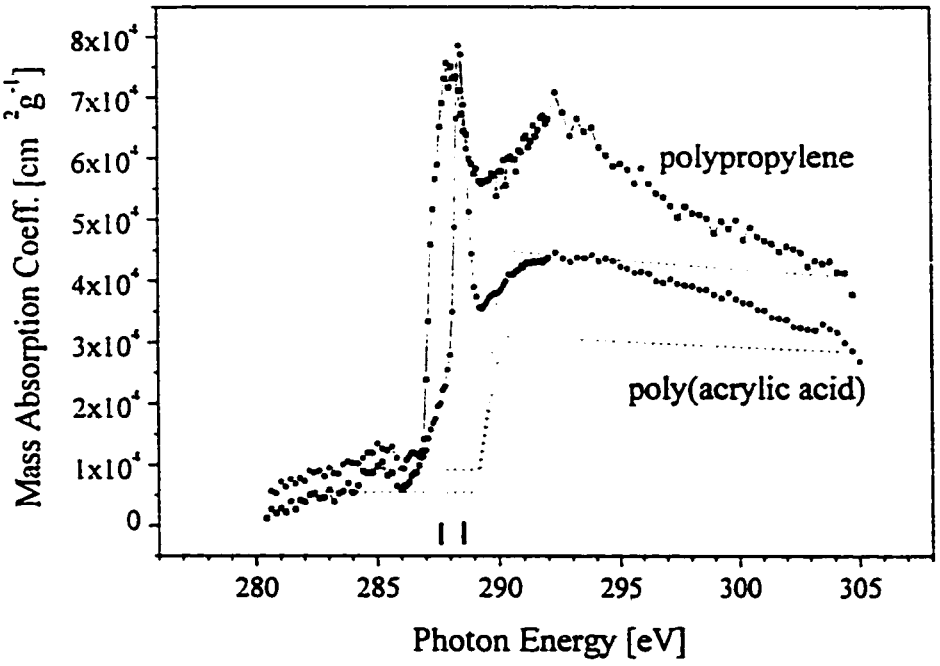

Figure 5.6. NEXAFS spectra of poly(acrylic acid) gel and polypropylene obtained from a fine mesh sequence (every point is an image) compared to the spectrum of polypropylene, recorded on pure material. The spectra are plotted on quantitative mass thickness scales. The dashed line is the calculated elemental absorption of the pure materials, which was used to convert each spectrum to absolute mass absorption units. The two vertical lines at the bottom of the spectra represent the absorption maxima for polypropylene and poly(acrylic acid), respectively at 287. 6 and 288.6 eV.

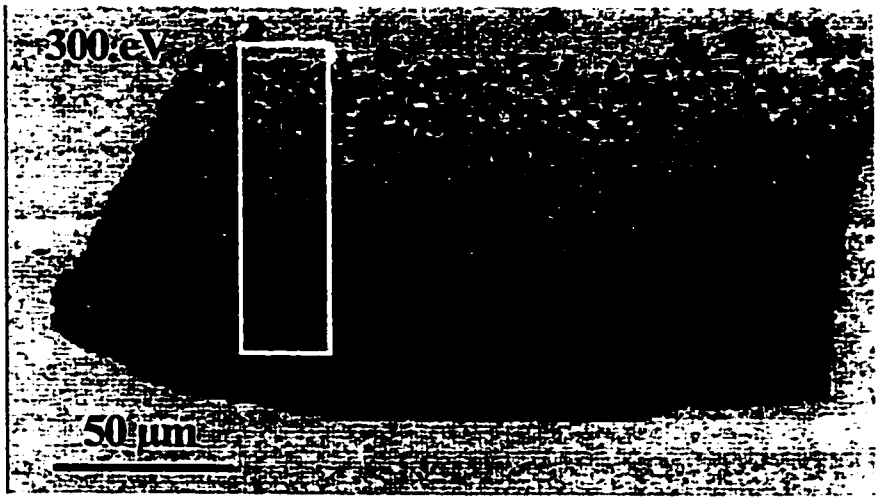

Figure 5.7. Transmission mode STXM image at 300 eV of a thin section (~300 nm) of membrane CTM 010. The polypropylene is the dark structure while the poly(acrylic acid) is the lighter grey area.

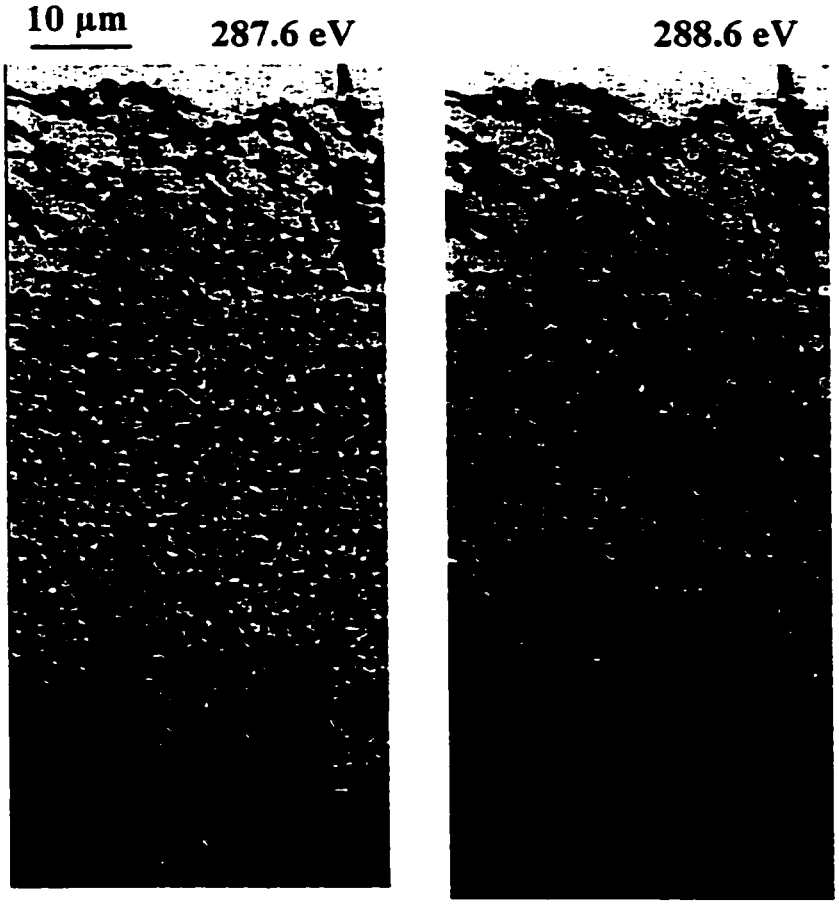

Figure 5.8. Images at 287.6 and 288.6 eV of the sub-region indicated in **figure 5.3**. Note the changes in contrast due to the different absorption properties of the two polymers at the different photon energies.

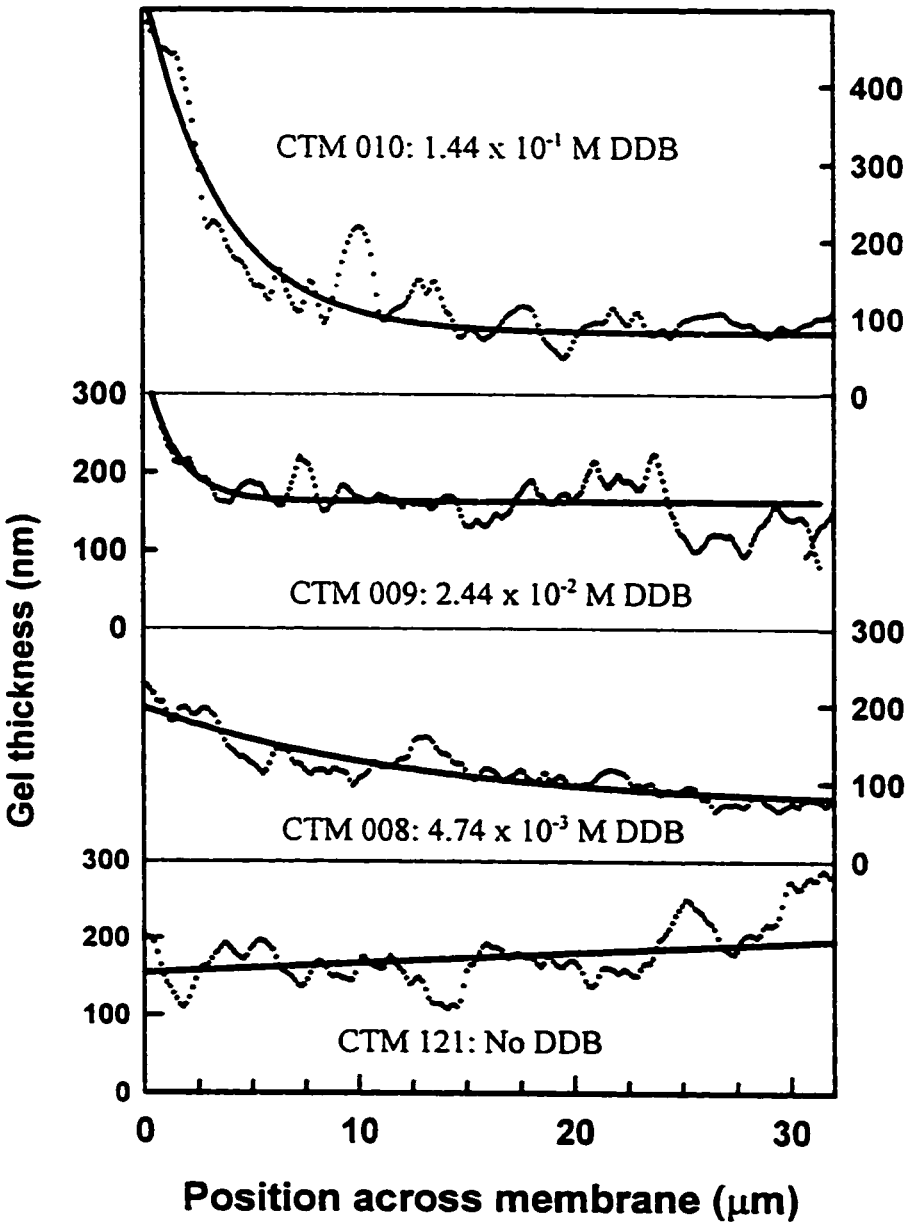

Figure 5.9. Normalized gel profile across first 30 microns of membrane. Solid lines represent exponential fits of the data.

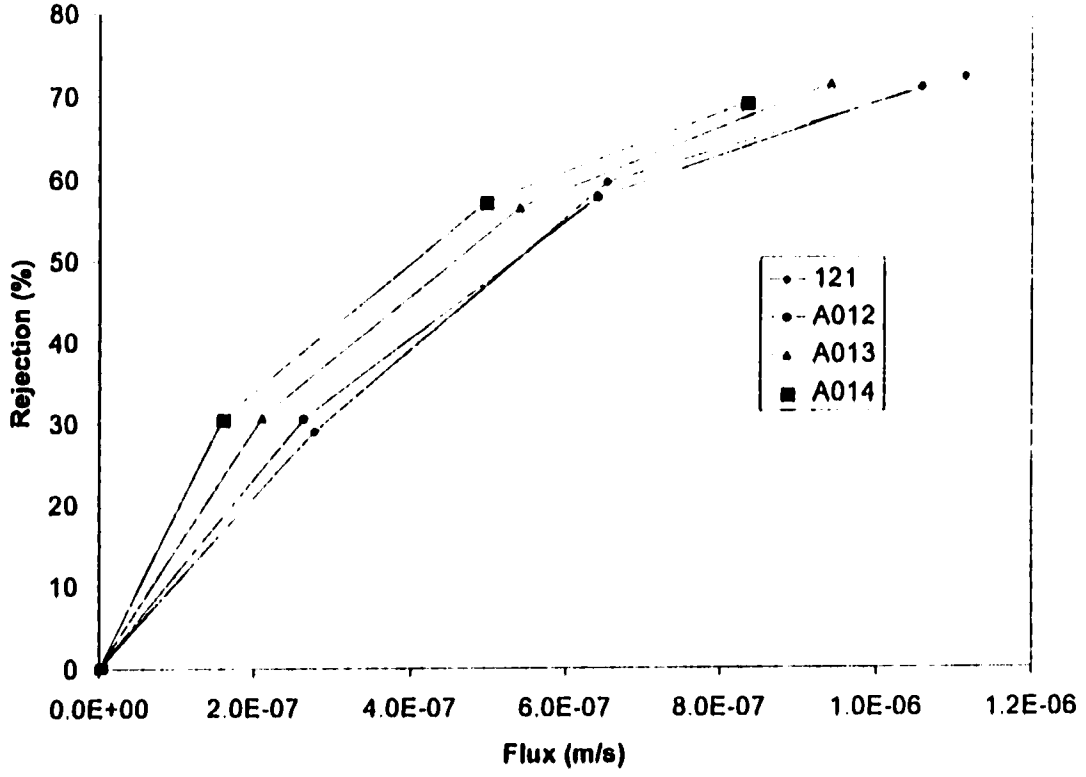

Figure 5.10. Nanofiltration of 5 mM NaCl by symmetric membrane CTM 121 (no photoblocker), and asymmetric membranes A012 (4.74 x 10^{-3} M DDB), A013 (2.44 x 10^{-2} M DDB) and A014 (1.44 x 10^{-1} M DDB).

Reference List

(1) Baker, R. W. *Membrane Technology and Applications*; McGraw-Hill: New York, 2000.

(2) Mika, A. M. and Childs, R. F. RO and NF membranes: The role of chemistry and morphology in membrane transport. 2001. A conference of the European Membrane Society. 9-9-2001.

(3) Mika, A. M. Unpublished work. 2001.

(4) Loeb, S.; Sourirajan, S. *Adv.Chem.Sev.* **1962**, *38*, 117.

(5) Lonsdale, H.; Merten, U.; Riley, R. *J.App.Polym.Sci.* **1965**, *9*, 1341.

(6) Lonsdale, H. K. *J.Membrane Sci.* **1982**, *10*, 81.

(7) Mulder, M. *Basic Principles of Membrane Technology*; Kluwer Academic Publishers: 1997.

(8) van de Witte, P.; Dijkstra, P. J.; van den Berg, J. W. A.; Feijen, J. *J.Membrane Sci.* **1996**, *117*, 1-31.

(9) Zeeman, L.; Fraser, T. *J.Membrane Sci.* **1994**, *84*, 93.

(10) Zeeman, L.; Fraser, T. *J.Membrane Sci.* **1994**, *87*, 267.

(11) Cadotte, J. E.; Peterson, R. J. Thin-film composite reverse osmosis membranes: origin, development and recent advances; In *Synthetic Membranes. Vol. I., Desalination*; Turbak, A. F., ed. American Chemical Society: Washington, 1981; p 305.

(12) Cadotte, J. E. Evolution of composite reverse osmosis membranes; In *Material Science of Synthetic Membranes*; Lloyd, D. R., ed. American Chemical Society: Washington, 1985; p 273.

(13) Hirose, M.; Ito, H.; Kamiyama, Y. *J.Membrane Sci.* **1996**, *121*, 3671.

(14) Hirose, M.; Minamizaki, H.; Kamiyama, Y. *J.Membrane Sci.* **1997**, *123*, 151.

(15) Koo, J.-Y. and Yoon, Y. S. Composite polyamide reverse osmosis membrane and method of producing same. (US6063278). 16-5-2000.

(16) Kwak, S.-Y.; Jung, S. G.; Yoon, Y. S.; Ihm, D. W. *J.Polym.Sci.B., Polym.Phys.* **1999**, *37*, 1429.

(17) Kwak, S.-Y. *Polymer* **1999**, *40*, 6361.

(18) Peterson, R. J.; Cadotte, J. E. Thin film composite reverse osmosis membranes; In *Handbook of Industrial Membrane Technology*; Porter, M. E., ed. Noyes Publications: Park Ridge, 1990; p 307.

(19) Tomaschke, J. E. and Ary, I. E. Interfacially synthesized reverse osmosis membranes and processesfor preparing same. (US5254261). 19-10-1993.

(20) Tomaschke, J. E. Interfacially synthesized reverse osmosis membranes and processes for preparing the same. (US5246587). 21-9-1993.

(21) Tomaschke, J. E. Amine monomers and their use in preparing interfacially synthesized membranes for reverse osmosis and nanofiltration. (US5922203). 13-7-1999.

(22) Fibiger, R. F., Colucci, M. J., Forgach, D. J., Wessling, R. A., and Schmidt, D. L. Rejection enhancing coatings for reverse osmosis membranes. (US4909943). 20-3-1990.

(23) Fibiger, R. F., Colucci, M. J., Forgach, D. J., Wessling, R. A., and Schmidt, D. L. Rejection enhancing coatings for reverse osmosis membranes. (US4894165). 16-1-1990.

(24) Mickols, W. E. Method of treating polyamide membranes to increase flux. (US5755964). 26-5-1998.

(25) Dytnerskii, Y. I.; Dmitriev, A. A.; Mchedlishvili, B. V.; Potokin, I. L. *Russ.Coll.* **1983** , 1024-1028.

(26) Uragami, T.; Fujimoto, M.; Sugihara, M. *Angew.Makromol.Chem.* **1981**, *95*, 45-54.

(27) Yokoyama, Y.; Tanioka, A.; Miyasaka, K. *J.Membrane Sci.* **1988**, *38*, 223-236.

(28) Yokoyama, Y.; Tanioka, A.; Miyasaka, K. *J.Membrane Sci.* **1989**, *43*, 165-175.

(29) Yamaguchi, T.; Nakao, S.; Kimura, S. *Macromol.* **1991**, *24*, 5522-5527.

(30) Yamaguchi, T.; Yamahara, S.; Nakao, S.; Kimura, S. *J.Membrane Sci.* **1994**, *95*, 39-49.

(31) Yeom, C. K.; Lee, K. H. *J.App.Polym.Sci.* **1996**, *59*, 1271-1279.

(32) Stachera, D. Ph.D. Thesis: Poly(4-vinylpyridine) membranes. 2000. McMaster University.

(33) Chris McCrory. Unpublished work on the formation of pore-filled poly(acrylic acid) membranes by plasma activation. 1998.

(34) Ge, J. and Childs, R. F. Unpublished work on asymmetric membranes. 2001.

(35) Childs, R. F.; Mika, A. M.; Pandey, A. K.; McCrory, C. T. C.; Mouton, S.; Dickson, J. M. *Sep.Purif.Technol.* **1999**, *22-23*, 507-517.

(36) Stohr, J. *NEXAFS Spectroscopy*; Springer-Velag: Berlin, 1992.

(37) Ade, H.; Smith, A. P.; Zhang, H.; Winn, B.; Kirz, J.; Rightor, E. G.; Hitchcock, A. P. *J.Electron Spectrosc.* **1997**, *84*, 53.

(38) Warwick, T.; Padmore, H.; Ade, H.; Hitchcock, A. P.; Rightor, E. G.; Tonner, B. P. *J.Electron Spectrosc.* **1997**, *84*, 85.

(39) Warwick, T.; Franck, K.; Kortwight, J. B.; Meigs, G.; Moronne, M.; Myeni, S.; Rotenberg, E.; Seal, S.; Steele, W. F.; Ade, H.; Garcia, A.; Cerasari, S.; Denlinger, J.; Hayakawa, S.; Hitchcock, A. P.; Tyliszczak, T.; Rightor, E. G.; Shin, H.-J.; Tonner, B. P. *Rev.Sci.Inst.* **1998**, *69*, 2964.

(40) Ade, H.; Urquhart, S. G. to be published as a chapter; In *Chemical application of sychrotron radiation*; Sham, T. K., ed. World Scientific Publishing: 200.

(41) Ade, H. Academic Press: New York, 1998; p 225.

(42) Kirz, J.; Jacobsen, C.; Howells, M. *Q.Rev.Biophys.* **1995**, *28*, 33.

(43) Ade, H.; Zhang, H.; Cameron, S.; Costello, C.; Kirz, J.; Williams, S. *Science* **1992**, *258*, 972.

(44) Ade, H.; Hsioa, B. *Science* **1992**, *262*, 1427.

(45) Ade, H.; Smith, A. P.; Cameron, S.; Cieslinski, R.; Costello, C.; Hsioa, B.; Mitchell, G. E.; Rightor, E. G. *Polymer* **1995**, *36*, 1843.

(46) Smith, A. P.; Ade, H. *Appl.Phys.Lett.* **1996**, *69*, 3833.

(47) Henke, B. L.; Gullikson, E. M.; Davis, J. C. *At.Nucl.Data Tables* **1993**, *54*, 181.

(48) Lloyd, D. R.; Kinzer, K. E.; Tseng, H. S. *J.Membrane Sci.* **1990**, *52*, 239.

(49) Jacobsen, C.; Wirik, S.; Flynn, G.; Zimba, C. *J.Microscopy* **2000**, *197*, 173.

(50) Cowie, J. M. G. *Polymers: Chemistry and Physics of Modern Materials*; Blackie Academic and Professional: Suffolk, 1991.

Chapter 6

Conclusions and Future Work

The feature that sets apart the pore-filled membranes from other nanofiltration membranes is the construct, which incorporates a polymer gel within the pores of a host substrate. It has been shown in this work that the morphology of the gel is a key factor in determining the performance of these types of membranes. Assumptions of a homogeneous gel morphology in the pore-filled membranes can clearly be an over simplification as these studies show that the monomer concentration, reaction solvent and cross-linking ratio all have a direct effect on the morphology of the gel fill and subsequently on the performance of the membranes.

The effect of gel heterogeneity on the performance of the pore-filled membranes is difficult to predict, even with conventional models. The method of free radical polymerization begs the question as to the origin of the gel heterogeneity. Understanding the formation of heterogeneity in the gel may be a key component in the overall understanding of the gel performance. Questions such as the density of draining and non-draining regions and influence of spatial charge distributions may be better understood if the gelation mechanism is known.

Much work has been done on the understanding of polymers in solution. However, the cross-over to gel systems is much more poorly understood. A more controlled system for gel membrane formation, backed up with research on polymers or polyelectrolytes of

interest in the semi-dilute regime, may also help in further understanding the effects of gel morphology on membrane properties. Such a system may exist in the method of pore-filling by cross-linking of pre-formed polymers developed in this group. The method involves a solution of polymer in which a cross-linking agent is added to form the gel network. Properties of the polymer solutions can be studied without cross-linking, to obtain information on the polymer properties under numerous conditions, including nanofiltration test conditions and gelation conditions. The polymer properties can further be studied in the semi-dilute regime, the area to which gel properties best relate to gel properties. One can now permanently fix the polymer lattice in place by chemical cross-linking and test the properties of the gel. Enough background knowledge should be obtained by these studies to tackle the problem of understanding the gel within a pore-filled membrane.

The asymmetry results are preliminary. It is clear that the asymmetric membranes produced here are capable of rejecting sodium chloride, but the expected improvement in performance due to a decrease in the gel layer was not observed. The work outlined in this thesis shows that the density of the gel layer is a key factor in enhancing the performance of the membrane. The gel density can be controlled through the concentration of the monomer in solution. A decrease in monomer concentration would produce a less dense, asymmetric gel network at infinite polymerization times. Future work in this area would require a systematic study of the effect of monomer concentration, at infinite polymerization time, on the gel density, thickness and performance of asymmetric pore-filled membranes.

Appendix

Experimental Data for Table 3.1.

Membranes synthesized in 1,4-Dioxane.

Membrane	Polymer Volume Fraction	Permeability (m^2)	NaCl Rejection 300 kPa
CTM 160	0.0998	1.1902E-18	66.8
CTM 161	0.0869	2.89616E-18	68.3
CTM 124	0.1826	9.08E-19	68.3
CTM 138	0.1132	2.16E-19	76.8
CTM 111	0.1095	6.16E-19	66.9
CTM 121	0.1442	1.69E-19	59.5
CTM 122	0.1403	1.95E-19	57.1

Membranes syntthesized in DMF

AR 011	0.0216	3.87E-18	59
CTM 123	0.149	2.68E-19	57.1
CTM 112	0.146	2.55E-19	53.1
CTM 142	0.0016	4.06E-14	0
CTM 140	0.0067	5.35E-14	0.000
CTM 145	0.0809	5.47E-19	58
CTM 153	0.0115	1.77E-16	0
CTM 153	0.0115	1.77E-16	0
CTM 154	0.0372	4.50E-18	61.5
CTM 155	0.0531	1.16E-18	59.8
CTM 148	0.0759	1.78E-18	59.3
CTM 149	0.056	3.31E-18	62

Example of a plot of volume flux versus pressure to obtain Darcy permeability, by equation 3.6, for membranes of 78 % and 120 % mass gain.